SCHOOL OF SCIENCE

Using Historic Satellite and 3D UAV Imagery to Map the Dynamics of the Coast at Sites with Anthropogenic Debris in Southland, New Zealand

Cassandra Newman 2022

A THESIS SUBMITTED TO AUCKLAND UNIVERSITY OF TECHNOLOGY IN PARTIAL FULFILMENT OF THE REQUIREMENTS FOR THE DEGREE OF MASTER OF SCIENCE (RESEARCH) IN GEOSPATIAL SCIENCE

Abstract

The coast is a naturally active margin that forms an important barrier system subjected to the forces of both the terrestrial and marine environment. Coastal erosion has become a problem where infrastructure and debris along the shore are being consumed by the ocean. The overall aim of this research was to investigate the ability of a generalised GIS methodology to quantify coastal dynamics at different locations with anthropogenic debris. This study investigated four sites along the southern coast of the South Island, New Zealand: Monkey Island, Colac Bay, Fortrose, and Porpoise Bay. Historic satellite imagery was used to investigate coastal dynamics by extracting the magnitude and rate of change occurring from past shorelines where patterns were interpreted to predict where the shorelines will be in the future. 3D UAV imagery was collected to analyse volumetric change on a seasonal basis. The main findings illustrate the importance of human intervention when interpreting the dynamics occurring along the coast and predicting where the future shoreline could be. Seasonal 3D UAV imagery and analysis highlights both the great deal of temporal and spatial change in these environments, as well as the complexity of understanding the dynamics of coastal areas. This study evaluates the validity of applying a generalised GIS methodology and makes recommendations for further research, which will, in turn, inform future monitoring and management of coastlines with anthropogenic debris.

Contents

Abstract i
Figures i
Tables x
Attestation of Authorship xi
Acknowledgements xii
Appendix xiii
Chapter 1 Introduction 1
1.1 The coastal system 1
1.2 Anthropogenic impacts and climate change 3
1.2.1 Coastal landfills and debris 4
1.3 Coastal monitoring 5
1.4 Applications of Geographic Information Systems (GIS) 6
1.4.1 Applications of Unmanned Aerial Vehicles (UAV) 6
1.5 Research aims and objectives 8
1.6 Structure of thesis 9
Chapter 2 Methodology 10
2.1 Study areas 10
2.1.1 Monkey Island 11
2.1.2 Colac Bay 13
2.1.3 Fortrose 15
2.1.4 Porpoise Bay 16
2.2 Datasets and acquisitions 18
2.2.1 Satellite imagery 18
2.2.2 UAV imagery 19
2.3 Software 20
2.4 Analysis and workflow 20
2.4.1 Satellite analysis workflow 21
2.4.2 Predicting future shorelines workflow 32
2.4.3 UAV analysis workflow to calculate seasonal change in volume 35
Chapter 3 Results 39
3.1 Results summary 39
3.2 Historic Shorelines 43
3.2.1 Monkey Island Historic Shorelines 43
3.2.2 Colac Bay Historic Shorelines 44
3.2.3 Fortrose Historic Shorelines 46
3.2.4 Porpoise Bay Historic Shorelines 47

3.3 Coastal Dynamics 50
3.3.1 Monkey Island Coastal Dynamics 50
3.3.2 Colac Bay Coastal Dynamics 51
3.3.3 Fortrose Coastal Dynamics 54
3.3.4 Porpoise Bay Coastal Dynamics 55
3.4 Prediction Maps 56
3.4.1 Monkey Island Prediction Maps 56
3.4.2 Colac Bay Prediction Maps 57
3.4.3 Fortrose Prediction Maps 60
3.4.4 Porpoise Bay Prediction Maps 61
3.5 Volume Maps 63
3.5.1 Monkey Island Volume Maps 63
3.5.2 Colac Bay Volume Maps 66
3.5.3 Fortrose Volume Maps 70
3.5.4 Porpoise Bay Volume Maps 73
Chapter 4 Discussion 76
4.1 Success and significance of research 77
4.1.1 Patterns in the shorelines 77
4.1.2 Predicting future shorelines 79
4.1.3 Human Intervention 80
4.1.4 3D UAV seasonal data 82
4.2 Recommendations 82
4.2.1 Recommendations for the Methodology 83
4.2.2 Site Specific Recommendations 87
4.3 Uncertainty and limitations 90
4.3.1 Imagery inaccuracy and sparse data 90
4.3.2 UAV data collection 92
4.3.3 Imagery doming 93
4.4 Conclusion 95
References 96

Figures

Figure 1.1. Processes that supply and remove sediment from the coast. There are many sources (where sediment joins the coastal system) and sinks (where it leaves the coastal system) of sediment showing that the coast is a very active environment with many different influences affecting it. These include fluvial (from rivers and streams) and aeolian (wind) transport, eroding cliffs, longshore drift and cross-shore exchange. Made by Cassandra Newman. 2

Figure 1.3. The changing formation of sediment at sandy beaches throughout the year. Sand builds up over the summer months on the shore (left-hand side of figure) then is pulled out by currents and wave action to create a bar offshore in winter months. This illustrates one of the many cycles the coastal system experiences at different temporal rates. Made by Cassandra Newman. 3

Figure 2.1. Study areas shown throughout the southern coast in Southland, New Zealand. **A.** The study areas are Monkey Island, Colac Bay, Fortrose, and Porpoise Bay. **B.** The right-hand map shows where the research took place in relation to New Zealand. 11

Figure 2.2. Monkey Island study area. Outlines show the shoreline being analysed with historic satellite imagery and the UAV flight area. Due to the nature of the shoreline, the width of the study area is dependent on the historic shorelines analysed. 12

Figure 2.3. The nature of the site at Monkey Island and the thin coastal margin before the metalled carpark. Along the study area there are pieces of discarded concrete and many pieces of rubbish in the face of the dune. The seaweed on the ground shows the water comes right up to the shoreline. 13

Figure 2.4. Colac Bay study area. Outlines show the shoreline being analysed with historic satellite imagery and where the UAV flight area is. Due to the nature of the shoreline, the width of the study area is dependent on the historic shorelines analysed. 14

Figure 2.5. Colac Bay as it is in 2021 looking south along where the coastal road was closed and where the 3D UAV flight captures imagery. Blocks in the bottom of the image show where vehicles no longer have access and the pebble substrate on the closed road shows how invasive the sea can be as well as the road being eaten away shown at the top of the image. 14

Figure 2.6. Fortrose study area. Outlines show the shoreline being analysed with historic satellite imagery and the area for the UAV flight plan. Due to the nature of the shoreline, the width of the study area is dependent on the historic shorelines analysed. 15

Figure 2.7. The nature of the site at Fortrose where the UAV flight plan captured imagery. A visualisation of the old building materials and bricks throughout the estuary edge. 16

Figure 2.8. Porpoise Bay study area. Outlines show the shoreline being analysed with historic satellite imagery and the area for the UAV flight plan. Due to the nature of the shoreline, the width of the study area is dependent on the historic shorelines analysed 17

Figure 2.9. Shows the nature of the site where the 3D UAV imagery is captured with a visualisation of the frontal dune along Porpoise Bay. 18

Figure 2.10. Screenshot of the flight plan on the Pix4D application on my phone. The plan was able to be duplicated for each time survey. The top lefthand corner shows the GSD which stands for 'Ground Sampling Distance' which measured how many centimetres were equal to one digital pixel. This was adjusted with the height of the flight which you can see on the left-hand side of the image. This flight is at 50 m above ground level. The same flight area for each site was done at 100 m above ground level to fix doming issue which occurred in the May survey. The bottom middle of the image shows the parameters of the flight plan which is 131 x 58 m. The time it will take for the flight to be completed is also shown in the box. This flight plan will take 21 minutes and 51 seconds. This is important to note because the battery in the drone can run for about 25 minutes before it needs to be replaced. 19
Figure 2.11. Overview of collecting, analysing, and presenting data for this research. The top blue is where the imagery came from. On the left workflow, the top grey step illustrates where the shorelines are extracted from the satellite imagery in ArcGIS Pro. The shorelines are used as an input for the DSAS software (dark grey), the coastal dynamics (grey) and are illustrated as a final output in the results. The coastal dynamics are illustrated in a map as a final output and used along with the DSAS software to predict where the shoreline will in 20 years which is also a final output of the study. The dark blue on the right workflow shows the processing of the UAV imagery in the Agisoft Metashape application. The output from this went into the CloudCompare application to extract volume values shown in the light blue. The volume values were imported into ArcGIS Pro in grey to have the symbology changed and to be presented in a map. Light grey is the final output. 21
Figure 2.12. Workflow of extracting the shoreline for each satellite image at each site and producing vector outputs. Cobalt blue represents the input into the workflow. The %Year% in some of the light blue steps is used as a substitute for listing all the outputs where only the year is different. The percentage signs on either side are used in python coding to process multiple inputs while keeping some features unique in the outputs. The dark blue below it iterates the raster layers, so each image goes through the same analysis step. Grey represents geoprocessing that occurs in ArcGIS Pro and white represents manual editing that occurs at that point of the workflow. The final output is a collecting of historic shoreline layers each representing a different year where the imagery was originally captured. This is shown in the grey box at the end of the workflow. 23
Figure 2.13. a. The study area was clipped then the *Iso Cluster Unsupervised Classification* tool was used to classify land cover. The *Iso Cluster Unsupervised Classification* tool divides the elements of the imagery into 5 classes to distinguish them from each other shown with the different colours..... 24
Figure 2.14. Workflow generating transect lines and merging them with each shoreline. The shorelines were merged with the transect layer and the most recent shoreline layer to distinguish the magnitude of change between the past and present. Transects were edited using the ArcGIS Pro *Planarize* and *Delete* tool so that the line between the shorelines analysed was all that was left of the transect. The outputs become inputs for the workflows illustrated in figure 20 and 21. Cobalt blue represents the transects being inputs into the workflow. Light blue represents outputs. Grey represents geoprocessing that occurred and white represents manual editing that occurred at that point of the workflow..... 25
Figure 2.15. **a**. Example of transect lines merged with 2021 shoreline then merged with 1948 shoreline to compute the length of erosion or accretion between the 1948 and 2021 shorelines. **b**. Resulting

transect lines between 1948 and 2021. Once edited, the transect shape length will be the magnitude of change between the shorelines. 26
Figure 2.16. An example of how the magnitude values were extracted. Each measurement occurs where the transect lines are but for demonstration in this figure, they have been separated along the shoreline so you can see them. The dark brown line is the 2021 shoreline. All measurements go towards this so that an increase or decrease in magnitude between the shorelines can be easily distinguished. The arrows show the direction of change. All shorelines in this example are eroding towards the 2021 shoreline except the 2013 shoreline that has accreted 1.21 m. 26
Figure 2.17. Example of the attributes table. 'ErosionAccretion' column states whether the shoreline was eroding to accreting towards the 2021 shoreline. 'AEPosNeg' is the shape length of each transect with all the erosion values as negative and accretion as positive. 'Year' is the years the measurement is between. Annual rate is the 'Shape_Length' divided by the number of years the measurement is between used as an estimate. 27
Figure 2.18. This workflow is for adding and populating fields with erosion / accretion data to go into an excel spreadsheet. The first transect attribute was populated with the 'shoreline year' to distinguish each set of transects when the outputs are merged. The other attributes were created to indicate if erosion or accretion was occurring between the survey times. If the earlier-date shoreline was on the seaward side of the 2021 shoreline, the attribute was labelled with 'Erosion' because the shore had eroded toward the most recent shoreline. If the shoreline was on the landward side of the 2021 shoreline, it was populated with 'Accretion'. The erosion values were calculated with a bit of code which says if 'Erosion' is in this column then I will populate this value with a negative, else keep value the same. 28
Figure 2.19. From the outputs of figure 16, the transects with corresponding historic shorelines such as the 1948 with the 1962 and the 1962 with the 1978 shoreline were merged. The 'Planarize' and' Delete' tool was used to extract the shape length of each transect between the shorelines. The rate of change between the different historical shorelines was then determined from the resultant transect line segment lengths divided by the number of years between the shorelines which then populated an 'Annual_Rate' attribute. Each layer was merged into one and the attribute table was saved as an excel worksheet using the *Table to Excel* tool in ArcGIS Pro. 30
Figure 2.20. Using the original transect lines, two attribute fields were added and populated with a pattern number and a matrix is produced to illustrate the coastal dynamics. Transects that produced high values for both categories were classed as 'unstable'. The values calculated are put back into ArcGIS Pro and added to the original transect lines. 31
Figure 2.21. This is the coastal dynamics matrix for categorising each transect line. You can expect to see this in the results chapter on the coastal dynamic's maps. Each transect was placed into a matrix based on the value of accretion and erosion it showed. If both these patterns are low, then the shoreline is stable resulting in a yellow transect line. If both are high, it is classed as unstable resulting in a black transect line. Brown shows a dominant erosion pattern and blue shows a dominant accreting pattern. The colours in between show a mix of dynamics. 32

Figure 2.22. Method to extract values for predicting the shoreline in 20 years. The transect layer and the 2020s shoreline layer were intersected using the *intersect* tool in ArcGIS Pro with the output being a point layer. To compute the estimated distance the shoreline would change in 20 years, the point layer was buffered using the values from the 'Estimate20' field. A new point layer was created, and points were manually created on top of where the transect and the buffer intercept or if the value was 0, on the same point as the previous point layer. 33

Figure 2.23. Method for the manual predictions in ArcGIS Pro. The key in the figure describes the different layers used to estimate the shoreline in 20 years. This method used several ArcGIS Pro geoprocessing tools to get the future shoreline prediction. A buffer using the values from the 'Estimate20' field was created at the point where the transect line and current shoreline intersect. Where the edge of this buffer and the transect intersect is the point where the shoreline is predicted to be in 20 years. A new point layer was created and placed along this intersect and then a line was drawn between the points with the *Point to Line* tool. 34

Figure 2.24. Inputs for the DSAS software to calculate statistics on the rate of change. The DSAS software requires two inputs: a baseline and multiple historic shorelines. The left shows the parameters you need to fill out for the baseline input and the right shows the shoreline parameters. The middle is an aerial view of the shorelines (green) and the baseline (purple) in ArcMap before the software has been run. 35

Figure 2.25. Model for extracting the volumetric change between the UAV surveys used for each site. To compare the point clouds into the same matrix, the August and December surveys were cloned using the *clone* tool in CloudCompare and each were clipped around an area with consistency throughout all surveys such as a road or building. The *Finely registers already (roughly) aligned entities (cloud or meshes)* tool was used with the August and December clipped layers onto the February layer. A transformation matrix is produced which was then copied and written into the *apply transformation* tool for the original August and December survey layers. 36

Figure 2.26. Surveys from side view of February and August layering one on top of the other instead of at the same elevation. The imagery shows two models before they are aligned properly, hence all the steps in figure 27. Once aligned the volumetric differences can be calculated. 37

Figure 2.27. The *Display XY data* tool is used to return the file to a point layer where a 'point to raster' geoprocessing tool is then used. The symbology is then modified to make analysis between the surveys more transparent for the final output. 37

Figure 3.1. A summary of all the dynamics occurring along each coastline. Each vertical line represents a transect which are spaced 20 m apart on the survey site. A scale bay shows the distance the transect lines cover at each shoreline. Colac Bay is showing more transects in a smaller area than Porpoise Bay because of the profile of the shoreline. From left to right shows transects 1 to the end of the shoreline surveyed. Each transect was placed into a matrix based on what level of accretion and erosion it showed. If both these patterns are low, then the shoreline is stable resulting in a yellow transect line. If both are high, it is classed as unstable resulting in a black transect line. Brown shows a dominant erosion pattern and blue shows a dominant accretion pattern. The colours in between show a mix of dynamics. 40

Figure 3.2. A summary of the main areas of interest where predictions are shown at each site. Monkey Island and Fortrose have the sea on the left-hand side of the shoreline and Colac Bay and Porpoise Bay have the sea on the right-hand side of the shoreline. Monkey Island showed little change between the current shoreline and the predicted shoreline in 20 years which is illustrated in the top left of the figure. This was the same as the Colac Bay predictions apart from between transects 65 – 75 where the automated prediction only showed an average of 5 m of retreat whereas the manual prediction estimates an average of 15 m of retreat shown in the upper right image. Transects 7 – 10 at Fortrose are predicted to retreat about 7 m on average shown on the lower left-hand corner of the figure. The manual prediction estimates the shoreline between 18 – 27 at Fortrose will retreat more than an average of 10 m in 20 years shown on the left middle picture of the figure. Porpoise Bay shoreline dominated by the DSAS software predicting accretion shown in the bottom right-hand images. 41

Figure 3.3. Historic shorelines at Monkey Island, derived from historic satellite imagery. The key shows the year the shorelines were extracted from. At Monkey Island there is a lot of overlap between the shorelines showing in some areas there has been minimal change occurring. The earliest year is 1946 shown in the dark blue. The corresponding years go to light blue, green, yellow, light brown and dark brown. Between transect 22 and 28 there is a pattern of erosion through the years shown by the brown being the most shoreward shoreline and then dark blue being the furthest seaward. 44

Figure 3.4. Historic Shorelines at Colac Bay. The earliest year is 1952 shown in the dark blue. The corresponding years go to light blue, green, yellow, light brown and dark brown. The coastline surveyed was 2500 m long with no significant change occurring over most of it. The following figures (34 and 35) are close ups of the boxed areas shown in this figure where change did occur along this coastline. 45

Figure 3.5. Historic shorelines at Colac Bay close up 1. This close up shows where the coastal road was closed due to continuous erosion after the 2014 satellite image was captured. You can see the significant erosion since then by the 2021 survey year being more shoreward compared to previous years. 46

Figure 3.6. Historic shorelines at Colac Bay close up 2. This figure shows just past the end of the road where the coastline goes into a natural dune system that has no engineered or hard protection. The blue (1963), green (1985) and bits of dark brown (2021) patches further back from the main shoreline show sparse vegetation throughout the dunes. 46

Figure 3.7. Historic shorelines at Fortrose, derived from satellite imagery. Between transects 4 – 16 and 18 – 28 there are distinct patterns of erosion especially from 1948 (dark blue) to 1962 (light blue). The shoreline begins to stabilise in recent years shown by the overlapping of the brown, and light brown shorelines. 34 out of the 49 transects have a net change of over 10 m of erosion. The maximum net change occurs on transect 4 with a result of 35.73 m of erosion. 47

Figure 3.8. Historic shorelines at Porpoise Bay. The earliest year is 1948 shown in the dark blue and the corresponding years go to light blue, green, yellow, light brown and dark brown. Over the whole shoreline, the net total change between 1948 and 2020 from all the transects was accretion of 4283.4 m. Since 1978 the net change was only 44.1 m of accretion. Between 2013 and 2020 there has been over 10 m of erosion occurring between transects 87 to 95 with transect 91 showing a rate of erosion averaging at ~2.63 m. per year 49

Figure 3.9. Coastal dynamics at Monkey Island, shown via transect lines 20 m apart. There are four main dynamics shown throughout the coastline which are eroding, accreting, stable and unstable. Erosion patterns at varying levels have occurred between transect 1 – 8, 13 – 15 and 22 - 32 with some of these areas not showing any record of accretion. Transects 2, 5, 8, 9, 11, 16 – 18 had positive net change. Areas around transect 8 – 11 and 17 – 19 are classed as stable as the change throughout the years and the overall net change were insignificant. The yellow shows a stable dynamic where movement of the shoreline throughout the years has been minimal. There is no blue transects which show a dominant accreting pattern, but a few are brown which shows a dominating eroding pattern. 51
Figure 3.10. Coastal dynamics at Colac Bay, shown via transect lines 20 m apart. There are four main dynamics shown throughout the coastline which are eroding, accreting, stable and unstable. For most of the coastline at Colac Bay, a stable dynamic is shown with the yellow transect lines. Blue shows a dominant accreting pattern which is not shown at this site and brown shows a dominating eroding pattern which is shown between transects 65 - 75. The grey and tan colours at the north-eastern end show transects 109 - 119 where a small flux between erosion and accretion is illustrated..... 52
Figure 3.11. Coastal dynamics at Colac Bay, shown via transect lines 20 m apart. There are four main dynamics shown throughout the coastline which are eroding, accreting, stable and unstable. Brown shows a dominating eroding pattern which is shown between transects 65 - 75. Transect 67 shows extreme erosion between the 2014 and 2021 shorelines and the dynamic is expressed as such. 53
Figure 3.12. Coastal dynamics at Colac Bay, shown via transect lines 20 m apart. There are four main dynamics shown throughout the coastline which are eroding, accreting, stable and unstable. A matrix was created to measure the patterns shown on the transects that illustrated multiple dynamics over the years. The yellow shows a stable dynamic where movement of shoreline throughout the years has been minimal. The green on transect 119 shows an unstable dynamic with more of an accreting pattern being dominant. The grey transect lines shown in this figure show slight erosion and accretion and the tan shows a slight erosion pattern. 53
Figure 3.13. Coastal dynamics at Fortrose, shown via transect lines 20 m apart. The yellow shows a stable dynamic where movement of shoreline throughout the years has been minimal which is shown in the northern part of the survey area. The opposite of this is black where major erosion and accretion is shown throughout the shoreline on the same transect line. There is a dominant erosion pattern shown by the dark brown transect lines along the site. Some transects show little erosion and are tan coloured (e.g., 15 - 17) whereas others show strong blue / green illustrating they are patterns of accretion. 54
Figure 3.14. Coastal dynamics at Porpoise Bay, shown via transect lines 20 m apart. The black shows where major erosion and accretion is shown throughout the shoreline on the same transect line. Blue shows a dominant accreting pattern. This shoreline shows varying degrees of instability. The bluer transects around transect 40 are in front of the houses that encroach onto the beachfront while the unstable transects around transect 90 and 115 boarders along sheep paddocks. Even though there are major cycles of erosion and accretion, net change has remained quite small after 1978. 55
Figure 3.15. Shoreline prediction in 20 years at Monkey Island derived from automated predictions with the DSAS software and manual predictions. The blue line is the DSAS shoreline prediction with an uncertainty margin spanning 20 m either side of the shoreline. The DSAS software discarded transect 25

because it could not predict a pattern along that transect. The manual shoreline prediction has gaps between transect 4 – 6, 33 – 35, 38 – 42 and 45 – 47 because the values extracted show no clear patterns that I could manually predict. The current shoreline in 2021 is below the prediction layers in this map so when you cannot see it, the predictions show no change in the position of the shoreline. .. 57

Figure 3.16. Shoreline prediction in 20 years at Colac Bay derived from automated predictions with the DSAS software and manual predictions. The blue line is the DSAS shoreline prediction with an uncertainty margin spanning 20 m either side of the shoreline. Both manual and automated predictions are mostly the same as the 2021 shoreline except between transects 65 – 75 and 109 – 119 which are illustrated in figures 46 and 47. 58

Figure 3.17. Shoreline prediction in 20 years at Colac Bay close up 1 derived from automated predictions with the DSAS software and manual predictions. The blue line is the DSAS shoreline prediction with an uncertainty margin spanning 20 m either side of the shoreline. Both the manual and automated software shows further erosion of this area in the next 20 years shown by the dark brown and blue lines being shoreward of the 2021 shoreline (light brown). The manual prediction is further shoreward because it illustrates the pattern shown from the 2014 survey onwards where human intervention was stopped. 59

Figure 3.18. Shoreline prediction in 20 years at Colac Bay derived from automated predictions with the DSAS software and manual predictions. The manual prediction shows a similar shoreline to the 2021 shoreline and the automated shoreline (blue) shows accretion in some areas around transects 111, 113 - 114, 117 – 118, 121 and 125. The blue line is the DSAS shoreline prediction with an uncertainty margin spanning 20 m either side of the shoreline. The left hand of the close up shows the DSAS software predicted erosion on transects 107 and 108 where the manual prediction stayed the same as the 2021 shoreline. 59

Figure 3.19. Shoreline prediction in 20 years at Fortrose derived from automated predictions (blue) with the DSAS software and manual predictions. The current shoreline in 2021 is below the prediction layers in this map so when you cannot see it, the predictions show no change in the position of the shoreline. The blue line is the DSAS shoreline prediction with an uncertainty margin spanning 20 m either side of the shoreline. The DSAS software predicts more erosion than the manual prediction between transects 2-3, 5, 6 and 33-35. Between transects 7 – 10, the manual and DSAS software predicted the shoreline to have eroded around 7 metres in the next 20 years. 60

Figure 3.20. Shoreline prediction in 20 years at Porpoise Bay derived from automated and manual predictions. The current shoreline in 2021 is below the prediction layers in this map so when you cannot see it, the predictions show no change in the position of the shoreline. The DSAS software predicted large areas will accrete significantly in 20 years. Between transects 38 and 45, the manual prediction based this shoreline off the fact that the accretion occuring was a human intervention and that although it will not continue along this pattern, it is likely it will continue to be maintained at the current shoreline. 62

Figure 3.21. Relative height between the February and August point cloud survey at Monkey Island. There is 235.759 m^3 of added volume and 94.989 m^3 of removed volume. The coastline itself shows

small hotspots of erosion and accretion both up to 1.5 m by the blue and dark brown patches shown in the middle and at the top of the survey area. 63
Figure 3.22. Relative height between the August and December point cloud survey at Monkey Island. 731.101 m³ have been taken away where only 33.373 m³ had been added. There is a distinct line of erosion along the shoreline with up to 1.75 m of negative change between the surveys shown with the dark brown line. The seaward site of the survey area shows slight erosion and stability with the yellow and lighter brown colours. 64
Figure 3.23. Relative height between the February and December point cloud survey at Monkey Island. 17.745 m³ of volume was added throughout the year and 574.241 m³ was removed. The yellow brown across the whole survey shows there is little significant change of the volume. There are very small patches of erosion throughout the shoreline, the most significant being at the top of the survey area. Little accretion has occurred. 66
Figure 3.24. Relative height between the February and August point cloud survey at Colac Bay. 152. 859 m³ of volume was added which is over double the value of removed volume at 68.780 m³. there is a distinct line of removed volume along the south-eastern part of the survey shown by the darker brown areas. The blue added volume in the northern length of the survey area is overlaying the coastal road. 67
Figure 3.25. Relative height between the August and December point cloud survey at Colac Bay. 301.903 m³ of sediment is removed shown by the dominant brown along the southern length of the survey and only 17.233 m³ of volume was added. Throughout the middle of the survey area are rounded brown sections which show the removal of substrate encroaching on the eroding coastal road. 68
Figure 3.26. Relative height between the February and December point cloud survey at Colac Bay. 218.616 m³ of volume was removed and only 9.353 m³ was added. This shows that the dominant dynamic was erosion with dark brown patches shown throughout the bottom left of the survey area and minimal volume added with faint blue patches throughout the middle and right side of the survey area. 69
Figure 3.27. Relative height between the February and August point cloud survey at Fortrose. There is slight erosion along the estuary shown on the seaward side of the point cloud. Erosion is shown along the south-eastern end of the shoreline with the dark brown line spanning 30 m of the survey area. There are little patches of added volume in the of the survey site on the landward side of the brown line of removed volume. Erosion is the dominant dynamic between these surveys with 1766.031 cubic metres of substrate being removed and only 23.355 added 70
Figure 3.28. Relative height between the August and December point cloud survey at Fortrose. Major accretion is shown along the sand on the seaward side of the shoreline. This illustrates the change in volume in an estuary environment throughout the year. Accretion is the dominant dynamic because 2489.657 m³ of volume was added and 84.821 m³ was removed from the survey site. There is a dark brown point of removed volume which aligns with a point of accretion in the February to August point cloud. 71
Figure 3.29. Relative height between the February and December point cloud survey at Fortrose. The overall volume change was 1105.011 m³ of added volume and 214.123 m³ removed. The accretion is

from the sand at the base of the shoreline. The shoreline itself shows little change apart from the removed volume at the south-eastern end of the survey site shown by the brown line. 72
Figure 3.30. Relative height between the February and August point cloud survey at Porpoise Bay. This map shows major erosion in the middle of the survey area both along the shoreline and the sand on the beach. 1870.292 m^3 of volume has been removed from the survey area and 271.400 m^3 has been added. 73
Figure 3.31. Relative height between the August and December point cloud survey at Porpoise. 1108.910 m^3 of sediment is removed shown by the dominant brown along the seaward side of the survey and 881.907 m^3 of volume was added. Added volume is shown throughout the sand on the beach and the vegetation behind the shoreline. 74
Figure 3.32. Relative height between the February and December point cloud survey at Porpoise Bay. Overall, there was 1984.994 m^3 of volume removed from the survey area. There are little patches of added volume at the north and south ends of the survey area which adds up to 136.234 m^3. 75
Figure 4.1. Images of the doming issue of the May. This was a result of inadequate camera calibration or lack of information for the Agisoft Metashape software to process correctly. The blue shapes are the 2D images taken from the drone and the sparce image is the point cloud created with structure from motion photogrammetry explained in the introduction. Manual tie points were added to fix the doming issues but only made it worse as shown in the bottom screenshots of this figure where the point cloud became more curved. 94

Tables

Table 3.1 Removed and added volume (measured in m^3) values between each survey and site. The added and removed volume between each survey is standardised to 100m^2 to simplify comparisons between each site. The 'Figure #' states the figure correspondent with the row the data is from. 42
Table 3.2 Monkey Island removed and added volume (measured in m^3) values between each survey. The added and removed volume between each survey is standardised to 100m^2 to simplify comparisons. Matching cells measure the certainty of the values given with a confidence percentage derived from the CloudCompare software. The 'Figure #' states the figure correspondent with the row. The final row shows the change between the first and last surveys to illustrate the sum of the change in volume. 65
Table 3.3 Colac Bay removed and added volume (measured in m^3) values between each survey. The added and removed volume between each survey is standardised to 100m^2 to simplify comparisons. Matching cells measure the certainty of the values given with a confidence percentage derived from the CloudCompare software. The 'Figure #' states the figure correspondent with the row. The final row shows the change between the first and last surveys to illustrate the sum of the change in volume. 69
Table 3.4 Fortrose removed and added volume (measured in m^3) values between each survey. The added and removed volume between each survey is standardised to 100m^2 to simplify comparisons. Matching cells measure the certainty of the values given with a confidence percentage derived from the CloudCompare software. The 'Figure #' states the figure correspondent with the row. The final row shows the change between the first and last surveys to illustrate the sum of the change in volume. 72
Table 3.5 Porpoise Bay removed and added volume (measured in m^3) values between each survey. The added and removed volume between each survey is standardised to 100m^2 to simplify comparisons. Matching cells measure the certainty of the values given with a confidence percentage derived from the CloudCompare software. The 'Figure #' states the figure correspondent with the row. The final row shows the change between the first and last surveys to illustrate the sum of the change in volume. 75

Attestation of Authorship

"I hereby declare that this submission is my own work and that, to the best of my knowledge and belief, it contains no material previously published or written by another person (except where explicitly defined in the acknowledgements), nor material which to a substantial extent has been submitted for the award of any other degree or diploma of a university or other institution of higher learning."

Date: 21 June 2022

Acknowledgements

Special thanks to my supervisors Bradley Case, Graham Hinchliffe, and Hannah Buckley, who have put in the time to help me develop this research, which I am very proud of, as well as advancing my academic skills to get me to this point.

I am also grateful for the New Zealand's Changing Coastline project group from the National Science Challenge, particular Murray Ford for sharing with me historic satellite imagery for my research. It would have been an expensive exercise without it!

Thank you to Andrew Wilson for assisting with my first drone surveys and sharing with me historic satellite imagery from Environment Southland for my research.

I would like to express my deepest appreciation to my friends and to my mum, Jo, who has been my biggest support throughout this whole journey. Without whom the road here would have been a whole lot rockier.

Appendix

Each sites magnitude of change between corresponding years at each transect line. The net change, total accretion and total erosion added up for each transect line are on the right three columns……109

Chapter 1 Introduction

1.1 The coastal system

The coast is a naturally active margin that forms an important barrier system subjected to the forces of both the terrestrial and marine environment. Climate change, rising sea levels and anthropogenic influences are impeding the natural fluctuations of the coast (Nicholls & Cazenave, 2010; Romaine et al., 2021; Rouse et al., 2017). Coastal erosion has become an environmental and economic issue as numerous communities and cities around the world are located along the 'coastal zone'. There are many dynamics and influences that make the coast a unique environment. The featured coasts you see at the seaside are shaped by the supply and removal of sediment from the land and ocean (Hesp, 1989). Processes that supply sediment to the coast include erosion of cliffs, wave currents and both aeolian and fluvial transport (Fig. 1.1) (Addo et al., 2008; Walling, 2006). Fluvial transport is estimated to contribute 95% of sediment supply to the coasts (Syvitski, 2003; Walling, 2006). Energy of currents, waves and wind have great influence over the movement of vast volumes of sediment along a shoreline (Addo, 2018; Ashton et al., 2001; Seibold & Berger, 2017). Storms can take large volumes of sediment offshore and are the main cause for sudden erosion events around the world (Walling, 2006). Movement of sediment between the marine and terrestrial environment is a unique characteristic of the coast so it hosts unique vegetation that adapts to this.

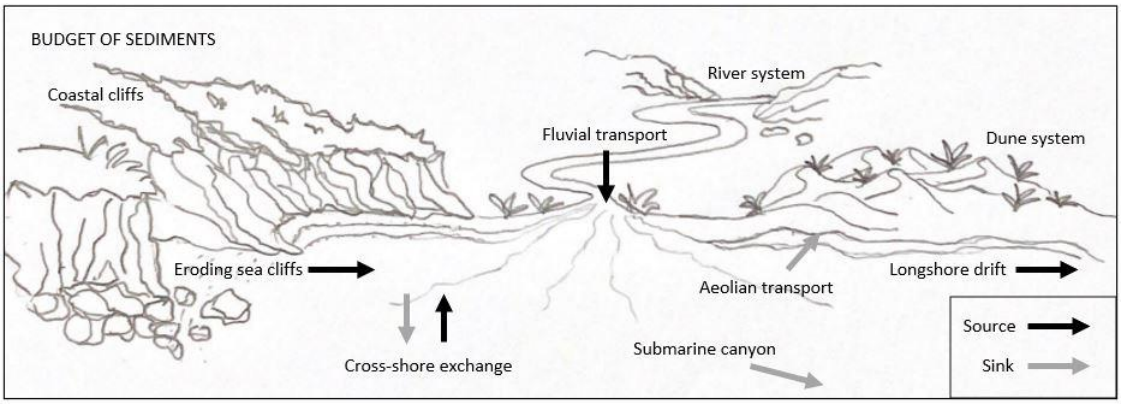

Figure 1.1. Processes that supply and remove sediment from the coast. There are many sources (where sediment joins the coastal system) and sinks (where it leaves the coastal system) of sediment showing that the coast is a very active environment with many different influences affecting it. These include fluvial (from rivers and streams) and aeolian (wind) transport, eroding cliffs, longshore drift, and cross-shore exchange. Made by Cassandra Newman.

Vegetation fluctuates with the movement of dunes and plays an important part in how active or stable a dune system is (Martínez et al., 2001). These dune environments are critical in the natural erosion and accretion cycles of the coast but are easily damaged by anthropogenic influences such as removal or manipulation for land use change or direct damage from vehicles and people (Burger, 1994; Nordstrom et al., 2000; Nordstrom & Mauriello, 2001; Taylor et al., 1997; Thompson & Schlacher, 2008). It is important to note that dunes and coastal systems have great resilience to undergo changes caused by natural stresses and fluctuations between patterns such as erosion and accretion. Figure 1.2 shows that seasonal changes between summer and winter can cause significant changes in coastal morphology (Thanh et al., 2018). This illustrates that there are many long- and short-term cycles related to the coastal environment. Due to changing climatic factors or coastal anthropogenic manipulation, 70% of the sandy beaches around the world are retreating with minimal accretion because of their stress threshold being exceeded (Bird, 2005). With our growing population, these dynamics and influences that shape our coastlines are being manipulated and distorted causing long-term shoreline retreat.

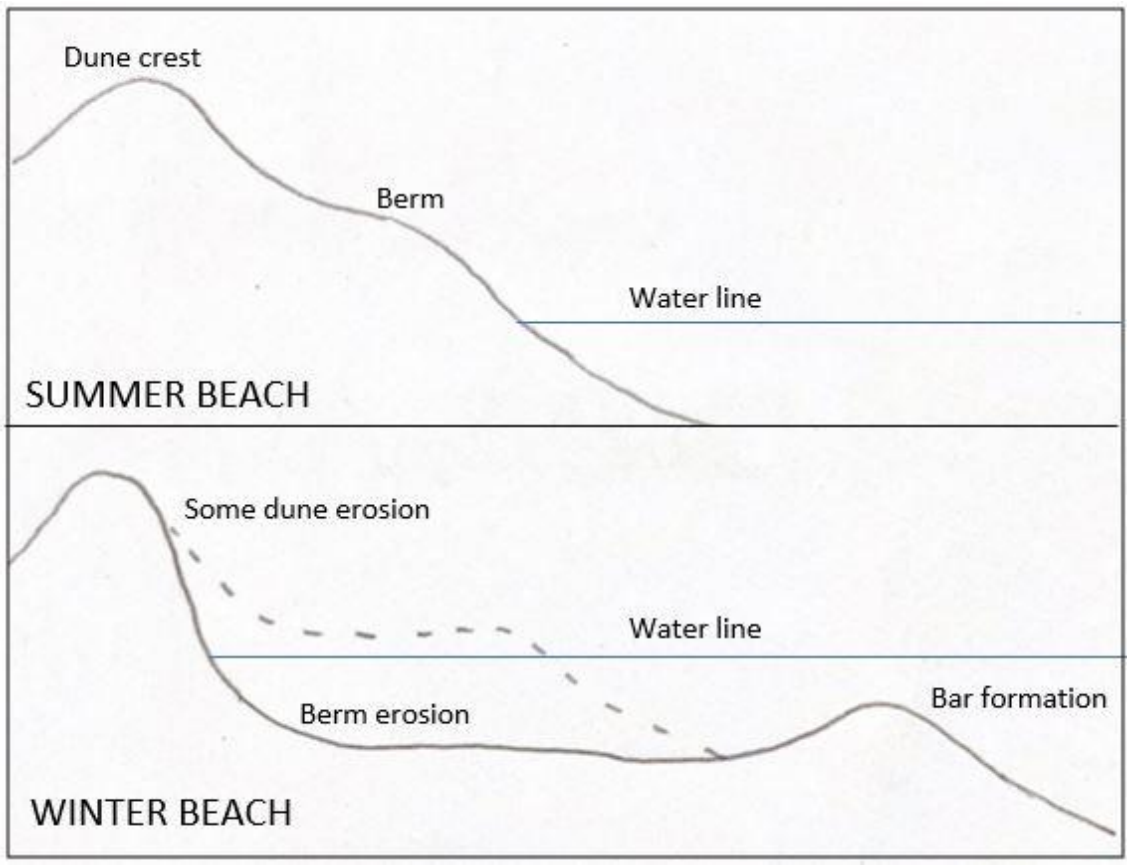

Figure 1.2. The changing formation of sediment at sandy beaches throughout the year. Sand builds up over the summer months on the shore (left-hand side of figure) then is pulled out by currents and wave action to create a bar offshore in winter months. This illustrates one of the many cycles the coastal system experiences at different temporal rates. Made by Cassandra Newman.

1.2 Anthropogenic impacts and climate change

Our species dominates the worlds coastlines with 10% of the population estimated to inhabit in the margin up to 10 metres above sea level and 60% of the world's population inhabiting the 'coastal zone' (Boye et al., 2018; Church et al., 2006; Domingues et al., 2018; McGranahan et al., 2007) . Shores have been eroded and degraded because of growth of coastal urbanisation, tourism, and industrialisation due to their attractiveness both visually and for commercial accessibility (Van Der Meulen & Salman, 1996). The coast is exploited and threatened yet hosts essential ecosystems as the margin between the terrestrial and marine environments (Dayton et al., 2005; Pascucci et al., 2018). One of the main risks associated with climate change in New Zealand is the impacts to coastal communities and ecosystems (Rouse et al., 2017). Sea level rise, more extreme storms, storm-induced erosion, and long-term shoreline retreat are some of the types of coastal hazards exacerbated by climate change (Nicholls & Cazenave, 2010; Romaine et al., 2021; Rouse et al., 2017). A study at Faro

beach, Southern Portugal, showed that even with extreme risks from coastal hazards, residents accept that there is a high probability of personal damages but the benefits to mental health and livelihoods of living close to the coast outweigh that (Costas et al., 2015; Domingues et al., 2018). Along coastlines where human influence is not an immediate complication, erosion around isolated coastlines has also shown signs of manipulated acceleration over the past few decades (Jeong, 2019). Human causes go inland where damming of rivers decreases sediment supply, or on the beaches themselves where mining sand and gravel in the surf zone depletes littoral coasts of their sand supply, causing more erosion (Anthony, 2014; Jenks, 2018; Toffi, 2008). The Manapouri Dam in Southland, New Zealand became fully operational in 1972 after taking eight years to build. This dam has reduced the flow of the Waiau river and hindered sediment supply to Te Waewae Bay (Beentjes, 2010). Rivers supply a vast majority of coastlines with sediment and dams reduce water volume and energy to transport sediment downstream, starving the coast of this fluvial supply (Addo, 2018). With lower sediment supply caused by anthropogenic infrastructure, the coast undergoes continuous erosion due to the beach profile not being sustained (Short, 1999; Walling, 2006). Increased sea level rise and coastal erosion also leads to an infiltration of the marine on the terrestrial environment which means that low lying aquifers, rivers and freshwater stores will be victim to salination (Taillie et al., 2019). Ecosystems are also vulnerable to pH and temperature changes caused by invasive rising seas and degradation of our coastlines (Nicholls & Cazenave, 2010; Pennings et al., 2005). The unpredictable patterns in consequence of oceano-climatic processes further complicate the management and restoration of these coastal margins where changes are becoming more extreme and less predictable (Addo, 2018; Muthusankar et al., 2018). Coastal planning is highly affected by these extra risks and more sustainable shoreline management is crucial. However, there are financial and logistical constraints associated with funding, stakeholders, and the physical restoration of coastlines. We need to adapt to this socio-ecological system where resource management is becoming a driver for action.

1.2.1 Coastal landfills and debris

The coast is an active system undergoing constant change, despite this, we built, developed, and laid our waste along its shores. In parts of New Zealand, debris from

historic landfills or other anthropogenic structures that were established near our coastlines are uncovering because of shoreline retreat or sudden erosion events. Landfills are deposits of waste materials buried under soils or sand. The waste or debris can be anything from household rubbish, toxic waste, old building material or other waste produced as a by-product from our path to convenience. Studies have brought to light the challenges that managing coastal landfills and leftover structures will bring as sea levels rise and coastlines retreat (Beaven et al., 2020; Sayers et al., 2017). Landfills can cause harm to human and environmental health when chemicals leach from liquid or solid waste (Beaven et al., 2020; Njue et al., 2012). The coast experiences extreme weathering so the sense of urgency to manage this waste before it becomes an issue should be a priority.

1.3 Coastal monitoring

New Zealand has about 15,000 km of coastline which has always been a subject of interest due to the role it plays in our economy and personal lives (Bell & Gibb, 1996). In New Zealand, coastal monitoring is a requirement under the Resource Management Act for each region. New Zealand has a variety of coastal environments and regions have different strategies specific to these environments. Some of these strategies include assessing ecological health, species presence and changes over time, creating baselines on water quality, fine scale monitoring and creating models to predict future patterns (Addo, 2018; Pascucci et al., 2018; Tiernan, 2012). The global strategies for monitoring the coast stretch even further which reiterates how diverse and complicated the coastal system is. With the expanded use of Geographic information systems (GIS) for spatial and temporal analysis, software has been created to automate future shoreline predictions and assist in coastal monitoring and management. Digital Shoreline Analysis System (DSAS) is a software used for exactly that. DSAS has been an important tool for the U.S. Geological Survey's Coastal Change Hazards Project as it can analyse large volumes of data at an accurate and reliable rate (Baig et al., 2020; Sebat & Salloum, 2018). The DSAS software has been used for shoreline research globally over large areas of the coast to monitor patterns for prioritising areas that are retreating for shoreline management (Baig et al., 2020; Baral et al., 2018; Kale et al., 2019; Sebat & Salloum, 2018; Yan et al., 2020). This software is

just one example of some of the technologies that can be utilised for more superior coastal management around the world.

1.4 Applications of Geographic Information Systems (GIS)

Geographic information systems (GIS) have become a globally used resource for mapping and analysing geographic data. In the coastal zone, GIS is used to measure and map spatial patterns that are not immediately detectable to us. GIS have been used heavily to create risk assessment models in association with coastal hazards and has assisted researchers with coastal planning and restoration (Fraser et al., 2017; Ma et al., 2011; Narra et al., 2019). Models created are based on the social aspect of the locations of risk, resulting in urban or built-up areas to be deemed at the highest risk of erosion in coastal areas (Narra et al., 2019). The social aspect of planning for risks and hazards is essential in our socio-ecological system and GIS helps with large scale and regional coastal studies which greatly informs government decisions and planning (Casella et al., 2016; Fraser et al., 2017; Ruiz-Beltran et al., 2019). Many models that analyse the risk from coastal hazards do so using past trends of the coastline and how coastal characteristics interact with our infrastructure (Fraser et al., 2017; Narra et al., 2019). Past trends of the coastline are extracted from overlapping historic satellite imagery as this is easily accessible and reasonably accurate to provide rough estimates of what the shoreline will look like in the future such as in the DSAS software (Romine et al., 2009, 2013). This monitoring technique has been coupled with storm events to measure the extent of damage or general change that storms have on the shoreline (Casella et al., 2016). Satellite aerial imagery is useful for regional or large-scale image extraction but some analysis benefits greatly from local scale imagery, where atmospheric conditions, cost and observation times are not limiting factors (Berni et al., 2009; Watts et al., 2012; Wulder et al., 2004). Unmanned Aerial Vehicles or UAVs are a revolutionary piece of GIS equipment used for capturing aerial imagery with the above benefits.

1.4.1 Applications of Unmanned Aerial Vehicles (UAV)

A multi rotor winged or fixed wing miniature aircraft fitted with a camera that can capture a range of features and observations of the ground has expanded science and commercial uses of aerial imagery over recent years with their utilisation only

expanding. There has been an acceleration in using unmanned aerial vehicles (UAV) for scientific research, monitoring and imagery collection (Anderson & Gaston, 2013; Colomina & Molina, 2014; Everaerts, 2008; Floreano & Wood, 2015). UAV Imagery provides similar results to that of more traditional image extraction such as from satellite imagery but there are benefits and trade-offs with both applications. The time it takes to collect imagery from a UAV is reduced by 80% resulting in more control of the time the imagery is gathered at (James & Robson, 2012). UAV data collecting is dictated by the weather as not all UAVs are waterproof and cannot be flown in the rain or wind speeds greater than 38kph whereas satellite imagery quality is dictated by atmospheric conditions where clouds can be present in the imagery. Because of the lithium battery in a UAV, there is also a temperature threshold of -10 to 40° where the battery can underperform when temperatures get too close to the limits of the threshold. 3D imagery collected by a UAV gives a more approximate value in analysis which is beneficial when measuring slow, variable changes such as shoreline erosion and accretion over localized areas (Yu et al., 2020).

1.4.1.1 Satellite verses UAV imagery

Because of the extensive historic imagery archives, satellite imagery is better with measuring long-term shoreline patterns of erosion and accretion. Unlike satellite imagery, UAVs can capture 3D imagery with the right capturing and processing applications. This is because of the significant advancement in photogrammetry, particularly Structure from Motion (SfM). Structure from motion is the process of creating 3-dimentional models with 2-dimentional images (Cullen et al., 2018). The development of this technology has meant that it is more widely available because it does not require specific expertise to run. The UAV captures overlapping images at different angles and orientations and software processes these images into a single point cloud (3D model consisting of many points). Due to the complexity of coastal barrier systems, UAVs that capture high detail 3D imagery are becoming more frequently used to map the horizontal and vertical structure of specific coastal margins (Casella et al., 2016; Drummond et al., 2015; Ierodiaconou et al., 2016; Yu et al., 2020). UAVs are also utilised in profile surveys, detailed aerial mapping and 3D sampling. A 3D limit equilibrium was created using GIS technologies to measure slope stability (Yu et al., 2020). This research goes more into the stress distribution, outcomes and sliding

directions of landslides but shows the practicality and versatility of 3D imagery captured by UAVs. Storm driven changes have been mapped using UAVs in southern Australia in 2014 showing dramatic results of dune movement and erosion before and after an event (Ierodiaconou et al., 2016). The use of digital elevation models and 3D imagery to capture seasonal change in shorelines is a novel approach to monitoring these systems for management and restoration options. Satellite and UAV imagery both have values and limiting factors and this research will evaluate their applications for monitoring the dynamics of the coast.

1.5 Research aims and objectives

The overall aim of this research was to investigate the ability of a generalised GIS methodology to quantify coastal dynamics at different locations with anthropogenic debris. The impact of anthropogenic debris along the coast needs to be addressed. Landfills, roads, urban areas, cemeteries, and debris along New Zealand's coastlines are at risk of being consumed by the threat of rising seas, more extreme weather, and other climatic events causing erosion. The Southland region of New Zealand at the bottom of the South Island is known for its diverse coastlines and biodiversity. The shores host endemic penguin species including the Fiordland crested penguin and the yellow-eyed penguin, sea lions and seals as well as the southern populations of Hectors dolphin (Hamner et al., 2017; Presswell & Bennett, 2021; Seddon et al., 2013). Southland also has some of New Zealand's most polluted estuaries (Lee & Partridge, 1983) which are essentially the kidneys of our rivers before water goes into the sea. Coastal erosion has become a problem along the southern coast where infrastructure and debris along the shore are being consumed by storms and the ocean. Adaptive management is the key for preventing the risk to wildlife and the natural environment so understanding the dynamics of the coast is important. Within this Southland coastal context, I will specifically address the following questions as my objectives:

1. What GIS processes are applicable to characterising historic shorelines in order to understand past dynamics occurring at each site?
2. Can the past trends characterised in (1) be used to predict where future shorelines will be?

3. Does characterising the seasonal volumetric changes occurring along the coastline provide additional insight into the temporal and spatial patterns of shoreline change?

To address these questions, this research will investigate four sites along the southern coast where anthropogenic debris has or will become an issue for local government management. The sites investigated are Monkey Island, Colac Bay, Fortrose, and Porpoise Bay (Further detail on sites in Chapter 2). Three out of the four sites border marine mammal sanctuaries so as per the Department of Conservation regulations, I ensured there were no marine mammals within 150 m of UAV flights. GIS imagery captured by satellite and UAV will predict the rate of erosion to aid in management decisions to help prepare for rising seas and changing climates at sites with anthropogenic debris.

1.6 Structure of thesis

After this introduction of the research and background of the study, the methodology of this thesis is described in Chapter 2. Field data were collected for the 3D UAV imagery and Satellite imagery were geoprocessed using model builder and manual editing. Chapter 3 presents the results from the analysis. Historic shorelines, coastal dynamics, prediction maps and volume maps illustrate how the research objectives were met. The results gathered in the study are discussed and compared to relevant literature in Chapter 4.

Chapter 2 Methodology

This chapter presents the four study areas and illustrates why each were selected for this research. A map shows the location of these areas in terms of New Zealand and the southern coast. The data used in the study, how they were acquired and what software was used to analyse them is explained. The methodology description is divided into workflows together with corresponding models. The workflows are divided into 'satellite analysis workflow' where the satellite imagery method is used to produce the historic shorelines, coastal dynamics and prediction maps presented in the results chapter. The final part of this chapter is the 'UAV analysis workflow' which explains the processing and analysing of the 3D UAV imagery to get the volume maps shown in the results chapter.

2.1 Study areas

Four sites along the southern coast of the South Island of New Zealand have been selected for this study because each have anthropogenic features susceptible to current or future erosion. All sites have unique factors that may affect the dynamics of the coastline to help contrast how a generalised method approach may work with specific coastlines. These sites are (from west to east) Monkey Island, Colac Bay, Fortrose, and Porpoise Bay (Fig. 2.1). Three out of the four sites border marine mammal sanctuaries. Colac Bay, the exception to this has a local Hector's dolphin community in the summertime which are the smallest and rarest dolphins in the world second only to its almost identical subspecies, the Maui dolphin (Baker et al., 2002). Consequences may be detrimental to species living around these coastlines if ongoing erosion unveils the anthropogenic debris at any site.

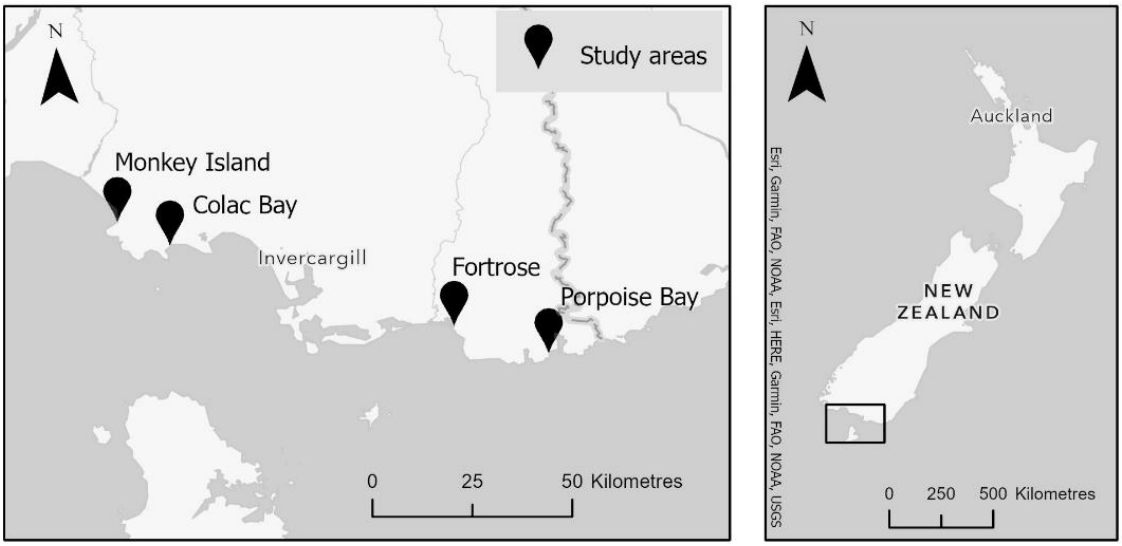

Figure 2.1. Study areas shown throughout the southern coast in Southland, New Zealand. The left map shows the study areas are Monkey Island, Colac Bay, Fortrose, and Porpoise Bay. The right map shows where the research took place in relation to New Zealand.

2.1.1 Monkey Island

The length of the coastline analysed in this research at Monkey Island is 1170 m (Fig. 2.2). Monkey Island is found on the eastern end of Te Waewae Bay on the south coast of the South Island, New Zealand. This site is chosen because of the concrete and layer of rubbish throughout the shoreline and the popular freedom camping area directly behind it which is vulnerable to future erosion (Fig. 2.3). The layer of rubbish at this site was distinctly positioned about 40 cm below the ground and transverses for about 200 m along the shoreline. The nature of this rubbish was mainly small plastics and from past knowledge of the consequences of small plastics in the marine environment, I knew this would be a significant area to add to my study. The geology layer describes the site as pebbly to bouldery gravel, sand, and minor peat underlying marine benches behind old sea cliffs dominated by gravel quartz (GNS Science Web Map Service). The 3D UAV imagery captures 15 x 167 m of the coastline at the southeast end of the survey area at 46°18'00.5"S 167°43'41.4"E.

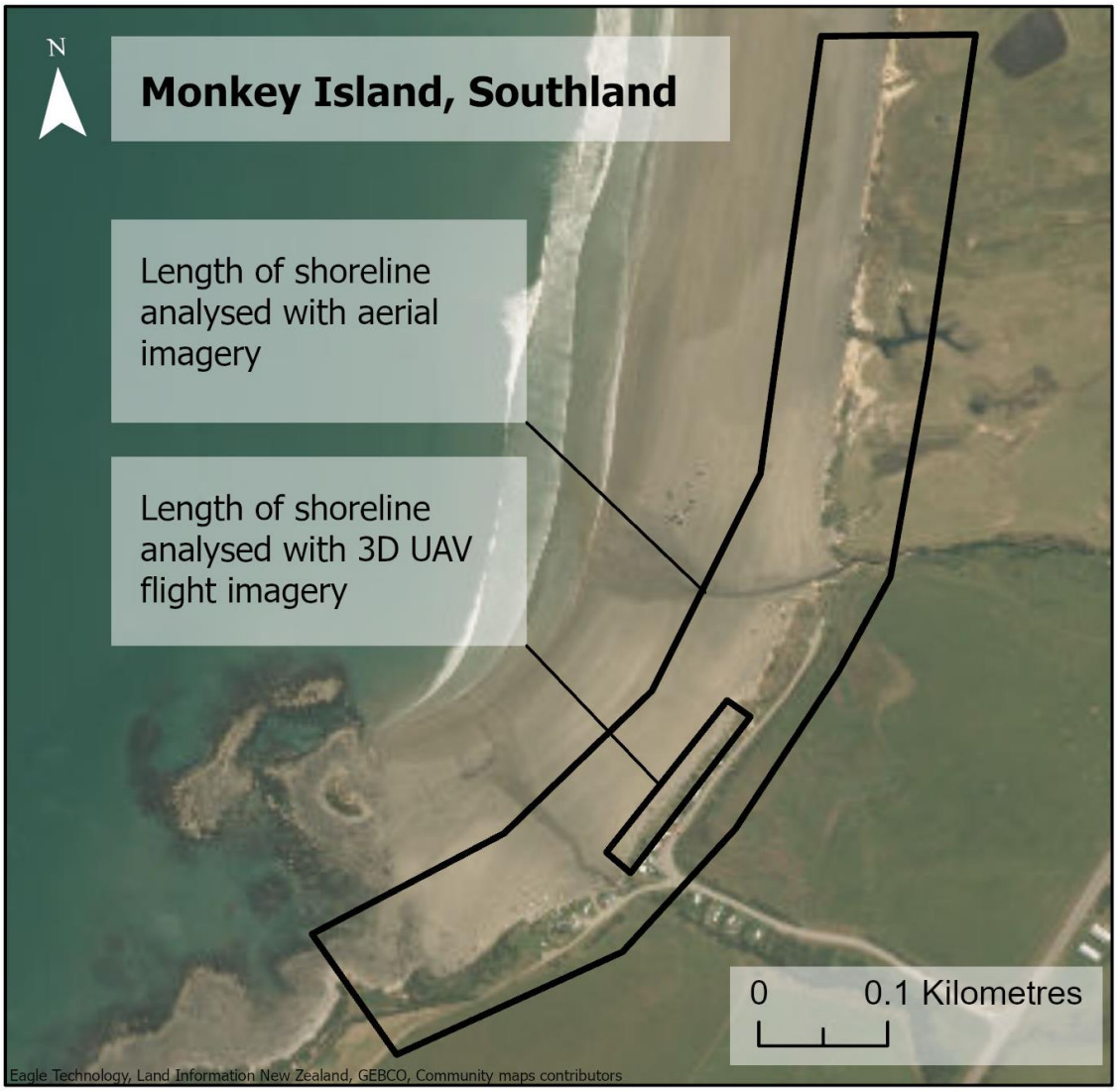

Figure 2.2. Monkey Island study area. Outlines show the shoreline being analysed with historic satellite imagery and the UAV flight area. Due to the nature of the shoreline, the width of the study area is dependent on the historic shorelines analysed.

Figure 2.3. The nature of the site at Monkey Island and the thin coastal margin before the metalled carpark. Along the study area there are pieces of discarded concrete and many pieces of rubbish in the face of the dune. The seaweed on the ground shows the water comes right up to the shoreline.

2.1.2 Colac Bay

Colac Bay is a southeast facing bay known for its consistent surf and local Hector's dolphin community in the summertime. The length of the coastline analysed is 2500 m (Fig. 2.4). The 3D UAV imagery captures 7 x 144 m of that coastline located at 46°21'37.3"S 167°53'36.5"E. The geology layer describes the surrounding location as stable longitudinal and parabolic sand dunes with peat in the hollows from the Holocene period (GNS Science Web Map Service). The shoreline is covered with pebbles where the analysis occurs (Fig. 2.5) but towards the northeast end of the beach it changes to sand dunes. This site is chosen because after decades of placing rock barriers along the beach, the coastal road could no longer be maintained from storm surge damage so was permanently closed in 2015. Where the road is closed, the shoreline is left to erode right in front of a historic landfill. Historic coastal protection has been going on at Colac Bay since the 1930s (Zammit et al., 2018).

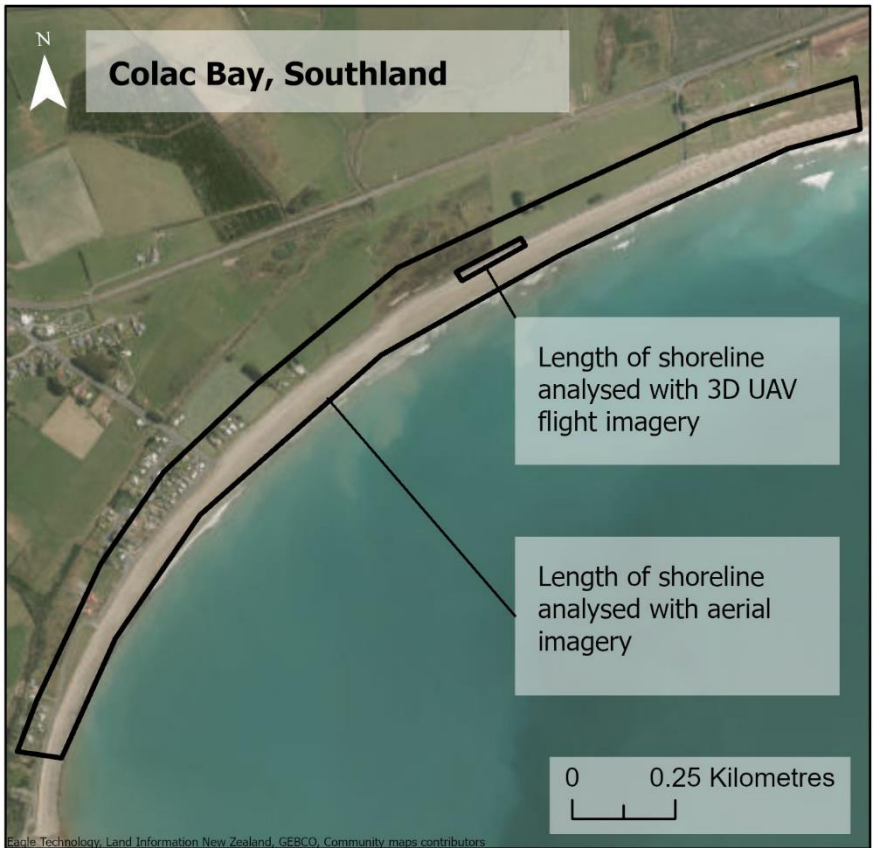

Figure 2.4. Colac Bay study area. Outlines show the shoreline being analysed with historic satellite imagery and where the UAV flight area is. Due to the nature of the shoreline, the width of the study area is dependent on the historic shorelines analysed.

Figure 2.5. Colac Bay as it is in 2021 looking south along where the coastal road was closed and where the 3D UAV flight captures imagery. Blocks in the bottom of the image show where vehicles no longer have access and the pebble substrate on the closed road shows how invasive the sea can be as well as the road being eaten away shown at the top of the image.

2.1.3 Fortrose

Fortrose is a small township bordering the eastern side of an estuary with the same name, at the mouth of the Mataura River. The length of the coastline analysed is 1150 m and the 3D UAV imagery captures 180 x 22 m of the coastline (Fig. 2.6). The location of the survey site is 46°34'40.5"S 168°48'04.2"E. Going down to the estuary from Boat Harbour Road (road next to UAV study site) (Fig. 2.6), the shoreline is covered with bricks, concrete and other old building materials used as riprap to build up an erosion barrier in the shoreline (Fig. 2.7). Fortrose was chosen for this research because erosion has been recorded for over a century along the township where early Computer-aided design (CAD) files show land designated with property lines which have completely eroded away into the estuary proving it to be an area of interest. The geology layer describes the site as peat in swamps and on actively growing peat mounds, with incursions of sand and silt which were formed in the Holocene period (GNS Science Web Map Service).

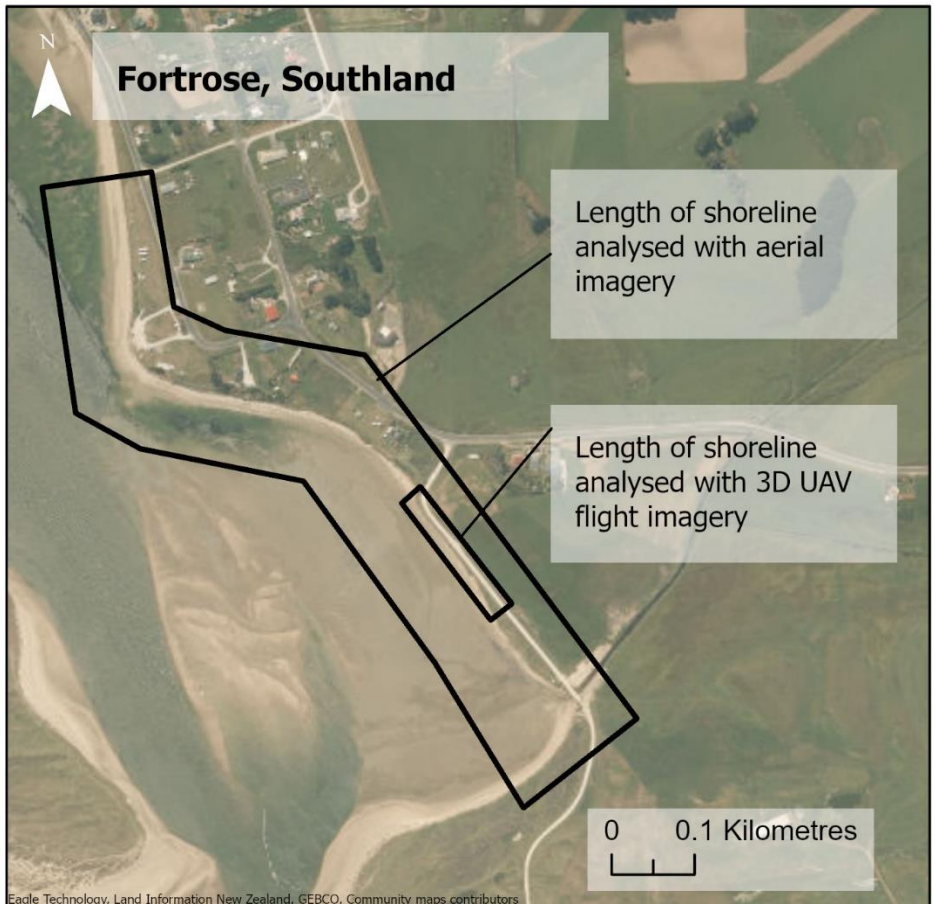

Figure 2.6. Fortrose study area. Outlines show the shoreline being analysed with historic satellite imagery and the area for the UAV flight plan. Due to the nature of the shoreline, the width of the study area is dependent on the historic shorelines analysed.

Figure 2.7. The nature of the site at Fortrose where the UAV flight plan captured imagery. A visualisation of the old building materials and bricks throughout the estuary edge.

2.1.4 Porpoise Bay

A small housing development is being built along the beach front where the substrate beneath the development is sand. Coastal housing developments are an anthropogenic feature that are at extreme risk if the coastline erodes making it an area of interest for this study. The length of the coastline analysed in this research at Porpoise Bay is 3000 m (Fig. 2.8). I have mapped an area of 15 x 196 m for the 3D UAV imagery further along the beach from these houses to not encroach on private property while still getting an understanding of the coastal dynamics occurring (Fig. 2.9). The location of the UAV survey site is at 46°39'02.3"S 169°06'15.9"E. The geology layer composes of sand and gravel; back-beach ridges and tidal platforms which originally formed in the Holocene period (GNS Science Web Map Service).

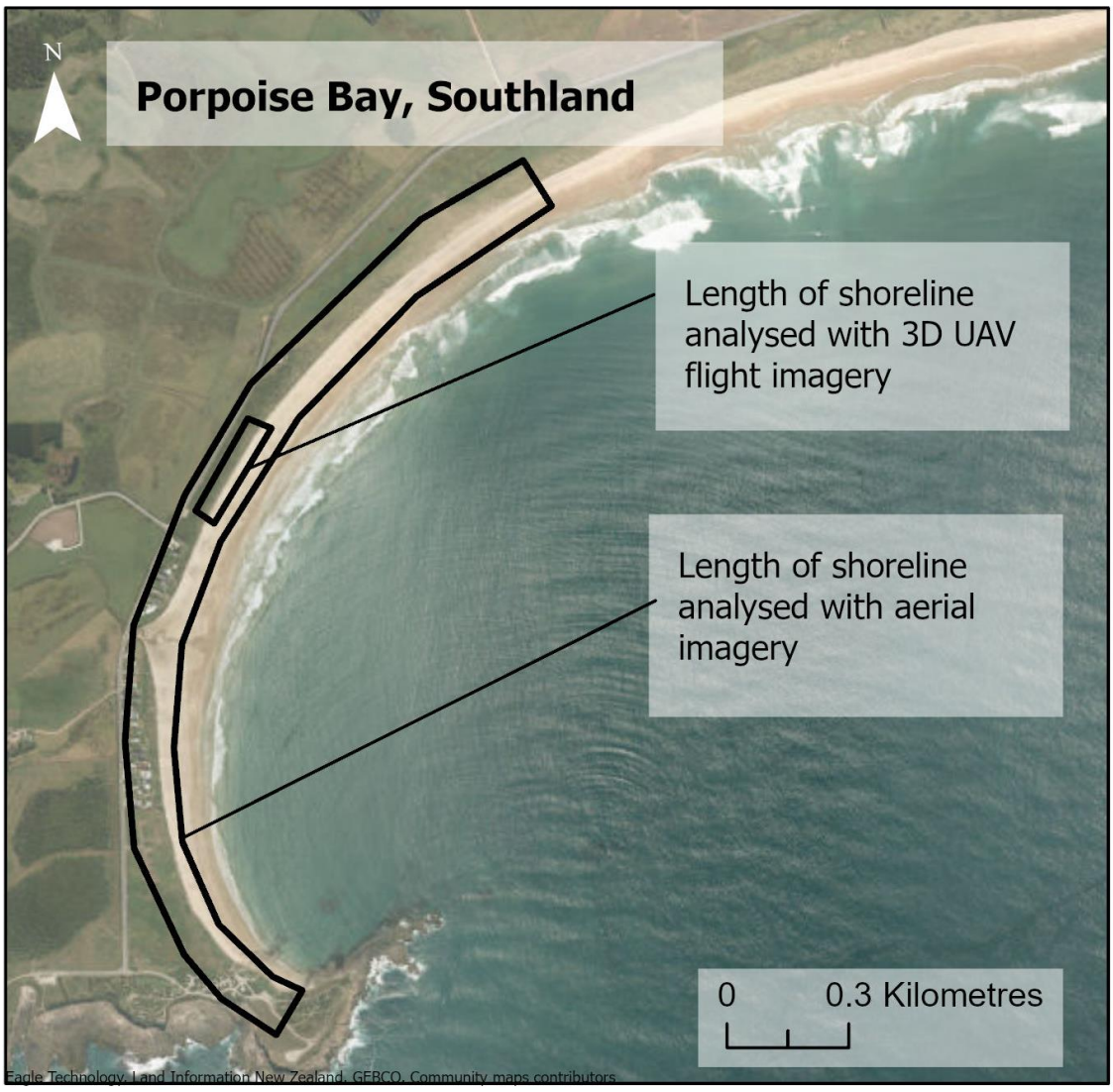

Figure 2.8. Porpoise Bay study area. Outlines show the shoreline being analysed with historic satellite imagery and the area for the UAV flight plan. Due to the nature of the shoreline, the width of the study area is dependent on the historic shorelines analysed

Figure 2.9. Shows the nature of the site where the 3D UAV imagery is captured with a visualisation of the frontal dune along Porpoise Bay.

2.2 Datasets and acquisitions

Satellite imagery used for this research was either collected from the internet, shared by organisations, or purchased. Field trips to Southland to collect UAV imagery at the four site locations were undertaken during February, May, August, and December 2021. The surveys were taken at this time because it was the end of every season except November due to Covid-19 lockdown pushing back the Spring data collection to December.

2.2.1 Satellite imagery

Free and open-source aerial imagery was taken from the LINZ and Retrolens websites, resulting in roughly one image from each decade at each site, 1946 onwards. The period between consecutive images varied depending on the availability of the imagery. Some layers were generously given to me by the New Zealand's Changing Coastline project group in the National Science Challenge or Environment Southland. One aerial image taken in 2021 of Monkey Island was purchased from Apollo Mapping. All layers were manually georeferenced on ArcGIS Pro (ArcGIS Pro 2.7.1, Esri, 2020). An

area of interest between one to three kilometres of coastline was used to encompass a sufficient portion of the shore for the satellite and 3D UAV image collection at each site location.

2.2.2 UAV imagery

A Mavic 2 Pro was used to capture the seasonal 3D UAV imagery. Pix4D (Pix4D, 2019) was used to create and programme a double grid flight plan for the UAV for each site (Fig. 2.10). The settings for each flight had 90% front and side overlap with each image to get a thorough coverage of the area for the model software. The angle of the camera was 45° to get the vertical surfaces. Each site had a different area based on the geometry of the coastline. Data was collected in February, May, August, and December 2021 on days with low wind and no rain. All surveys were flown at an altitude of 50 m. The August and December surveys were flown with an additional flight at 100 m to fix a doming issue that occurred in the May survey.

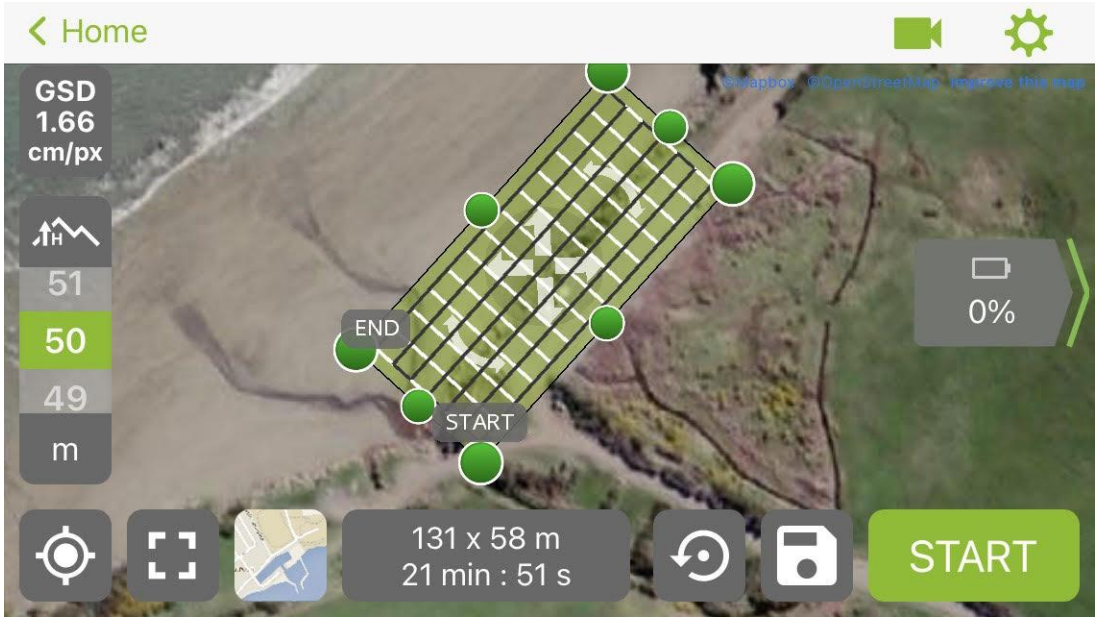

Figure 2.10. Screenshot of the flight plan on the Pix4D application on my phone. The plan was able to be duplicated for each time survey. The top lefthand corner shows the GSD which stands for 'Ground Sampling Distance' which measured how many centimetres were equal to one digital pixel. This was adjusted with the height of the flight which you can see on the left-hand side of the image. This flight is at 50 m above ground level. The same flight area for each site was done at 100 m above ground level to fix doming issue which occurred in the May survey. The bottom middle of the image shows the parameters of the flight plan which is 131 x 58 m. The time it will take for the flight to be completed is also shown in the box. This flight plan will take 21 minutes and 51 seconds. This is important to note because the battery in the drone can run for about 25 minutes before it needs to be replaced.

2.3 Software

Pix4D was the mobile application for creating and flying the 3D UAV flight plans (Pix4D, 2019, Version 4.5). This software was easy to use as I was able to duplicate flight patterns for consistency between the timeframes at each site. ArcGIS Pro (ArcGIS Pro 2.7.1, Esri, 2020) is a versatile software that was used for most of the analysis for the historic satellite imagery. ArcMap (ArcGIS 10.8.1, Esri, 2020) was used to host the Digital Shoreline Analysis System (DSAS 5.0 version, USGS, 2018) to automate shoreline predictions which were compared with manual predictions. Agisoft Metashape Professional (Agisoft Metashape 1.7.2, Agisoft LLC, 2021) was used to process the images captured by the Mavic 2 Pro. Each image was processed to create a point cloud. Cloud Compare (CloudCompare 2.11.2, 2020) is a free software that was used to compare volumetric change between the point clouds at each site.

2.4 Analysis and workflow

An overview of the analysis and workflow is illustrated in figure 2.11. My research workflow is divided into two sections. A ‘Satellite analysis workflow’ with multiple models where the satellite imagery method is explained to produce the historic shorelines, coastal dynamics and prediction maps presented in the results chapter. The ‘UAV analysis workflow’ explains the process and analysis of the 3D UAV imagery to get the volume maps presented in the results chapter. I elaborate on these sets of workflows, in order, below.

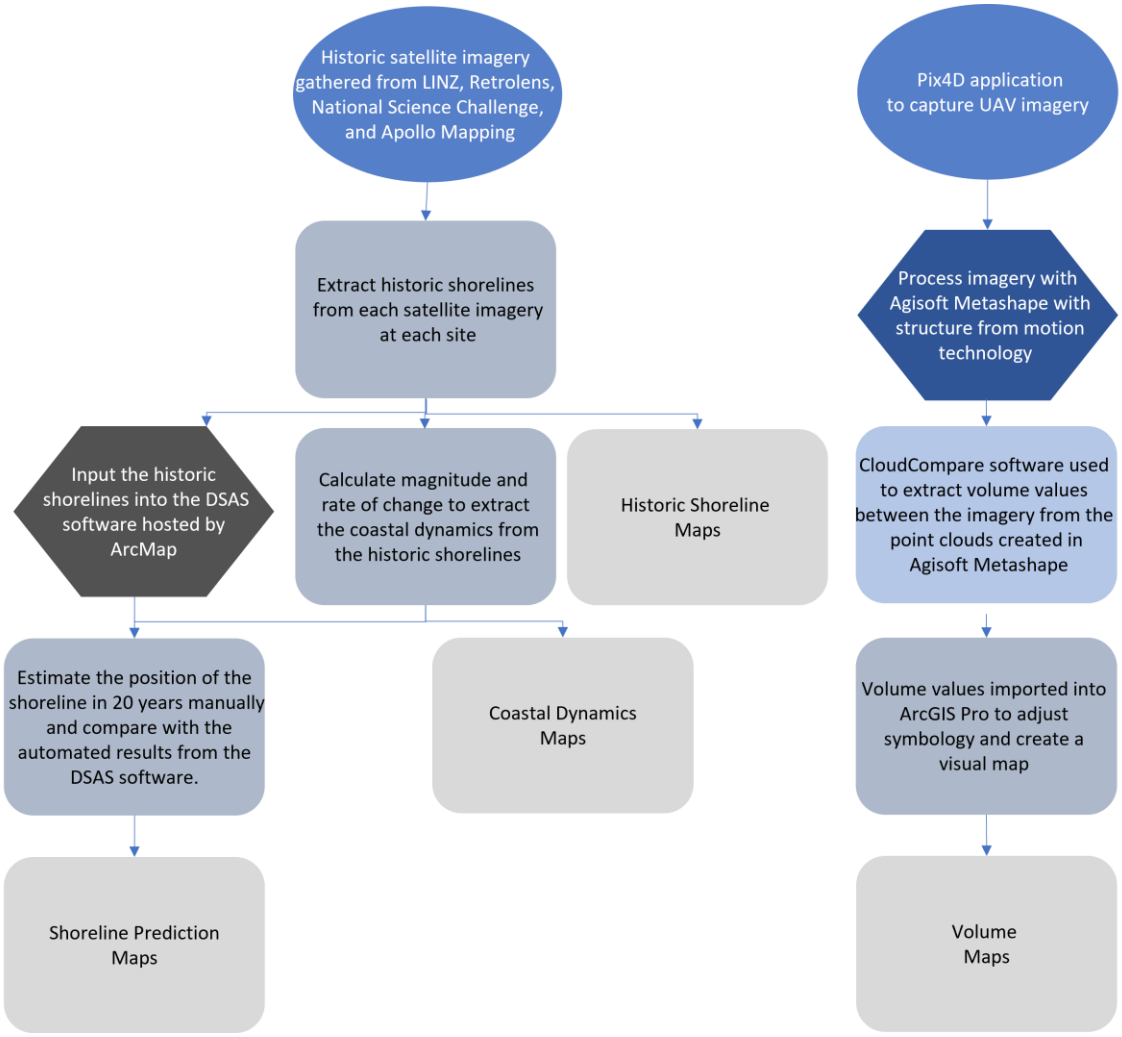

Figure 2.11. Overview of collecting, analysing, and presenting data for this research. The top blue is where the imagery came from. On the left workflow, the top grey step illustrates where the shorelines are extracted from the satellite imagery in ArcGIS Pro. The shorelines are used as an input for the DSAS software (dark grey), the coastal dynamics (grey) and are illustrated as a final output in the results. The coastal dynamics are illustrated in a map as a final output and used along with the DSAS software to predict where the shoreline will in 20 years which is also a final output of the study. The dark blue on the right workflow shows the processing of the UAV imagery in the Agisoft Metashape application. The output from this went into the CloudCompare application to extract volume values shown in the light blue. The volume values were imported into ArcGIS Pro in grey to have the symbology changed and to be presented in a map. Light grey is the final output.

2.4.1 Satellite analysis workflow

The first step in determining overall shoreline change at the study sites was to process the historic satellite imagery. This was achieved using the following GIS procedures:

1. Create GIS shoreline features from historic satellite imagery for each available year (Section 2.4.1.1 Fig. 2.12).

2. Compute the distance of shoreline change between years (Section 2.4.1.2 Fig. 2.14)
3. Assign the shoreline change information to the data table associated with each layer (Section 2.4.1.3 Fig. 2.18)
4. Calculate the rate of change between the historic shorelines (Section 2.4.1.4)
5. Characterise the symbology of the data for visualisation (Section 2.4.1.5 Fig. 2.20)

These steps are described further in the following subsections.

2.4.1.1 Creating GIS shoreline features from historic satellite imagery

To create a line feature of the shoreline from the initial satellite images, a workflow was created in ArcGIS Pro (Esri, 2020) and repeated over all the sites. To start, each georeferenced satellite imagery (raster layer) was clipped to the area of interest extents with the ‘Clip Raster’ tool (Fig. 2.12).

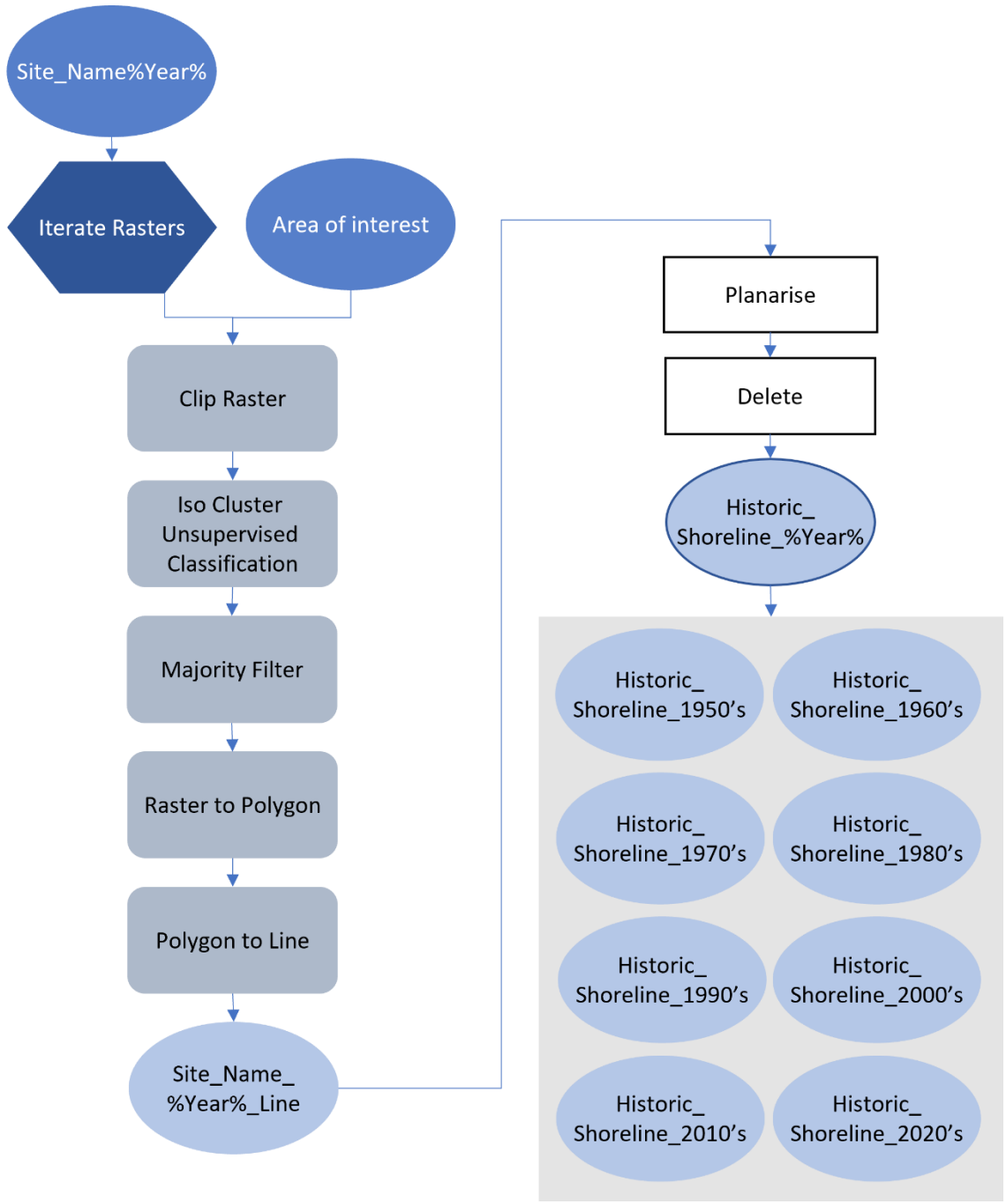

Figure 2.12. Workflow of extracting the shoreline for each satellite image at each site and producing vector outputs. Cobalt blue represents the input into the workflow. The %Year% in some of the light blue steps is used as a substitute for listing all the outputs where only the year is different. The percentage signs on either side are used in python coding to process multiple inputs while keeping some features unique in the outputs. The dark blue below it iterates the raster layers, so each image goes through the same analysis step. Grey represents geoprocessing that occurs in ArcGIS Pro and white represents manual editing that occurs at that point of the workflow. The final output is a collecting of historic shoreline layers each representing a different year where the imagery was originally captured. This is shown in the grey box at the end of the workflow.

The outputs of the *Clip Raster* in figure 2.12 were then used as inputs for an *Iso Cluster Unsupervised Classification* to separate the satellite image by land cover which uses colour of pixels to classify imagery into 5 different classes (Fig. 2.13, map on far left). To clean up noisy pixels of the resultant classification output the M*ajority Filter* tool was used. The raster output was then converted into a vector line layer which was then subsequently manually edited with the 'planarize' and 'delete' tools in ArcGIS Pro until only the line that divided the vegetation from the sand remained (Fig. 2.13, map on far right). The advantage of this is that it reduces human error or bias on where the shoreline could be. A limitation with this is that there is an error margin from the pixel size which was 40 cm for most of the imagery. This was completed for each satellite image of each site.

Figure 2.13. (From left to right). The study area was clipped then the *Iso Cluster Unsupervised Classification* tool was used to classify land cover. The *Iso Cluster Unsupervised Classification* tool divides the elements of the imagery into 5 classes to distinguish them from each other shown with the different colours. The *Polygon to Line* tool creates a vector layer (line). The raster output from map on the left is processed into a vector line layer so that the outlines from the landcover are all that are remaining. The map on the right shows the shoreline output after editing and deleting the excess lines so that the shoreline is the only part of the layer left.

2.4.1.2 Computing the distance of shoreline change between years

To compute the distance the shoreline moved between each satellite image, virtual transects were created at 20 m intervals along the coastline using the *Generate Transects Along Line* tool in ArcGIS Pro (Fig. 2.14). To extract the distance of change shoreward or seaward between each year, the transect layer was merged with each shoreline so that where they intercept can be recorded.

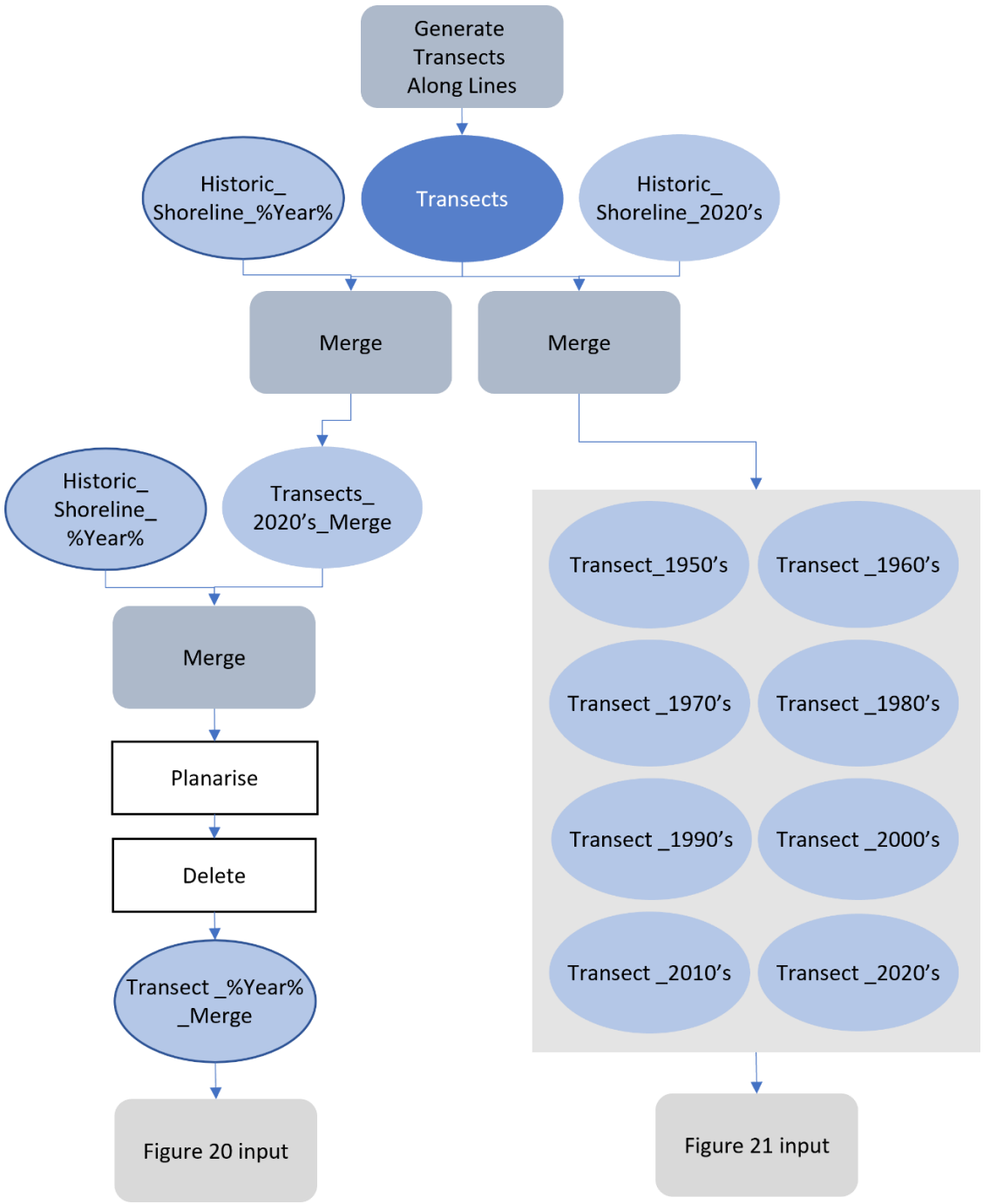

Figure 2.14. Workflow generating transect lines and merging them with each shoreline. The shorelines were merged with the transect layer and the most recent shoreline layer to distinguish the magnitude of change between the past and present. Transects were edited using the ArcGIS Pro *Planarize* and *Delete* tool so that the line between the shorelines analysed was all that was left of the transect. The outputs become inputs for the workflows illustrated in figures 2.18 and 2.19. Cobalt blue represents the transects being inputs into the workflow. Light blue represents outputs. Grey represents geoprocessing that occurred and white represents manual editing that occurred at that point of the workflow.

The historic shorelines were merged with the transect layer and the most recent shoreline layer to distinguish the magnitude of change determined from the resultant transect line segment lengths between the shorelines (Fig. 2.15 & 2.18).

Figure 2.15. Example of transect lines merged with 2021 shoreline then merged with 1948 shoreline to compute the length of erosion or accretion between the 1948 and 2021 shorelines is shown on left map. Resulting transect lines between 1948 and 2021 is shown on right map. Once edited, the transect shape length will be the magnitude of change between the shorelines.

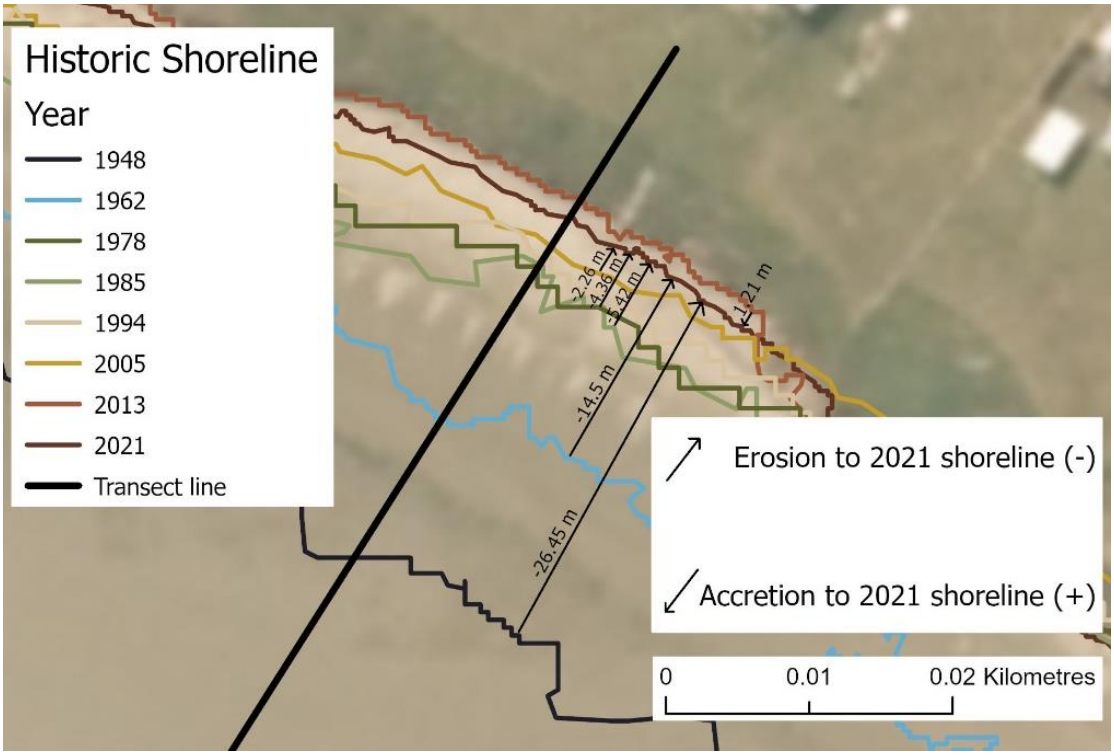

Figure 2.16. An example of how the magnitude values were extracted. Each measurement occurs where the transect lines are but for demonstration in this figure, they have been separated along the shoreline so you can see them. The dark brown line is the 2021 shoreline. All measurements go towards this so that an increase or decrease in magnitude between the shorelines can be easily distinguished. The arrows show the direction of change. All shorelines in this example are eroding towards the 2021 shoreline except the 2013 shoreline that has accreted 1.21 m.

2.4.1.3 Assigning the shoreline change information to the data table associated with each layer

Shoreline change information was assigned to each layer using the following workflow to create a set of descriptive attributes (Fig. 2.17). The attributes are associated with each transect that categorise whether the transects are eroding or accreting toward the 2021 shoreline (Fig. 2.18). The first transect attribute was populated using the *Calculate Field* tool with the 'Year' of the shoreline to distinguish each set of transects when the outputs are merged. The other attributes were created to indicate if erosion or accretion was occurring between the survey times. If the earlier-date shoreline was on the seaward side of the 2021 shoreline, the attribute was labelled with 'Erosion' because the shore had eroded toward the most recent shoreline. If the shoreline was on the landward side of the 2021 shoreline, it was populated with 'Accretion' (Fig. 2.17). Finally, an attribute was created that recorded the length of the transect between the shorelines; if the previous field indicated an accreting shoreline, the value was positive, and if an eroding shoreline, the value was negative (Fig. 2.17). Once all edits were complete, the attribute table was saved as an excel worksheet using the *Table to Excel* tool in ArcGIS Pro (Fig. 2.18).

Transect_Number	ErosionAccretion	AEPosNeg	Year	AnnualRate	Shape_Length
1	Accretion	2.04398	20142021	0.097332	2.04398
2	Erosion	-10.014211	20142021	-0.476867	10.014211
3	Erosion	-3.439827	20142021	-0.163801	3.439827
4	Erosion	-0.033175	20142021	-0.00158	0.033175
5	Erosion	-7.922752	20142021	-0.377274	7.922752
6	Erosion	-1.7525	20142021	-0.083452	1.7525
7	Accretion	0.097157	20142021	0.004627	0.097157
8	Accretion	0.26586	20142021	0.01266	0.26586

Figure 2.17. Example of the attributes table. 'ErosionAccretion' column states whether the shoreline was eroding to accreting towards the 2021 shoreline. 'AEPosNeg' is the shape length of each transect with all the erosion values as negative and accretion as positive. 'Year' is the years the measurement is between. Annual rate is the 'Shape_Length' divided by the number of years the measurement is between used as an estimate.

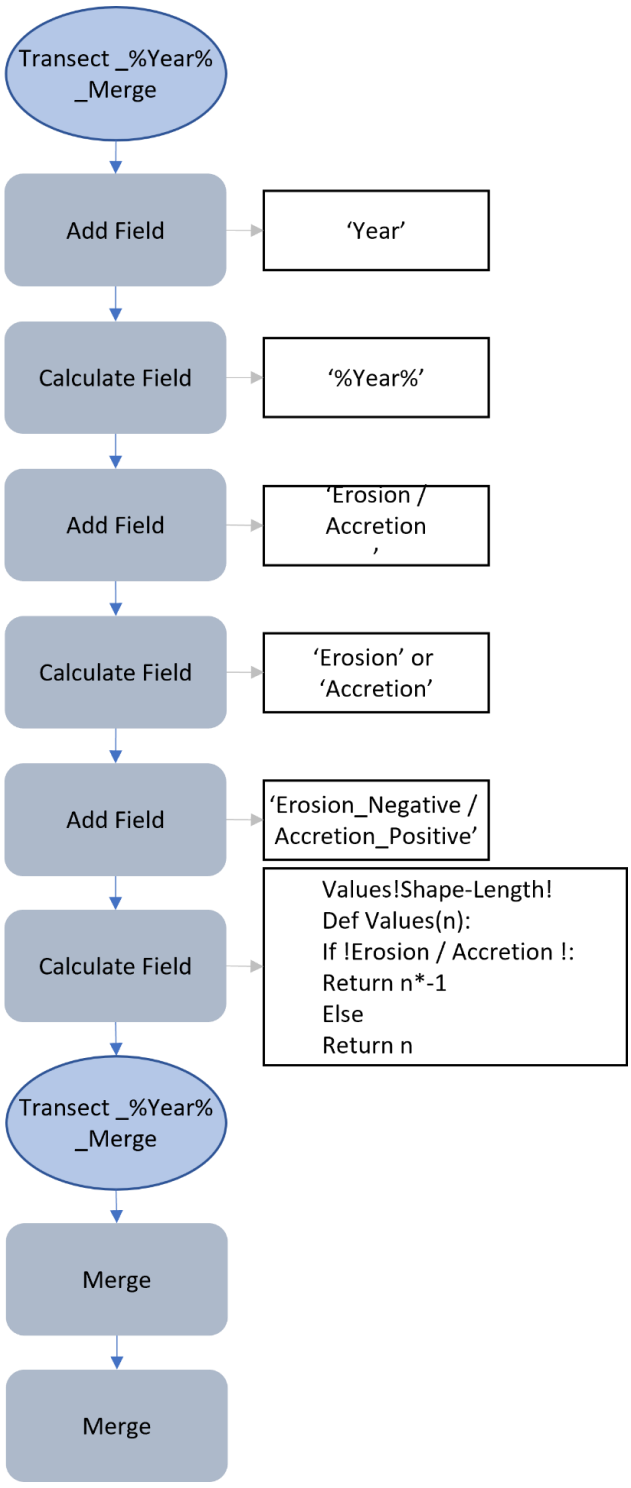

Figure 2.18. This workflow is for adding and populating fields with erosion / accretion data to go into an excel spreadsheet. The first transect attribute was populated with the 'shoreline year' to distinguish each set of transects when the outputs are merged. The other attributes were created to indicate if erosion or accretion was occurring between the survey times. If the earlier-date shoreline was on the seaward side of the 2021 shoreline, the attribute was labelled with 'Erosion' because the shore had eroded toward the most recent shoreline. If the shoreline was on the landward side of the 2021 shoreline, it was populated with 'Accretion'. The erosion values were calculated with a bit of code which says if 'Erosion' is in this column then I will populate this value with a negative, else keep value the same.

2.4.1.4 Calculating the rate of change between the historic shorelines

To calculate the rate of change I merged transects with corresponding historic shorelines such as the 1948 with the 1962 and the 1962 with the 1978 shoreline (Fig. 2.19). The 'Planarize' and' Delete' tool was used to extract the shape length of each transect between the shorelines. The rate of change between the different historical shorelines was then determined from the resultant transect line segment lengths divided by the number of years between the shorelines which then populated an 'Annual_Rate' attribute (Fig. 2.19). Each layer was merged into one and the attribute table was saved as an excel worksheet using the *Table to Excel* tool in ArcGIS Pro.

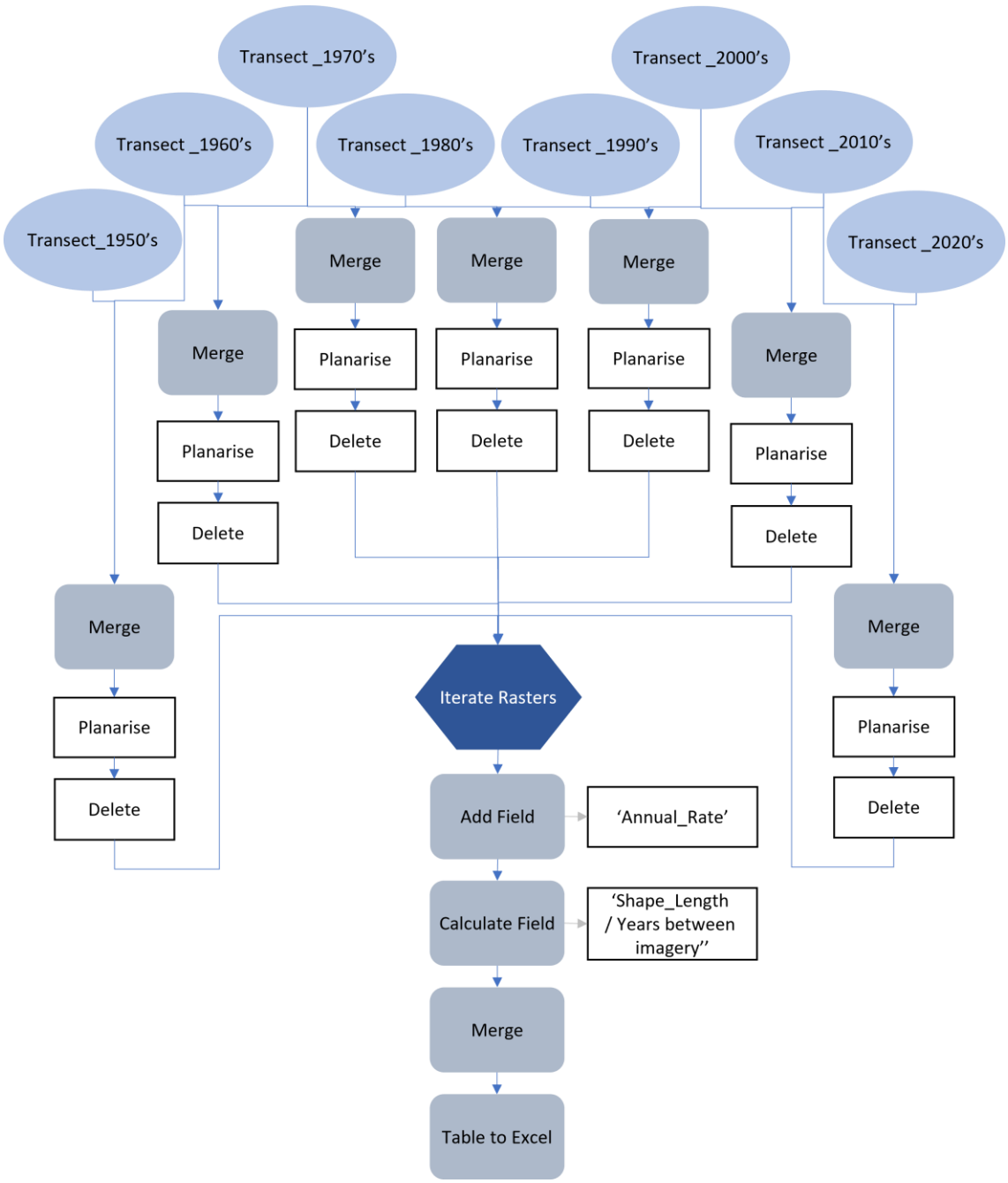

Figure 2.19. From the outputs of figure 2.14, the transects with corresponding historic shorelines such as the 1948 with the 1962 and the 1962 with the 1978 shoreline were merged. The 'Planarize' and' Delete' tool was used to extract the shape length of each transect between the shorelines. The rate of change between the different historical shorelines was then determined from the resultant transect line segment lengths divided by the number of years between the shorelines which then populated an 'Annual_Rate' attribute. Each layer was merged into one and the attribute table was saved as an excel worksheet using the *Table to Excel* tool in ArcGIS Pro.

2.4.1.5 Characterising the symbology of the data for visualisation

The magnitude and rate of change measurements produced from the above workflows were put in Microsoft Excel (see Appendix I). The net change, total accretion and total erosion were calculated for each transect. For the average rate of change calculations, 2 metres of change per year was extreme, 1 metre per year was major and half a metre was minor. Stable values were between -0.5 m and 0.5 m of annual change. Each transect was designated into two categories which were 'stable to erosion' and 'stable to accretion'. Transects that produced high rate of change values for both categories were classed as 'unstable'. The values calculated are put back into ArcGIS Pro and added to the original transect lines. Two attribute fields were added with corresponding names to the categories above (Fig. 2.20). These two attribute fields were used as the input for a symbology matrix to illustrate the patterns shown on each transect (Fig. 2.21).

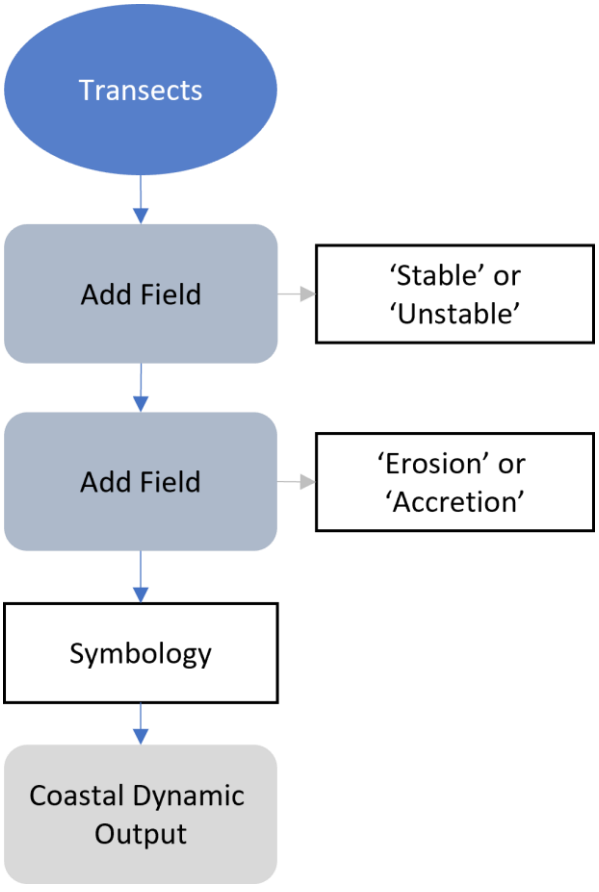

Figure 2.20. Using the original transect lines, two attribute fields were added and populated with a pattern number and a matrix is produced to illustrate the coastal dynamics. Transects that produced high values for both categories were classed as 'unstable'. The values calculated are put back into ArcGIS Pro and added to the original transect lines.

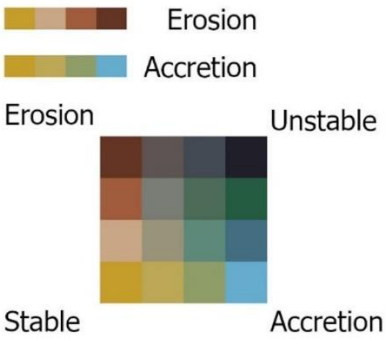

Figure 2.21. This is the coastal dynamics matrix for categorising each transect line. You can expect to see this in the results chapter on the coastal dynamic's maps. Each transect was placed into a matrix based on the value of accretion and erosion it showed. If both these patterns are low, then the shoreline is stable resulting in a yellow transect line. If both are high, it is classed as unstable resulting in a black transect line. Brown shows a dominant erosion pattern and blue shows a dominant accreting pattern. The colours in between show a mix of dynamics.

2.4.2 Predicting future shorelines workflow

This section of the research compares manually derived future shorelines predictions with future shorelines predicted with the Digital Shoreline Analysis System (DSAS) software (USGS, 2018) for ArcMap (Esri, 2020). This comparison will aid in evaluating adaptive methods for understanding and managing our coastlines.

2.4.2.1 Manually derived shoreline predictions

Basic calculations were undertaken to give a rough estimate of where the coastline of each site will be in 20 years. This calculation was completed from the satellite imagery as the short period of time the drone imagery was captured in, does not provide enough adequate information for these predictions. Transects at each site were analysed and if distinguishable patterns such as constant erosion, no movement or cycles between erosion and accretion for example were shown, the location the shoreline may be in 20 years was estimated. If there was no distinguishable pattern, the distance value would remain 'NULL'. Once all transect values were estimated, they were inputted into a new attribute field named "Estimate20" in the transect layer (Fig. 2.22).

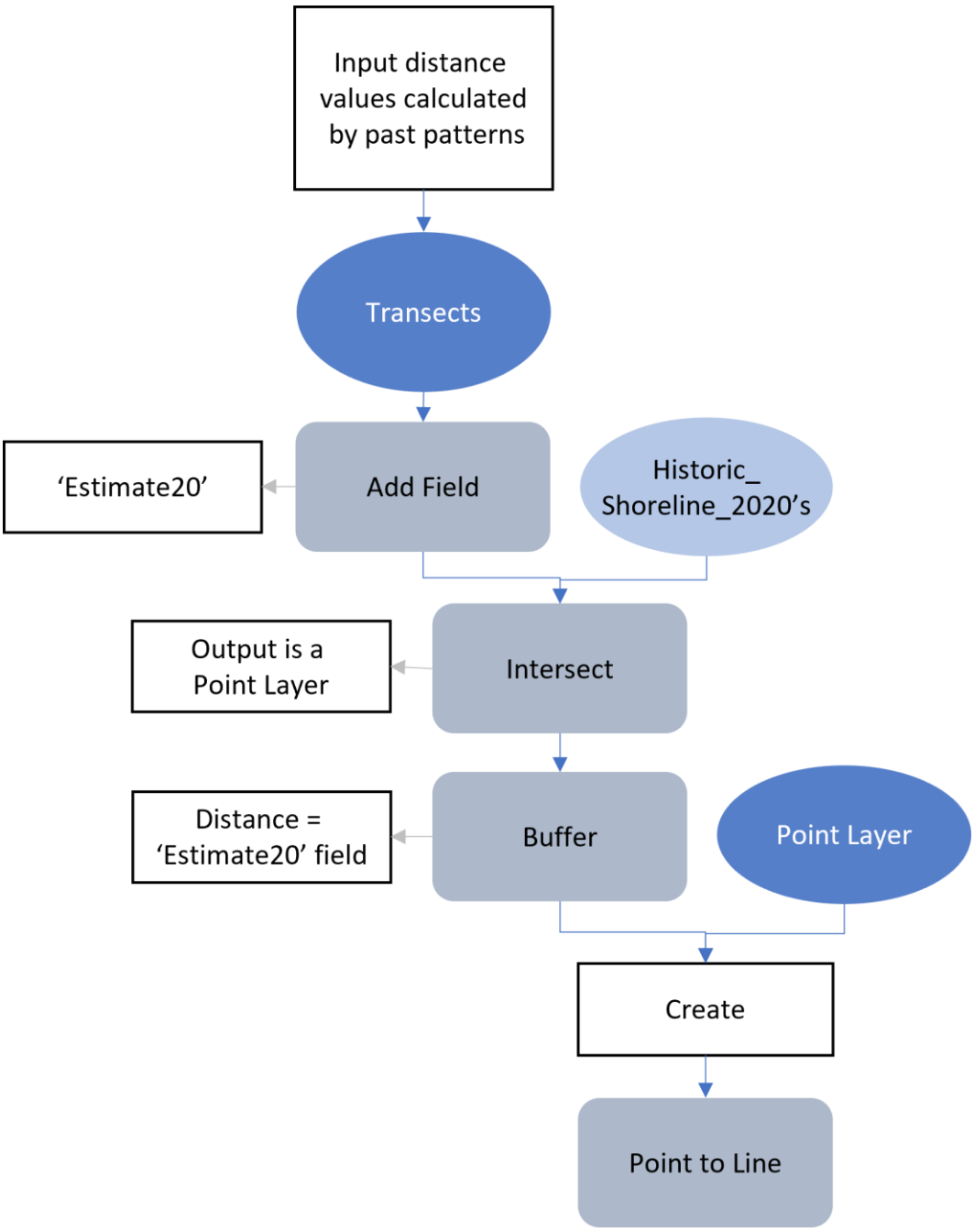

Figure 2.22. Method to extract values for predicting the shoreline in 20 years. The transect layer and the 2020s shoreline layer were intersected using the *intersect* tool in ArcGIS Pro with the output being a point layer. To compute the estimated distance the shoreline would change in 20 years, the point layer was buffered using the values from the 'Estimate20' field. A new point layer was created, and points were manually created on top of where the transect and the buffer intercept or if the value was 0, on the same point as the previous point layer.

The transect layer and the 2020s shoreline layer were intersected using the 'intersect' tool in ArcGIS Pro with the output being a point layer. To compute the estimated distance the shoreline changes in 20 years, the point layer was buffered using the values from the 'Estimate20' field. A new point layer was created, and points were

manually placed on top of where the transect and the buffer intersect or if the value was 0, on the same point as the previous point layer (Fig. 2.22). The points were then interpolated into a line using the *Point to Line* tool in ArcGIS Pro. The outcome is a rough estimate of what the shoreline may look like in 20 years to aid in adaptive management (Fig. 2.23).

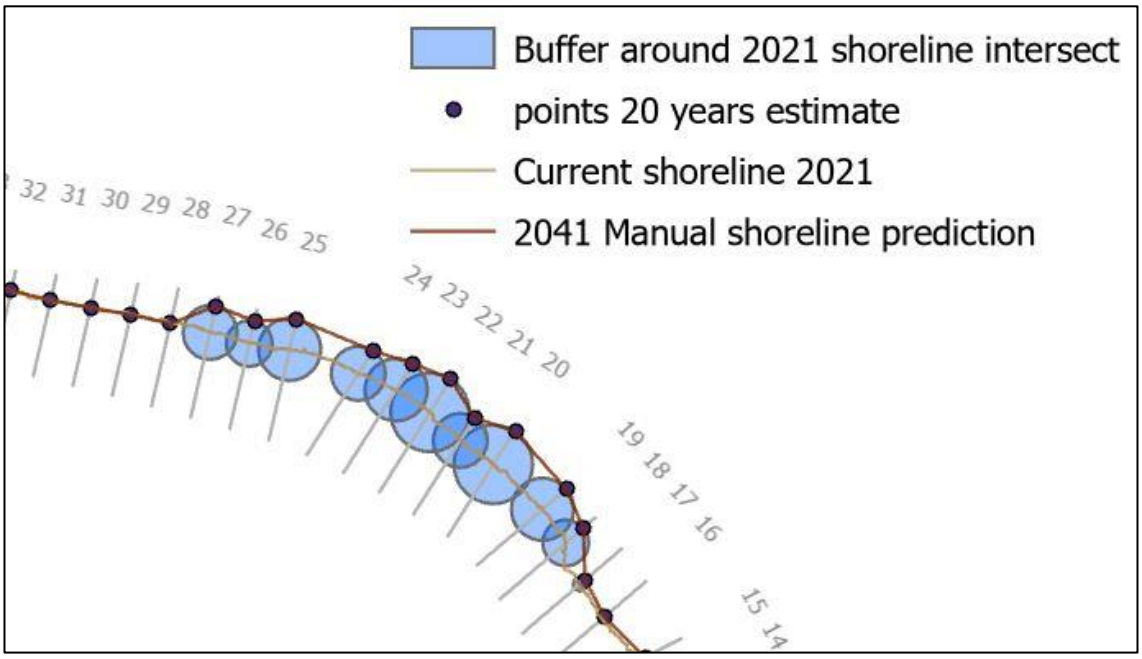

Figure 2.23. Method for the manual predictions in ArcGIS Pro. The key in the figure describes the different layers used to estimate the shoreline in 20 years. This method used several ArcGIS Pro geoprocessing tools to get the future shoreline prediction. A buffer using the values from the 'Estimate20' field was created at the point where the transect line and current shoreline intersect. Where the edge of this buffer and the transect intersect is the point where the shoreline is predicted to be in 20 years. A new point layer was created and placed along this intersect and then a line was drawn between the points with the *Point to Line* tool.

2.4.2.2 DSAS predicting shoreline

After completing the manual prediction, another software was evaluated on the competency of predicting future shorelines. The output of figure 2.12 was used as an input for the Digital Shoreline Analysis System (DSAS) software which provides an automated method to calculate the rate of change statistics. The software uses shoreline data and a baseline as the inputs (Fig. 2.24). It then generates transect lines at determined intervals and calculated outputs based on where the transects intersect the shorelines. There are several outputs which can be generated with this software including a shoreline change envelope and net shoreline movement as distance

measurements. The statistics includes end point rate, linear regression rate and weighted linear regression rate. From these outputs, you can predict the shoreline 10 years or 20 years into the future from the rate of change statistics through an automated process. For my comparison, I used the 20 years prediction and did the same working with my method above to observe the similarities and differences between the automated and manual workflow.

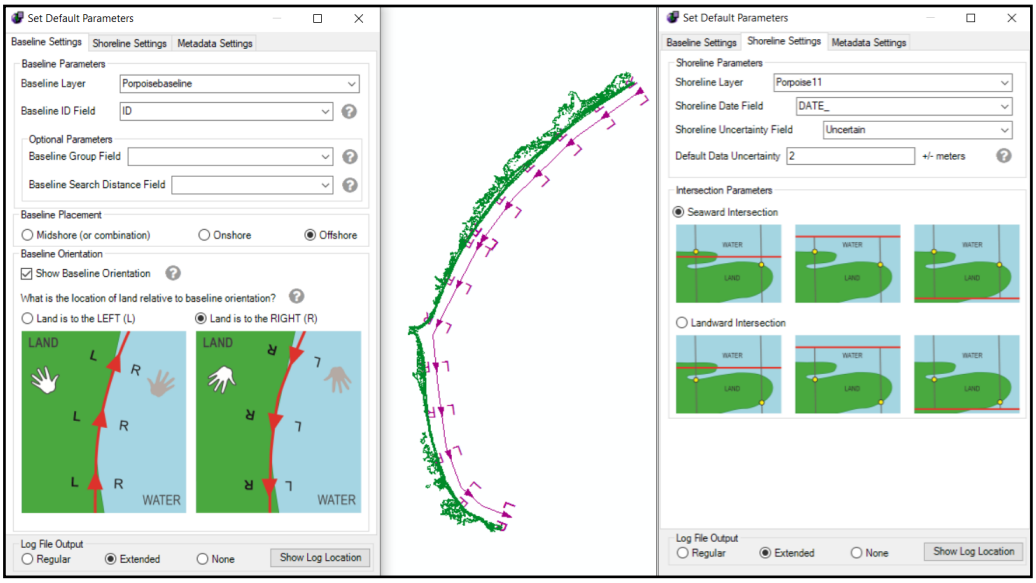

Figure 2.24. Inputs for the DSAS software to calculate statistics on the rate of change. The DSAS software requires two inputs: a baseline and multiple historic shorelines. The left shows the parameters you need to fill out for the baseline input and the right shows the shoreline parameters. The middle is an aerial view of the shorelines (green) and the baseline (purple) in ArcMap before the software has been run.

2.4.3 UAV analysis workflow to calculate seasonal change in volume

The UAV collected hundreds of images for each survey. These images were processed using the Agisoft Metashape software (Agisoft LLC, 2021) to create a 3D model comprised of many points, a point cloud. The dense point cloud was then exported into CloudCompare (CloudCompare 2020). To compare the volume between the surveys, the point clouds were transformed into the same matrix to fix any positioning error from imagery collection (Fig. 2.25). This transformation occurred before the comparison of the surveys because the elevations of each survey was based off the point at which the UAV took off from which was different at each survey.

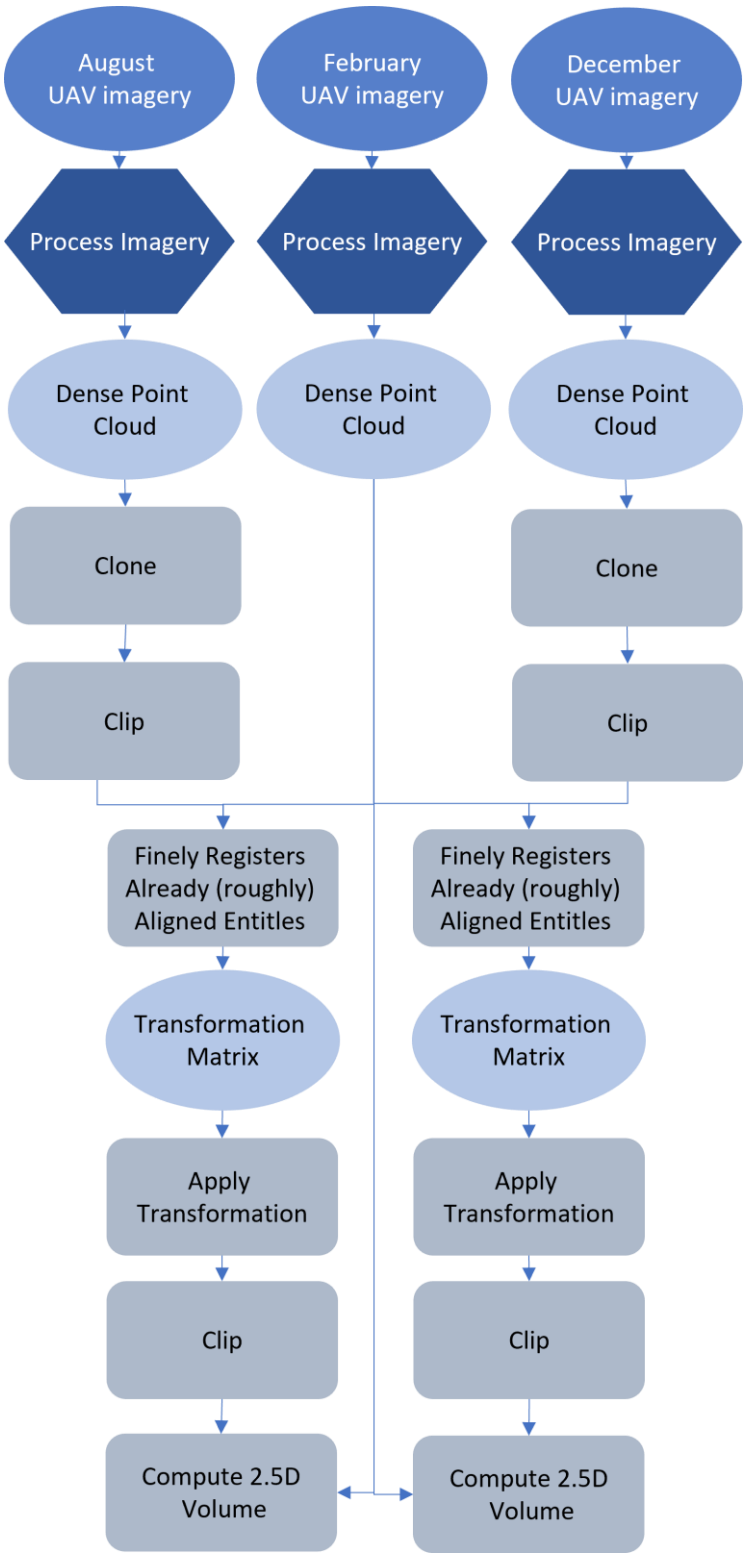

Figure 2.25. Model for extracting the volumetric change between the UAV surveys used for each site. To compare the point clouds into the same matrix, the August and December surveys were cloned using the *clone* tool in CloudCompare and each were clipped around an area with consistency throughout all surveys such as a road or building. The *Finely registers already (roughly) aligned entities (cloud or meshes)* tool was used with the August and December clipped layers onto the February layer. A transformation matrix is produced which was then copied and written into the *apply transformation* tool for the original August and December survey layers.

To join the point clouds into the same matrix, the August and December surveys were cloned using the *clone* tool in CloudCompare and each were clipped around an area with consistency throughout all surveys such as a road or building, excluding the shoreline (Fig. 2.25). This was to prevent the volume difference of each survey from interfering with the alignment process. The *Finely registers already (roughly) aligned entities (cloud or meshes)* tool was used with the August and December clipped layers onto the February layer (Fig. 2.26). A transformation matrix is produced which was then copied and written into the *apply transformation* tool for the original August and December survey layers.

Figure 2.26. Surveys from side view of February and August layering one on top of the other instead of at the same elevation. The imagery shows two models before they are aligned properly, hence all the steps in figure 2.25. Once aligned the volumetric differences can be calculated.

After the layers are in the same matrix (aligned properly), they are clipped to only include the relevant shoreline to prevent irrelevant values being computed. The *Compute 2.5D Volume* tool in CloudCompare was used to compare the volume difference between the February and August surveys, the August and December surveys and the February and December surveys of each site. This tool gives the net volume change, added volume, and removed volume. It also gives the percentage of cells matched between the surveys and the average neighbours per cell to aid in accuracy and error control.

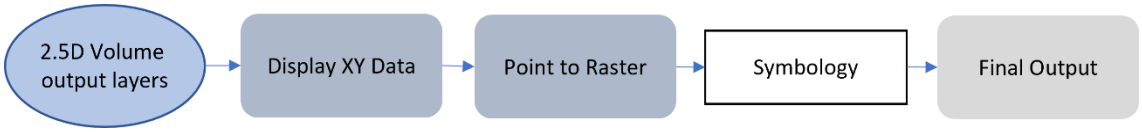

Figure 2.27. The *Display XY data* tool is used to return the file to a point layer where a 'point to raster' geoprocessing tool is then used. The symbology is then modified to make analysis between the surveys more transparent for the final output.

The point cloud between each survey year is exported into ArcGIS Pro as a txt document to present in a map. The *Display XY data* tool is used to return the file to a point layer where a *point to raster* geoprocessing tool is used to create a raster layer. This was because a raster creates a cleaner surface to display the volume change

results on (Fig. 2.27). The symbology is then modified to make analysis between the surveys more transparent.

Chapter 3 Results

3.1 Results summary

The results illustrate the success of a generalised GIS methodology used at different site locations with different factors affecting each shoreline. Comparison of the historic satellite imagery showed the changes to the position of the shorelines that have occurred over the past ~70 years. Transects were virtually generated 20 m apart and populated with the rate and magnitude of change occurring between the historic shorelines to produce coastal dynamics that were illustrated with a matrix. The four main dynamics were eroding, accreting, stable and unstable. Monkey Island and Colac Bay both showed a mainly stable coastline with specific areas of erosion or mixes of dynamics (Fig. 3.1). Monkey Island has areas of slight erosion, notably up to 60 m to the north of the two stream mouths along the shoreline analysed. Colac Bay has two main areas of interest in this study. The first is between transect 65 – 75 with erosion occurring in front of the coastal landfill and from transects 109 – 119 where the vegetation line takes over from the hard engineering seen throughout most of the coastline. Whereas at Fortrose, major erosion and stable dynamics were shown along the shoreline in specific areas. The shoreline between transects 18 – 28 has stabilised from a major erosion pattern in recent years. The entire length analysed is of concern due to 34 out of the 49 transects showing a net change of over 10 metres of erosion. Porpoise Bay showed an unstable coastline because of extreme cycles of erosion then accretion extracted from the historic shorelines. This is shown with the dark transect lines along the entire length of the shore (Fig. 3.1). The most unstable area of this coastline is between transects 87 – 95 with transect 91 showing a rate of erosion averaging at ~2.63 m per year.

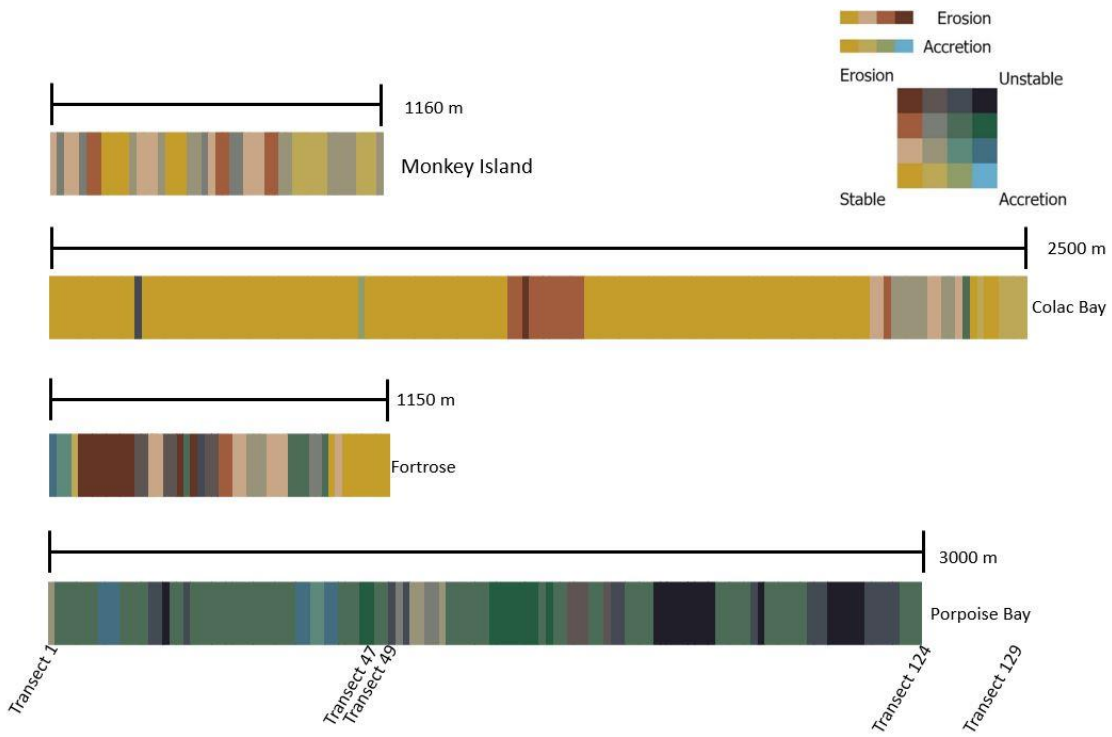

Figure 3.1. A summary of all the dynamics occurring along each coastline. Each vertical line represents a transect which are spaced 20 m apart on the survey site. A scale bar shows the distance the transect lines cover at each shoreline. Colac Bay is showing more transects in a smaller area than Porpoise Bay because of the profile of the shoreline. From left to right shows transects 1 to the end of the shoreline surveyed. Each transect was placed into a matrix based on what level of accretion and erosion it showed. If both these patterns are low, then the shoreline is stable resulting in a yellow transect line. If both are high, it is classed as unstable resulting in a black transect line. Brown shows a dominant erosion pattern and blue shows a dominant accretion pattern. The colours in between show a mix of dynamics.

Predictions were manually generated by hand and automatically generated with the DSAS software for where the location of the shoreline in 20 years will be. These were extracted from the historic shorelines and coastal dynamics at each site. Monkey Island showed little change between the current shoreline and the predicted shoreline in 20 years. This was for both the manual and automated predictions. This was the same as the Colac Bay predictions apart from between transects 65 – 75 where the automated prediction only showed an average of 5 m of retreat whereas the manual prediction estimates an average of 15 m of retreat over the next 20 years. The Fortrose automated prediction for the shoreline in 20 years is about the same as the current shoreline apart from between transects 7 – 10 where it is predicted to retreat 7 m. At Fortrose, the manual prediction estimates the shoreline between 18 – 27 will retreat more than an average of 10 m in 20 years. Porpoise Bay has a mix of predictions which

are dominated by the DSAS software predicting accretion for most of the shoreline (Fig. 3.2).

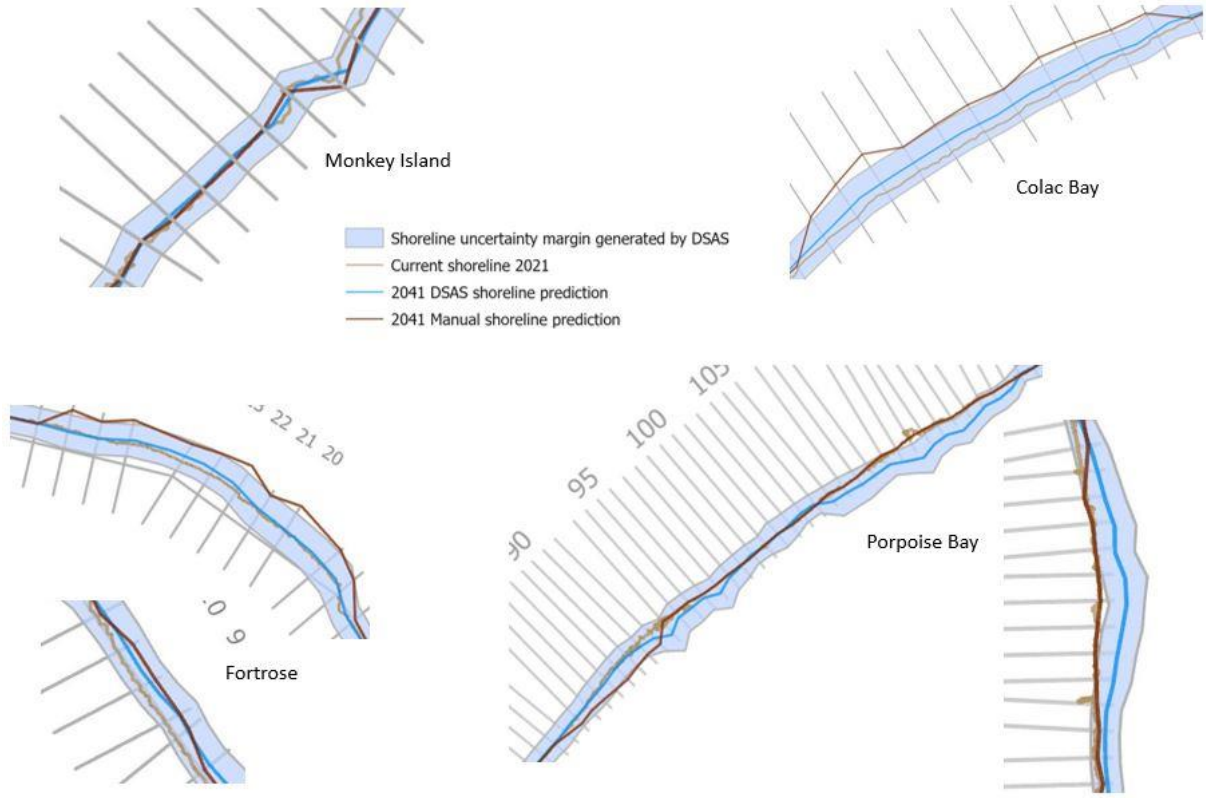

Figure 3.2. A summary of the main areas of interest where predictions are shown at each site. Monkey Island and Fortrose have the sea on the left-hand side of the shoreline and Colac Bay and Porpoise Bay have the sea on the right-hand side of the shoreline. Monkey Island showed little change between the current shoreline and the predicted shoreline in 20 years which is illustrated in the top left of the figure. This was the same as the Colac Bay predictions apart from between transects 65 – 75 where the automated prediction only showed an average of 5 m of retreat whereas the manual prediction estimates an average of 15 m of retreat shown in the upper right image. Transects 7 – 10 at Fortrose are predicted to retreat about 7 m on average shown on the lower left-hand corner of the figure. The manual prediction estimates the shoreline between 18 – 27 at Fortrose will retreat more than an average of 10 m in 20 years shown on the left middle picture of the figure. Porpoise Bay shoreline dominated by the DSAS software predicting accretion shown in the bottom right-hand images.

3D UAV imagery was collected at the four sites to extract volumetric changes from February to December 2021. These volumetric changes were calculated by overlaying point clouds of each survey with the other surveys taken. Empty cells were interpolated for the results. Table 3.1 illustrates the change in volume between the UAV surveys. The added and removed volume between each survey is standardised to 100m² to simplify comparisons between each site. Monkey Island and Colac Bay showed extremely similar results for the August to December comparison with 1.332

m^3 or 1.710 m^3 added and 29.186 m^3 or 29.951 m^3 removed. This was also observed for the February to December surveys with 0.708 m^3 or 0.928 m^3 added and 22.924 m^3 or 21.688 m^3 removed. Porpoise Bay showed the most volume removed through the study period with 63.615 m^3 removed between February and December, most of that occurring between February and August while 29.997 m^3 added and 37.718 m^3 removed volume between August and December are more similar. Overall, there was larger volume removed than added at Monkey Island, Colac Bay, and Porpoise Bay. Fortrose showed the opposite pattern between the August to December surveys where 62.870 m^3 was added and only 2.142 m^3 was removed. This was also observed at Fortrose for the February to December surveys where 27.904 m^3 was added and 5.407 m^3 was removed (Table 3.1).

Table 3.1 Removed and added volume (measured in m^3) values between each survey and site. The added and removed volume between each survey is standardised to 100m^2 to simplify comparisons between each site. The 'Figure #' states the figure correspondent with the row the data is from.

Survey	Site	Standardised added volume (100m^2)	Standardised removed volume (100m^2)	Figure #
February to August	Monkey Island	(+) 9.412	(-) 3.792	3.21
	Colac Bay	(+) 15.165	(-) 6.823	3.24
	Fortrose	(+) 0.590	(-) 44.597	3.27
	Porpoise Bay	(+) 9.231	(-) 63.615	3.30
August to December	Monkey Island	(+) 1.332	(-) 29.186	3.22
	Colac Bay	(+) 1.710	(-) 29.951	3.25
	Fortrose	(+) 62.870	(-) 2.142	3.28
	Porpoise Bay	(+) 29.997	(-) 37.718	3.31
February to December	Monkey Island	(+) 0.708	(-) 22.924	3.23
	Colac Bay	(+) 0.928	(-) 21.688	3.26
	Fortrose	(+) 27.904	(-) 5.407	3.29
	Porpoise Bay	(+) 4.634	(-) 67.517	3.32

The expanded value tables for each site can be found in Appendix I (excluding the volume tables which can be found in the results section divided by site). The rest of the chapter goes into more detail regarding the results of the study.

3.2 Historic Shorelines

3.2.1 Monkey Island Historic Shorelines

Monkey Island showed minimal movement of the shoreline over the past 75 years (Fig. 3.3). In Appendix I, there are a few major erosion values recorded for the distance change before 2005 where gaps between available data was large. The major erosion values do not exceed 13 m which, between the 1984 and 2005 satellite images is estimated to be less than 0.6 m a year. The rate of change table shows sporadic and minimal changes occurring. The largest recorded values of erosion and accretion occurred between 2013 and 2021 where transect 27 showed an average of 1.15 m of erosion.

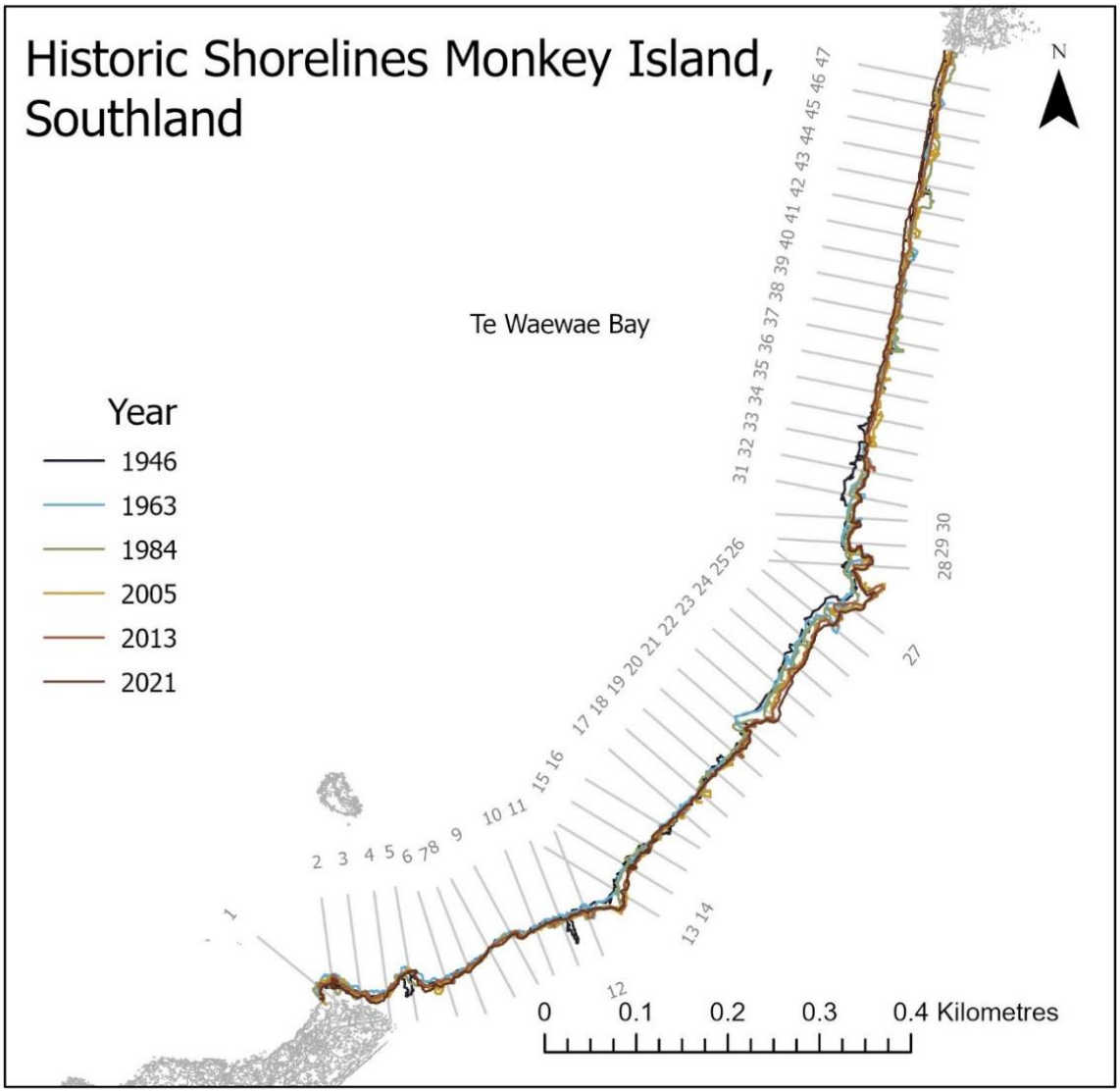

Figure 3.3. Historic shorelines at Monkey Island, derived from historic aerial imagery. The key shows the year the shorelines were extracted from. At Monkey Island there is a lot of overlap between the shorelines showing in some areas there has been minimal change occurring. The earliest year is 1946 shown in the dark blue. The corresponding years go to light blue, green, yellow, light brown and dark brown. Between transect 22 and 28 there is a pattern of erosion through the years shown by the brown being the most shoreward shoreline and then dark blue being the furthest seaward.

3.2.2 Colac Bay Historic Shorelines

Minimal change is observed at Colac Bay over the past 69 years. Over the whole shoreline, under 18% of transects show accretion for the net change. The total net change from all the transects was erosion of 371.8 m. This net change was added from the average of all the transects over each historic satellite image. There are two main areas of interest along the Colac Bay shoreline where significant change has occurred (Fig. 3.4). These areas are shown in figures 3.5 and 3.6 with close ups of the shoreline.

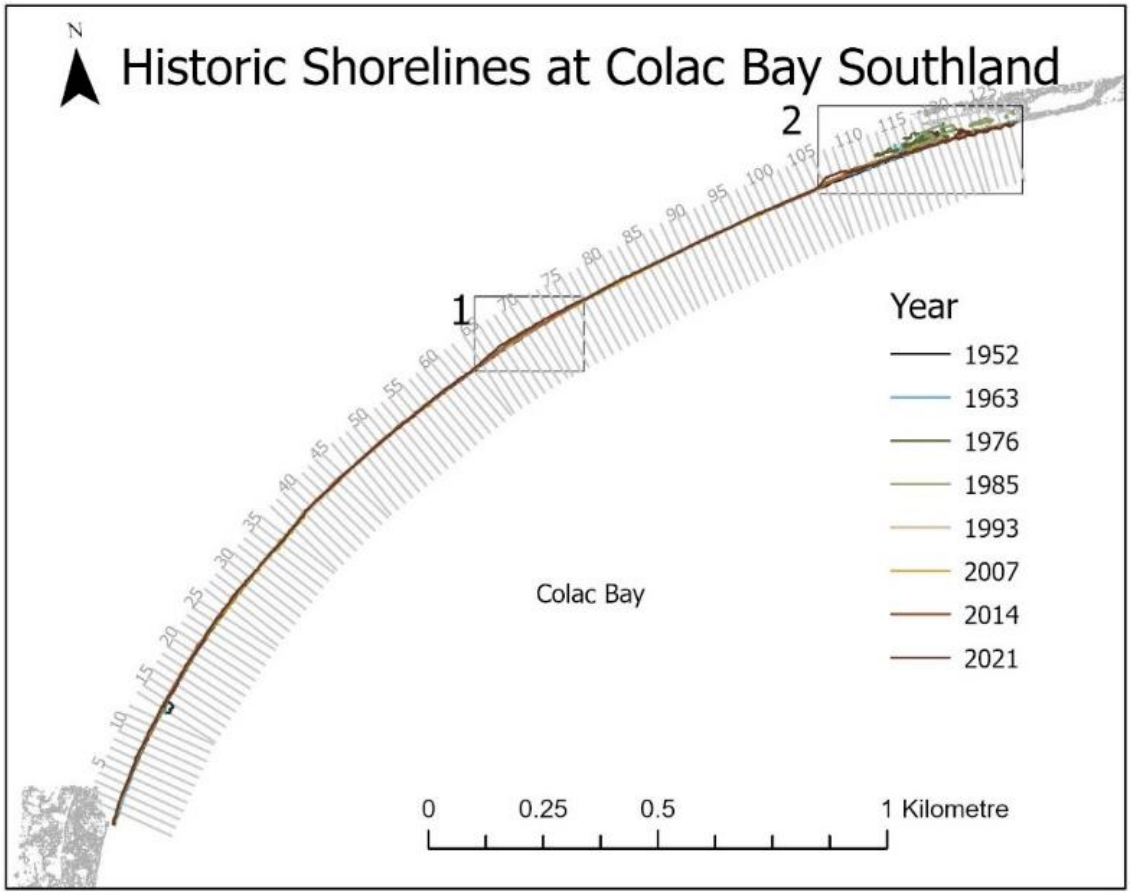

Figure 3.4. Historic Shorelines at Colac Bay. The earliest year is 1952 shown in the dark blue. The corresponding years go to light blue, green, yellow, light brown and dark brown. The coastline surveyed was 2500 m long with no significant change occurring over most of it. The following figures (3.5 and 3.6) are close ups of the boxed areas shown in this figure where change did occur along this coastline.

The first close up is along the shoreline where the road was closed between the 2014 and 2021 satellite images (Fig. 3.5). Since then, the coast has eroded up to 8.28 m at transect 67 which was an estimated average of 1.18 m a year. The second close up at Colac Bay shows the shoreline just past the northeast end of the coastal road when it goes back to a vegetated dune system (Fig. 3.6). Transect 94 - 127 are missing a shoreline from 1993 because of no available data which means there was a 22-year gap between the 1985 and 2007 shorelines. In this time the vegetation became less sparce and showed a stabilised shoreline from 2007 onwards.

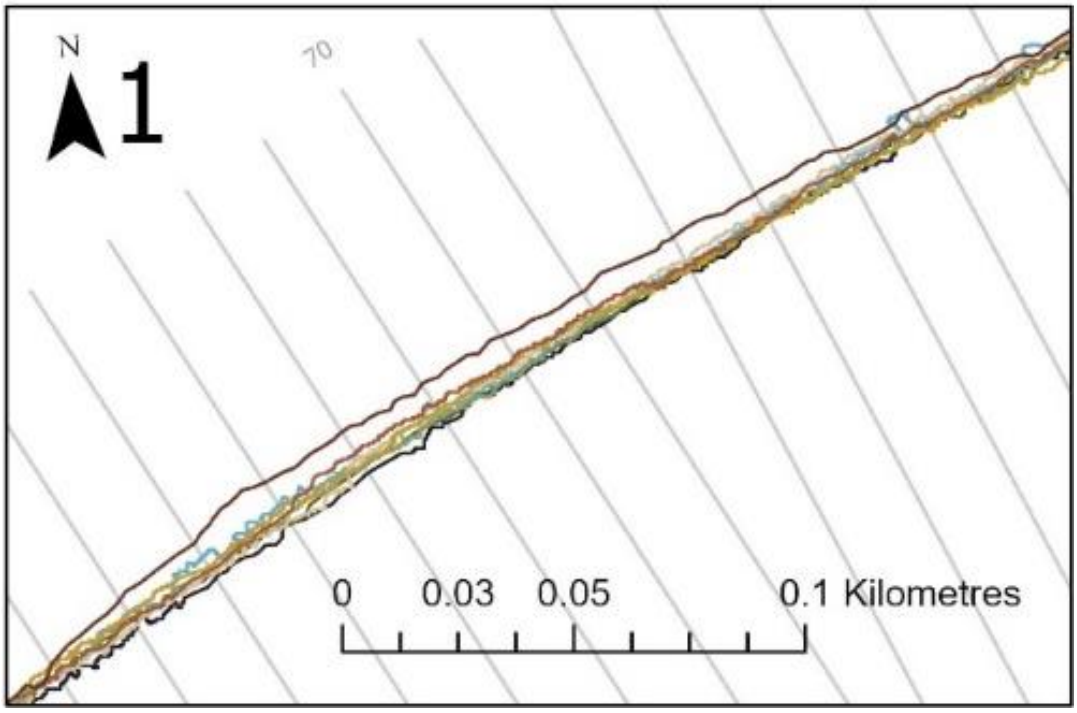

Figure 3.5. Historic shorelines at Colac Bay close up 1. This close up shows where the coastal road was closed due to continuous erosion after the 2014 satellite image was captured. You can see the significant erosion since then by the 2021 survey year being more shoreward compared to previous years.

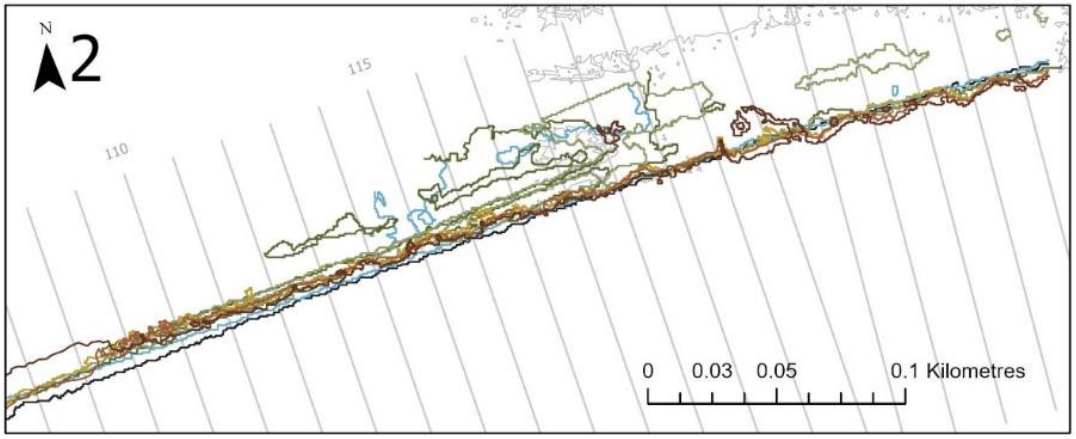

Figure 3.6. Historic shorelines at Colac Bay close up 2. This figure shows just past the end of the road where the coastline goes into a natural dune system that has no engineered or hard protection. The blue (1963), green (1985) and bits of dark brown (2021) patches further back from the main shoreline show sparse vegetation throughout the dunes.

3.2.3 Fortrose Historic Shorelines

Fortrose Estuary has shown some of the most prominent shoreline retreat throughout the last 73 years. Transects 1 and 2 showed major accretion in the first 30 years then stabilised from 1985 onward. Over the whole shoreline, the net total change from all the transects is erosion of 719.67 m. 34 out of the 49 transects have a net change of

over 10 m of erosion. The maximum net change occurs on transect 4 which has a result of 35.73 m of erosion. Transects 6, 7, 8 and 23 also have net changes above 30 m. (Fig. 3.7). Transects 7 - 10 have had minor erosion in the last 8 years up to 0.68 m on average a year for transect 9. The stabilisation in recent years is illustrated (Fig. 3.7).

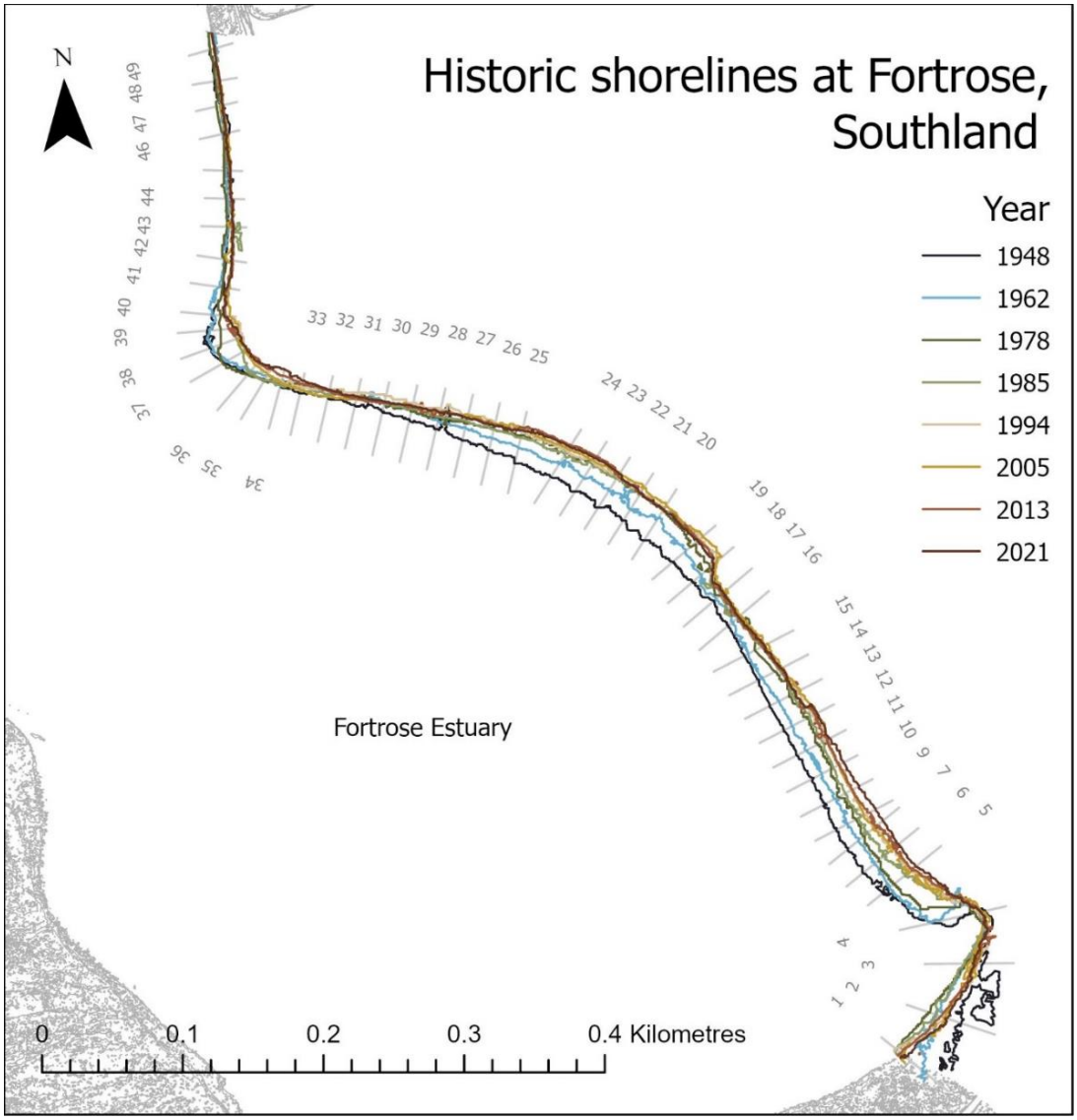

Figure 3.7. Historic shorelines at Fortrose, derived from satellite imagery. Between transects 4 – 16 and 18 – 28 there are distinct patterns of erosion especially from 1948 (dark blue) to 1962 (light blue). The shoreline begins to stabilise in recent years shown by the overlapping of the brown, and light brown shorelines. 34 out of the 49 transects have a net change of over 10 m of erosion. The maximum net change occurs on transect 4 with a result of 35.73 m of erosion.

3.2.4 Porpoise Bay Historic Shorelines

Major change has occurred along the shoreline at Porpoise Bay in the last 72 years with vast erosion and accretion occurring at different parts of the beach (Fig. 3.8). Over the whole shoreline, the net total change between 1948 and 2020 from all the

transects was accretion of 4283.4 m. Since 1978 the net change was only 44.1 m of accretion. Between 2013 and 2020 there has been over 10 m of erosion occurring between transects 87 to 95 with transect 91 showing a rate of erosion averaging at ~ 2.63 m. per year. The shoreline between transects 31 and 51 have accreted.

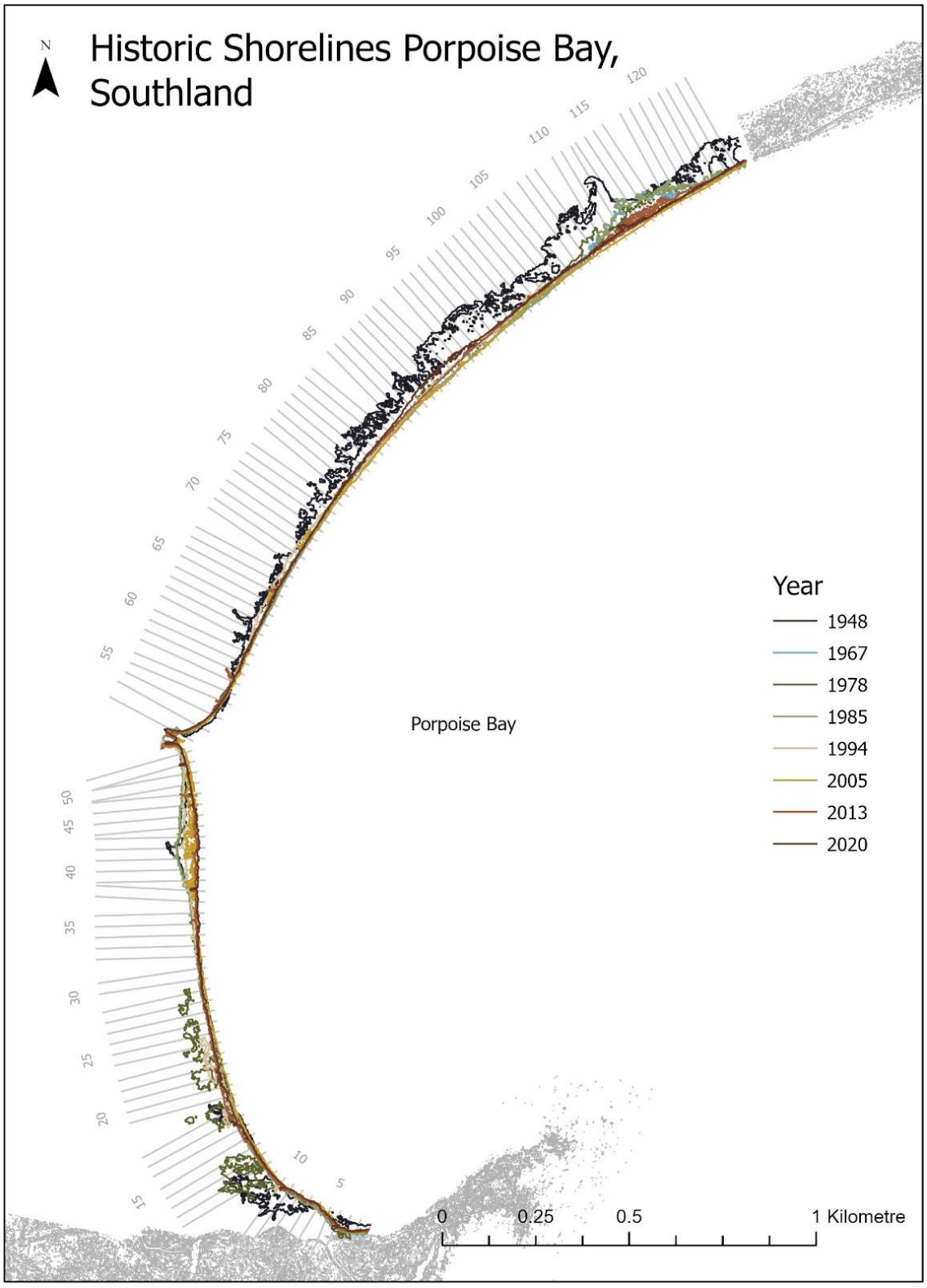

Figure 3.8. Historic shorelines at Porpoise Bay. The earliest year is 1948 shown in the dark blue and the corresponding years go to light blue, green, yellow, light brown and dark brown. Over the whole shoreline, the net total change between 1948 and 2020 from all the transects was accretion of 4283.4 m. Since 1978 the net change was only 44.1 m of accretion. Between 2013 and 2020 there has been over 10 m of erosion occurring between transects 87 to 95 with transect 91 showing a rate of erosion averaging at ~2.63 m. per year

3.3 Coastal Dynamics

3.3.1 Monkey Island Coastal Dynamics

Transect 27 showed the greatest net change of 24.3 m of erosion. The transects around transect 27 have shown erosion throughout the years excluding between 2005 and 2013 where the shoreline accreted 4.78 m. Erosion patterns at varying levels have occurred between transect 1 – 8, 13 – 15 and 22 - 32 with some of these areas not showing any record of accretion (Fig. 3.9). Transects 2, 5, 8, 9, 11, 16 – 18 had positive net change of accretion no larger than 6.84 m which was shown at transect 5. Areas around transect 8 – 11 and 17 – 19 are classed as stable as the change throughout the years and the overall net change were insignificant. Through the last 75 years, annual rate of change has not exceeded 1 m in accretion. The shoreline had been mostly stable between -0.5 m and 0.5 m of movement on average per year (Fig. 3.9). Between the 2013 and 2021 satellite imagery transect 27 exceeded 1 m/y of erosion.

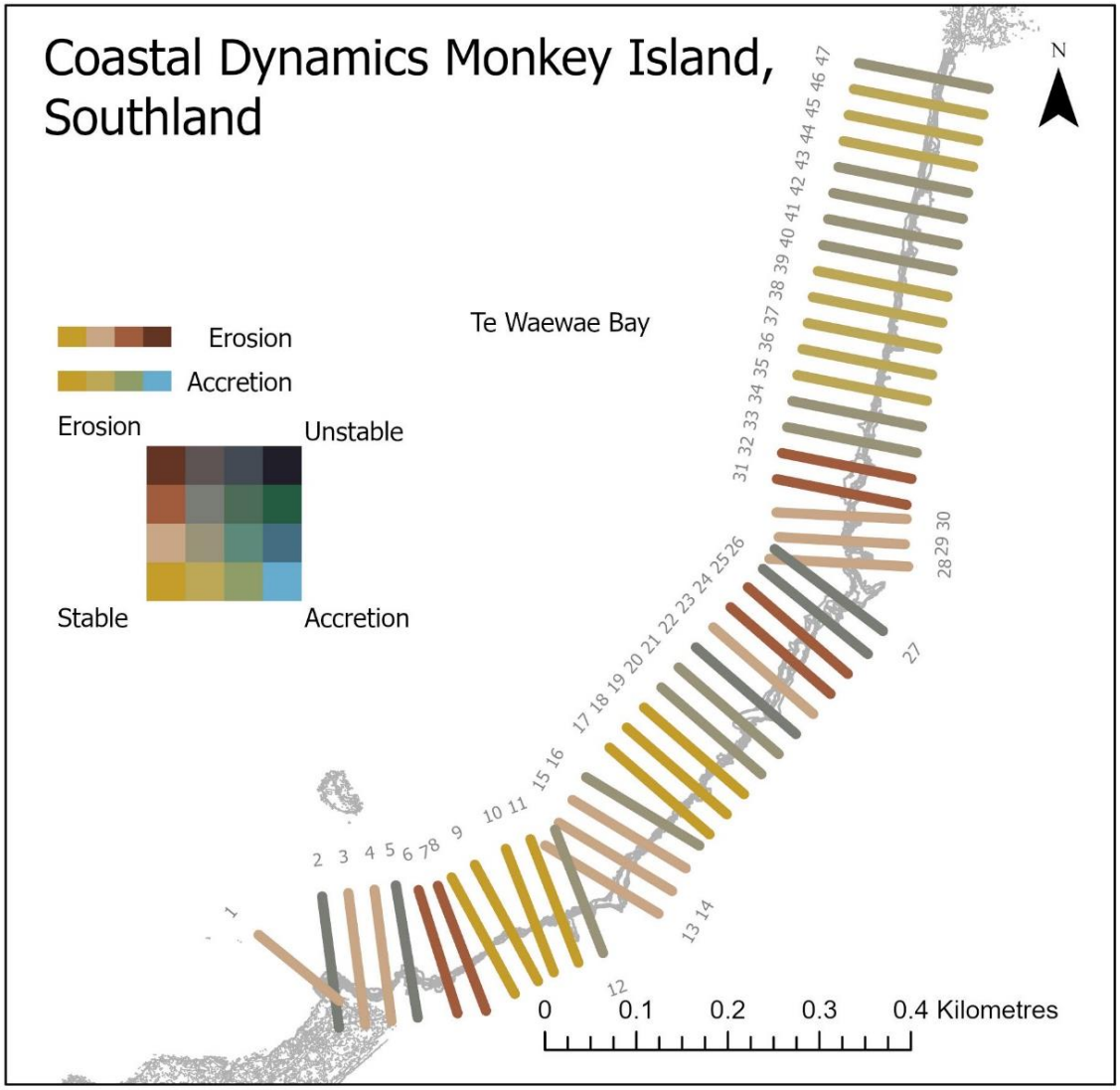

Figure 3.9. Coastal dynamics at Monkey Island, shown via transect lines 20 m apart. There are four main dynamics shown throughout the coastline which are eroding, accreting, stable and unstable. Erosion patterns at varying levels have occurred between transect 1 – 8, 13 – 15 and 22 - 32 with some of these areas not showing any record of accretion. Transects 2, 5, 8, 9, 11, 16 – 18 had positive net change. Areas around transect 8 – 11 and 17 – 19 are classed as stable as the change throughout the years and the overall net change were insignificant. The yellow shows a stable dynamic where movement of the shoreline throughout the years has been minimal. There are no blue transects which shows dominant accreting pattern, but a few are brown which shows a dominating eroding pattern.

3.3.2 Colac Bay Coastal Dynamics

Most of the transects show a stable dynamic (Fig. 3.10). There are two areas where this result is not shown. The first area is between transects 65 - 75 illustrated in figure 3.11. The second area is the dunes at the end of the analysed area show a small flux between erosion and accretion along transects 109 - 119 (Fig. 3.12).

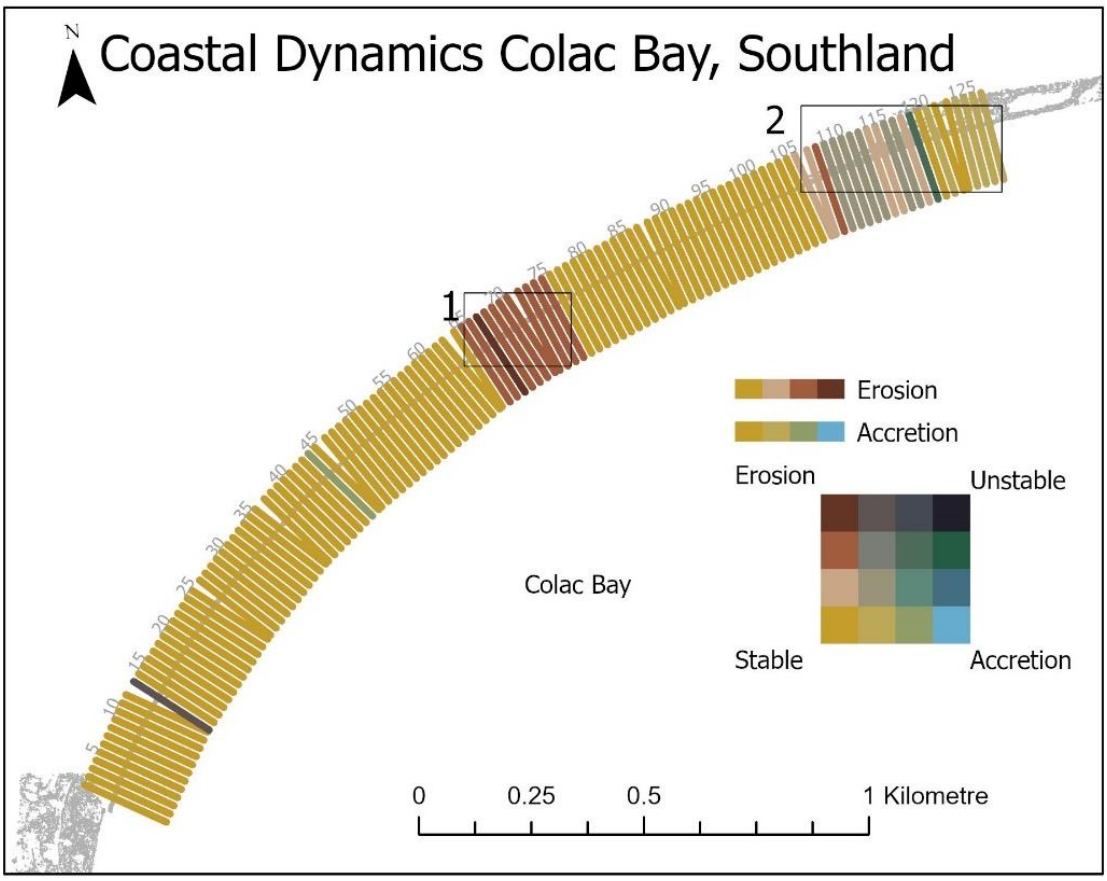

Figure 3.10. Coastal dynamics at Colac Bay, shown via transect lines 20 m apart. There are four main dynamics shown throughout the coastline which are eroding, accreting, stable and unstable. For most of the coastline at Colac Bay, a stable dynamic is shown with the yellow transect lines. Blue shows a dominant accreting pattern which is not shown at this site and brown shows a dominating eroding pattern which is shown between transects 65 - 75. The grey and tan colours at the north-eastern end show transects 109 - 119 where a small flux between erosion and accretion is illustrated.

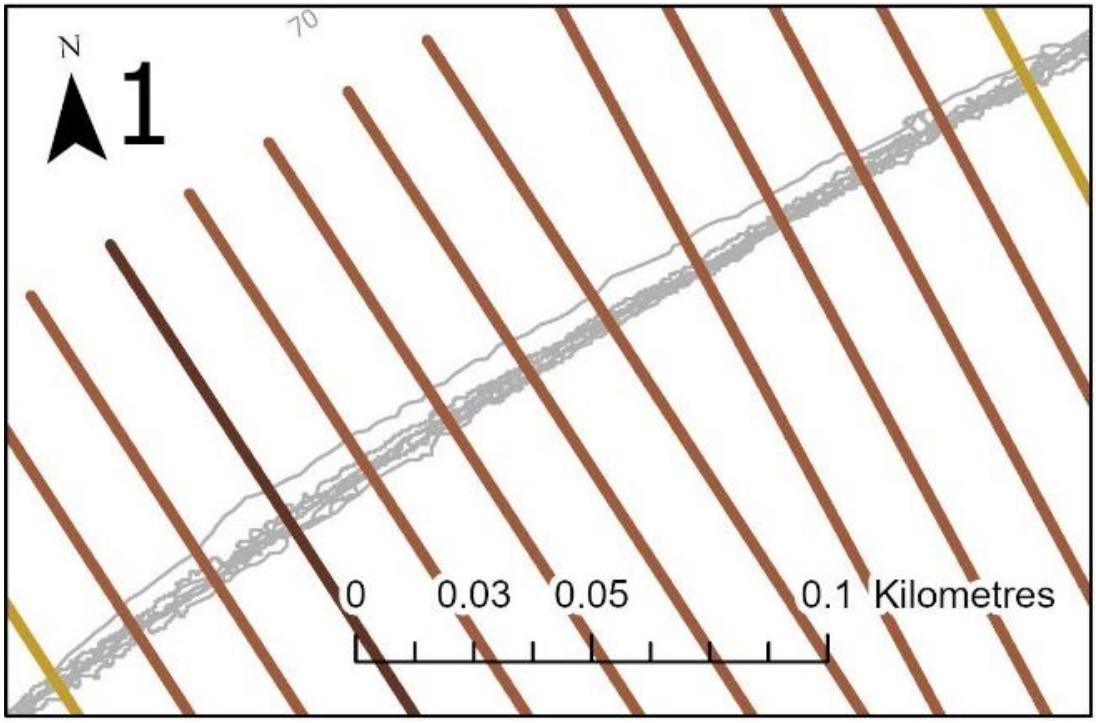

Figure 3.11. Coastal dynamics at Colac Bay, shown via transect lines 20 m apart. There are four main dynamics shown throughout the coastline which are eroding, accreting, stable and unstable. Brown shows a dominating eroding pattern which is shown between transects 65 - 75. Transect 67 shows extreme erosion between the 2014 and 2021 shorelines and the dynamic is expressed as such.

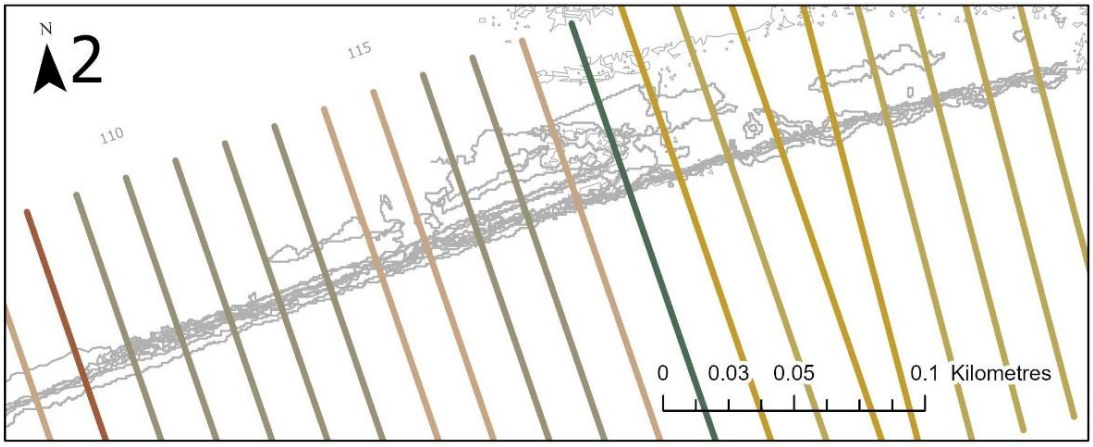

Figure 3.12. Coastal dynamics at Colac Bay, shown via transect lines 20 m apart. There are four main dynamics shown throughout the coastline which are eroding, accreting, stable and unstable. A matrix was created to measure the patterns shown on the transects that illustrated multiple dynamics over the years. The yellow shows a stable dynamic where movement of shoreline throughout the years has been minimal. The green on transect 119 shows an unstable dynamic with more of an accreting pattern being dominant. The grey transect lines shown in this figure show slight erosion and accretion and the tan shows a slight erosion pattern.

3.3.3 Fortrose Coastal Dynamics

Transects 5 to 12 show major erosion with no accretion. Major erosion or instability is shown from the darker transects between transect 5 and 27 (Fig. 3.13). Between these transects were extreme, major, and minor erosion occurring mainly between 1948 and 1978. Transects 45 - 49 show a stable dynamic (Fig. 3.13). There is instability shown between transects 37 – 40 and minor erosion to the southern side of those transects.

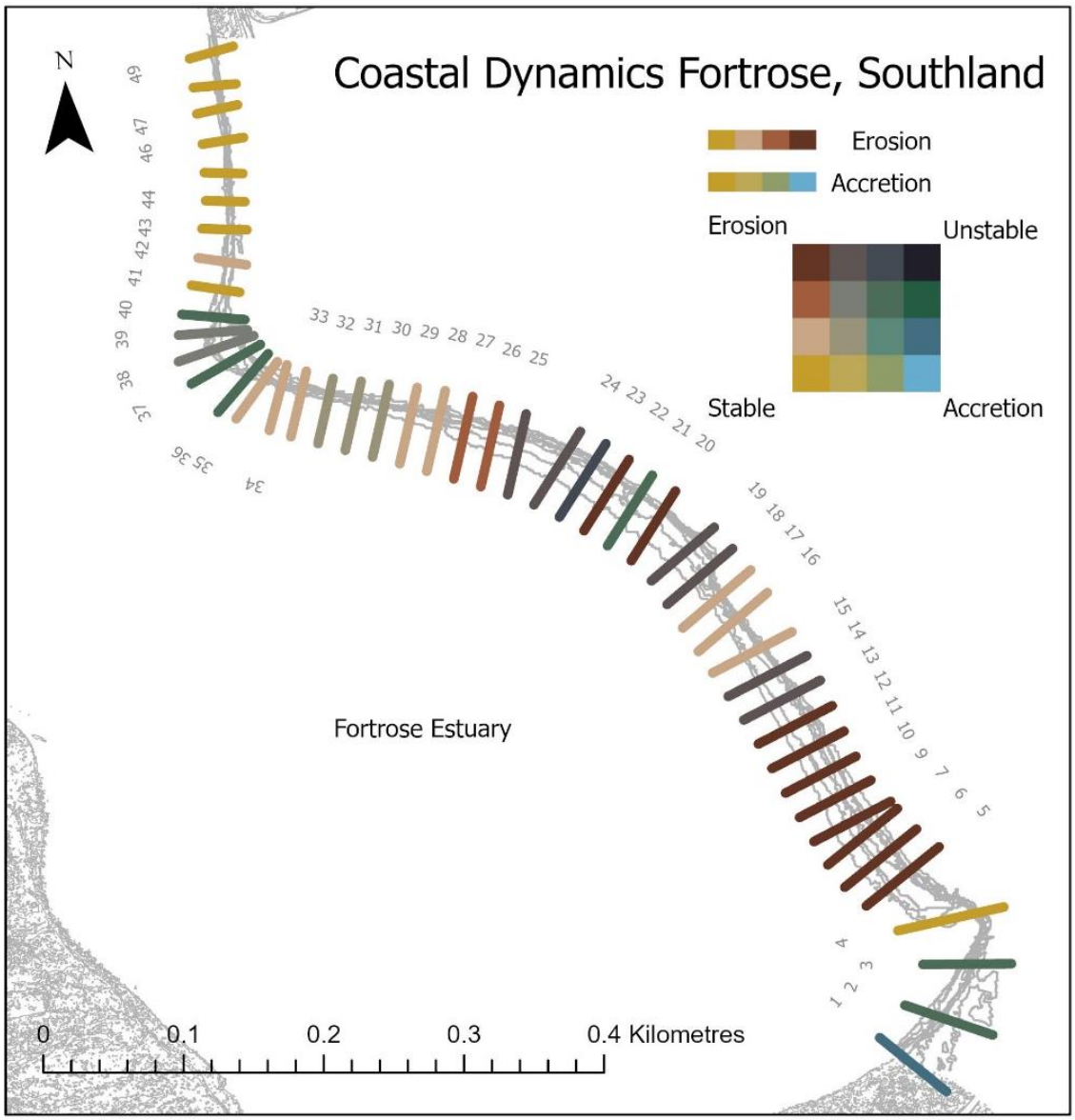

Figure 3.13. Coastal dynamics at Fortrose, shown via transect lines 20 m apart. The yellow shows a stable dynamic where movement of shoreline throughout the years has been minimal which is shown in the northern part of the survey area. The opposite of this is black where major erosion and accretion is shown throughout the shoreline on the same transect line. There is a dominant erosion pattern shown by the dark brown transect lines along the site. Some transects show little erosion and are tan coloured (e.g., 15 - 17) whereas others show strong blue / green illustrating they are patterns of accretion.

3.3.4 Porpoise Bay Coastal Dynamics

With each satellite image surveyed, there was a distinct jump between major erosion and major accretion resulting in the unstable dynamic shown throughout the entire coastline (Fig. 3.14). The bluer transects around transect 40 are in front of the houses that encroach onto the beachfront while the unstable transects around transect 90 and 115 border along sheep paddocks. As said above, even though there are major cycles of erosion and accretion, net change has remained quite small, excluding before 1978.

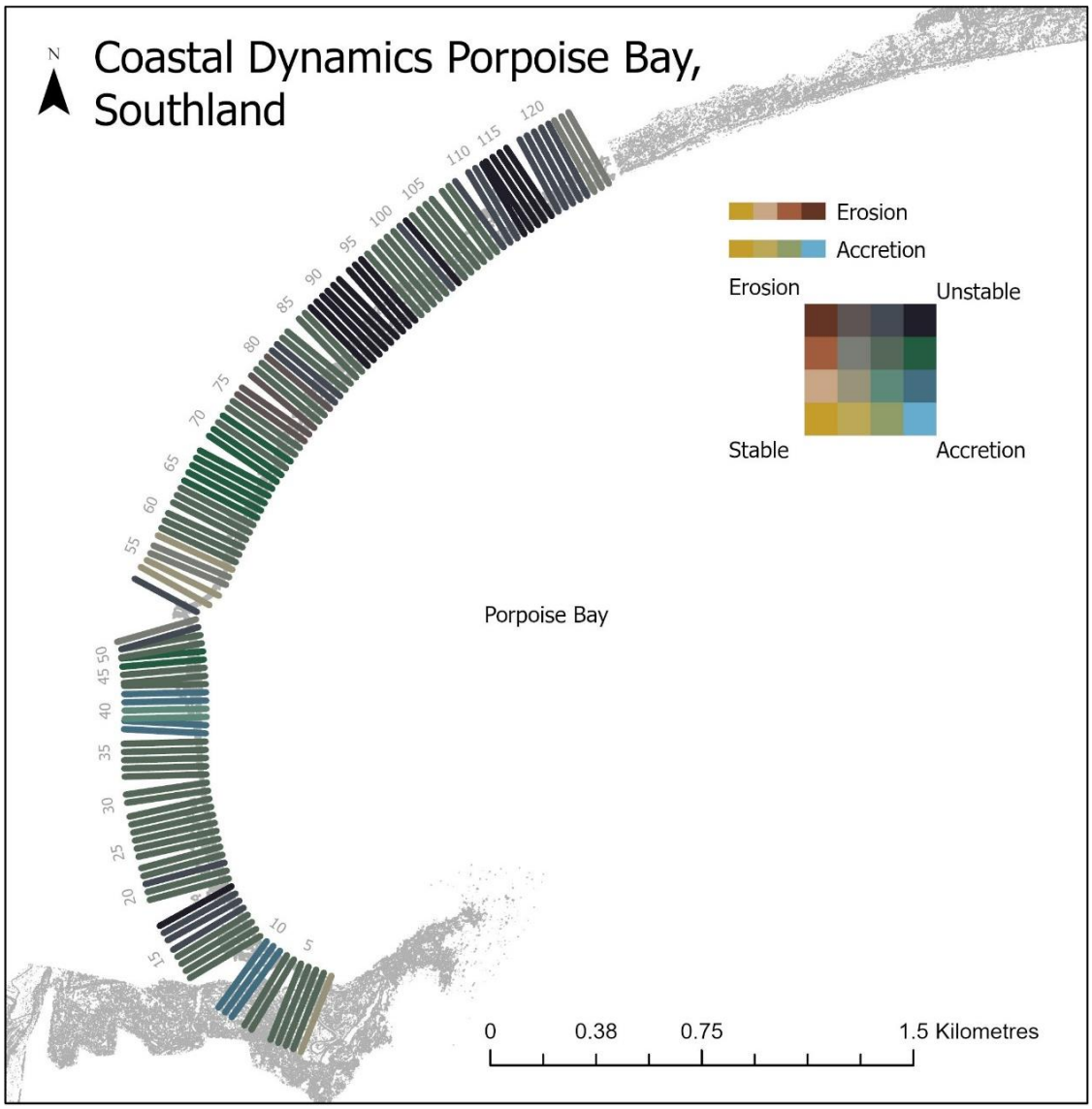

Figure 3.14. Coastal dynamics at Porpoise Bay, shown via transect lines 20 m apart. The black shows where major erosion and accretion is shown throughout the shoreline on the same transect line. Blue shows a dominant accreting pattern. This shoreline shows varying degrees of instability. The bluer transects around transect 40 are in front of the houses that encroach onto the beachfront while the unstable transects around transect 90 and 115 boarders along sheep paddocks. Even though there are major cycles of erosion and accretion, net change has remained quite small after 1978.

3.4 Prediction Maps

3.4.1 Monkey Island Prediction Maps

The shoreline in 20 years' time is predicted to stay close to what it is now (Fig. 3.15). Exceptions to this are between transects 22 – 33 with the manual forecast predicting erosion and some stretches of the shoreline accreting slightly. The gaps in the manual 2041 shoreline prediction show where there was not a significant enough pattern to predict where the shoreline would be or where interpolation would be skewed from the current shoreline between each transect. 21 transects spread along the coast have an insignificant change so are measured to stay in the same place as the current shoreline. The DSAS software predicts the shoreline will accrete a small amount between transects 42- 47 and will erode between transects 22 and 24. Data from the DSAS software is missing for transect 25.

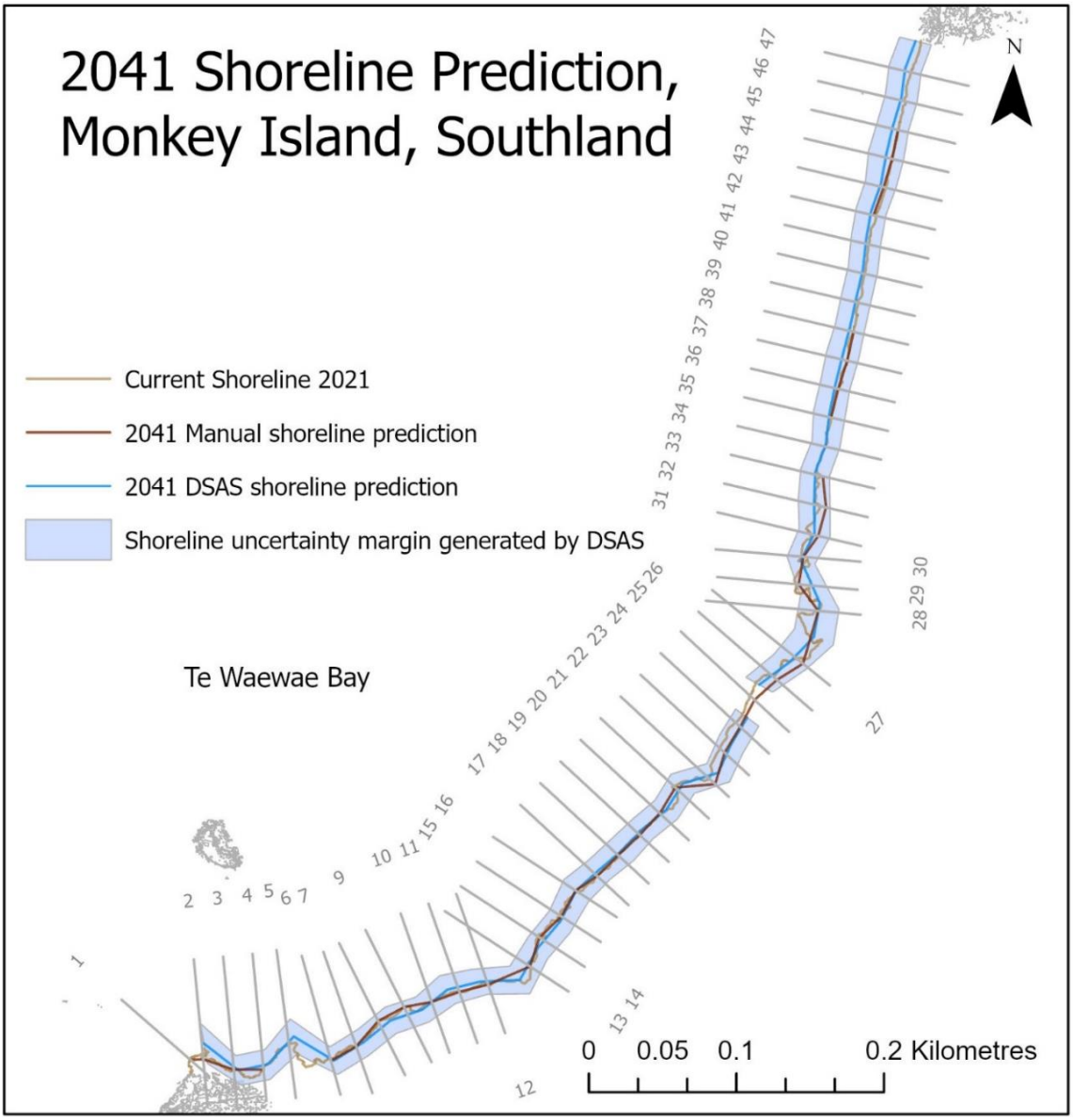

Figure 3.15. Shoreline prediction in 20 years at Monkey Island derived from automated predictions with the DSAS software and manual predictions. The blue line is the DSAS shoreline prediction with an uncertainty margin spanning 20 m either side of the shoreline. The DSAS software discarded transect 25 because it could not predict a pattern along that transect. The manual shoreline prediction has gaps between transect 4 – 6, 33 – 35, 38 – 42 and 45 – 47 because the values extracted show no clear patterns that I could manually predict. The current shoreline in 2021 is below the prediction layers in this map so when you cannot see it, the predictions show no change in the position of the shoreline.

3.4.2 Colac Bay Prediction Maps

The predictions of the shoreline in 20 years for Colac Bay is the same as it is now for most of the shoreline derived from manual and DSAS software predictions. The manual predictions for transects 65 – 75 are based off the average rate of change measure between the 2014 and 2021 satellite images which is between 0.65 and 1.18 metres of erosion. With an average annual estimated rate of change up to 1.18 metres, some of

the coastline may erode up to 23 metres in 20 years (Fig. 3.16). The DSAS software shows less dramatic erosion in figure 3.17. The average rate was calculated to be - 0.03 metres per year. At the most, the DSAS software predicted the shoreline to erode up to 6.3 metres on transect 67. The manual prediction shows the shoreline in 20 years will be very similar to what it is now (Fig 3.18). The DSAS software predicts accretion will occur sporadically along the coast between transect 110 and 127. Transects 106 to 109 are predicted to erode a further 4 metres from where it is now.

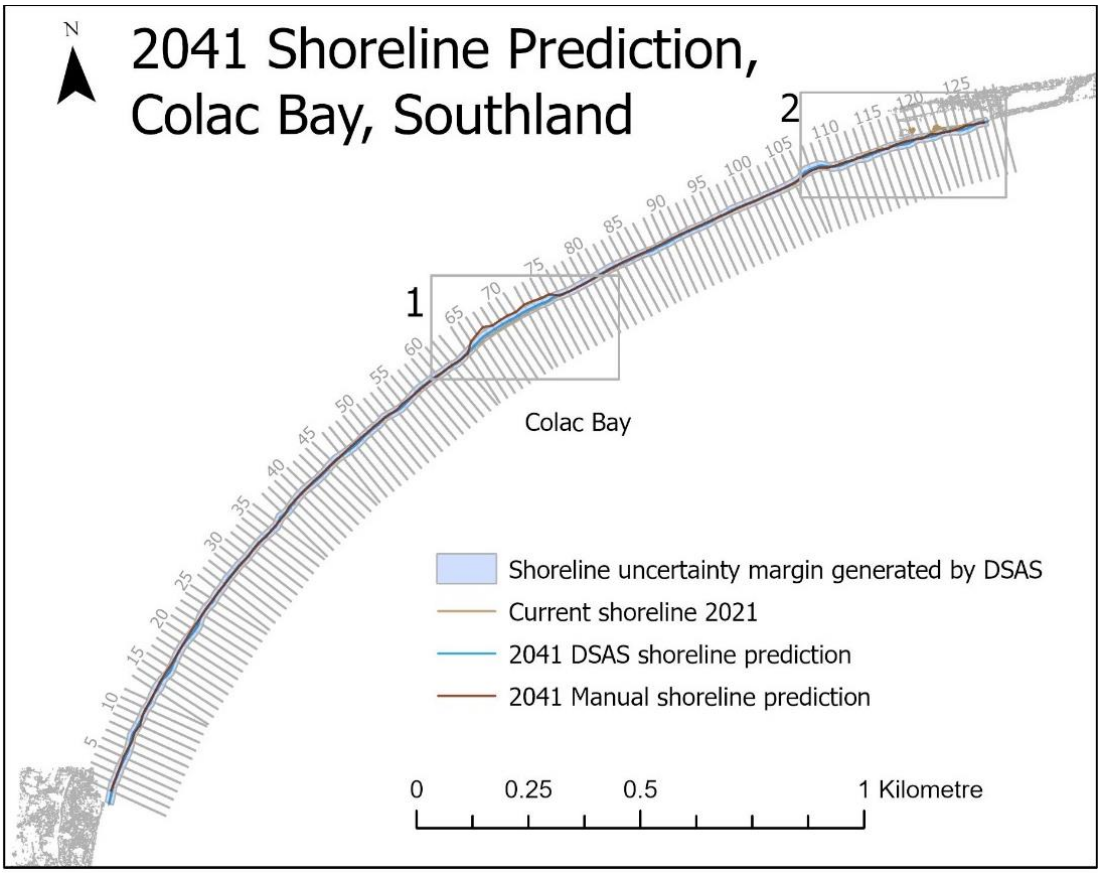

Figure 3.16. Shoreline prediction in 20 years at Colac Bay derived from automated predictions with the DSAS software and manual predictions. The blue line is the DSAS shoreline prediction with an uncertainty margin spanning 20 m either side of the shoreline. Both manual and automated predictions are mostly the same as the 2021 shoreline except between transects 65 – 75 and 109 – 119 which are illustrated in figures 46 and 47.

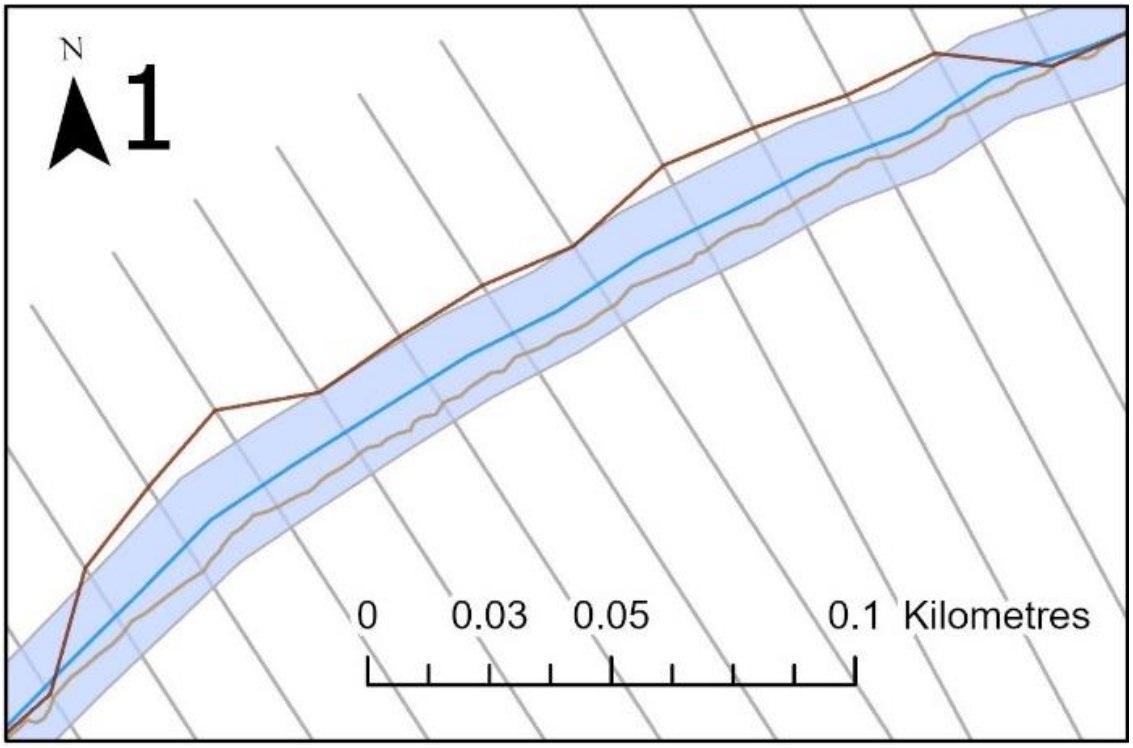

Figure 3.17. Shoreline prediction in 20 years at Colac Bay close up 1 derived from automated predictions with the DSAS software and manual predictions. The blue line is the DSAS shoreline prediction with an uncertainty margin spanning 20 m either side of the shoreline. Both the manual and automated software shows further erosion of this area in the next 20 years shown by the dark brown and blue lines being shoreward of the 2021 shoreline (light brown). The manual prediction is further shoreward because it illustrates the pattern shown from the 2014 survey onwards where human intervention was stopped.

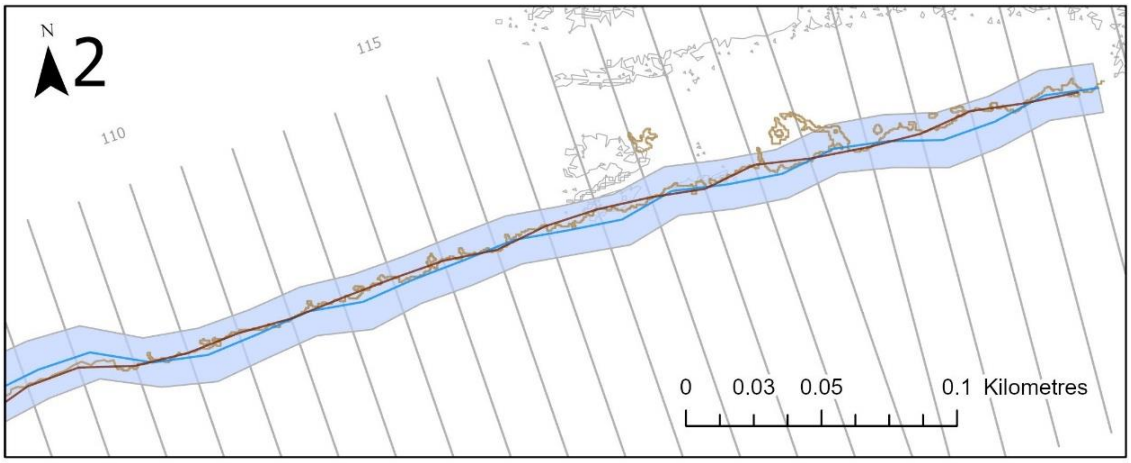

Figure 3.18. Shoreline prediction in 20 years at Colac Bay derived from automated predictions with the DSAS software and manual predictions. The manual prediction shows a similar shoreline to the 2021 shoreline and the automated shoreline (blue) shows accretion in some areas around transects 111, 113 - 114, 117 – 118, 121 and 125. The blue line is the DSAS shoreline prediction with an uncertainty margin spanning 20 m either side of the shoreline. The left hand of the close up shows the DSAS software predicted erosion on transects 107 and 108 where the manual prediction stayed the same as the 2021 shoreline.

3.4.3 Fortrose Prediction Maps

The manual predictions for the Fortrose shoreline are based on past rates of erosion without human intervention. The shoreline will be around the same as it is in 2021 which is shown with the DSAS software prediction (Fig. 3.19). The DSAS software predicts more erosion than the manual prediction between transects 2 - 3, 5, 6 and 33 - 35. Between transects 7 – 10, the manual and DSAS software predicted the shoreline to have eroded around 7 metres in the next 20 years.

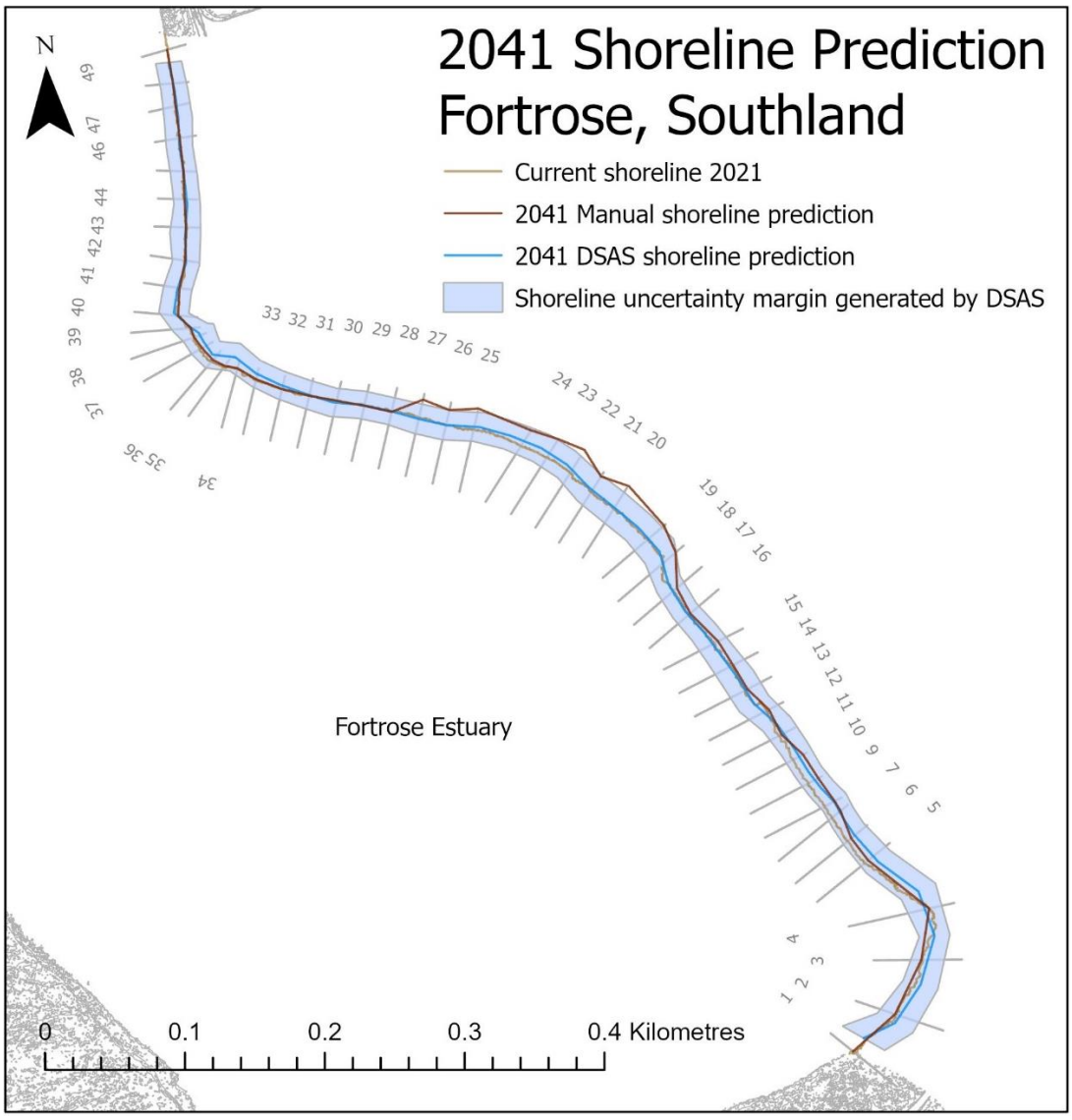

Figure 3.19. Shoreline prediction in 20 years at Fortrose derived from automated predictions (blue) with the DSAS software and manual predictions. The current shoreline in 2021 is below the prediction layers in this map so when you cannot see it, the predictions show no change in the position of the shoreline. The blue line is the DSAS shoreline prediction with an uncertainty margin spanning 20 m either side of the shoreline. The DSAS software predicts more erosion than the manual prediction between transects 2-3, 5, 6 and 33-35. Between transects 7 – 10, the manual and DSAS software predicted the shoreline to have eroded around 7 metres in the next 20 years.

3.4.4 Porpoise Bay Prediction Maps

The DSAS software predicted major accretion between transects 38 – 45 and 106 – 119 (Fig. 3.20). Transects 85 – 92 show the DSAS software predicting the shoreline will be the same as it is now in 20 years and the manual prediction to accrete up to 22 metres which is over 1 m/y.

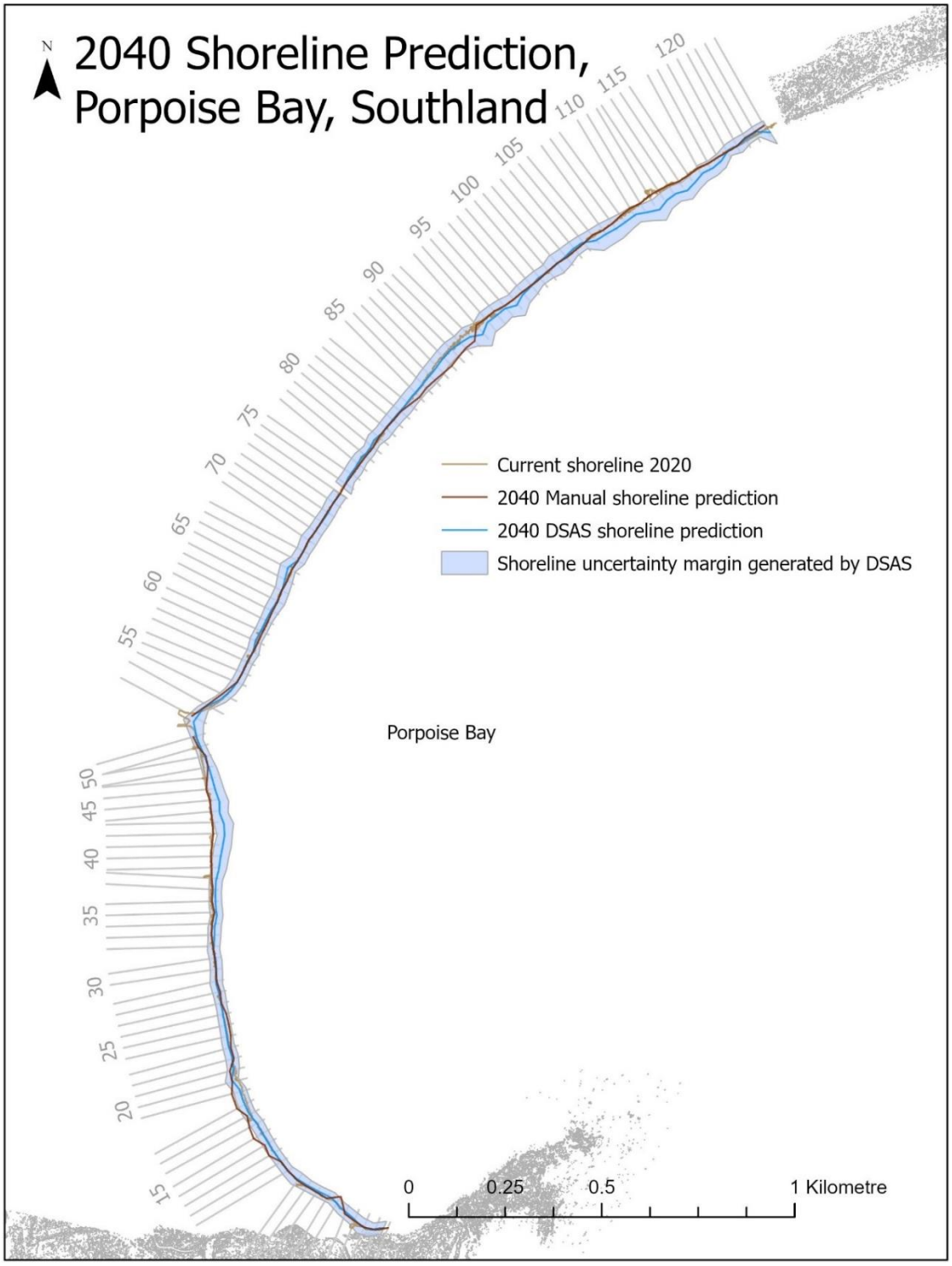

Figure 3.20. Shoreline prediction in 20 years at Porpoise Bay derived from automated and manual predictions. The current shoreline in 2021 is below the prediction layers in this map so when you cannot see it, the predictions show no change in the position of the shoreline. The DSAS software predicted large areas will accrete significantly in 20 years. Between transects 38 and 45, the manual prediction based this shoreline off the fact that the accretion occuring was a human intervention and that although it will not continue along this pattern, it is likely it will continue to be maintained at the current shoreline.

3.5 Volume Maps

3.5.1 Monkey Island Volume Maps

The following maps of Monkey Island each illustrate the relative height change between two temporal point clouds resulting in the volume change over the course of several months. There is a small build-up of sand on the beach illustrated between the February and August surveys (Fig. 3.21). The coastline itself shows small hotspots of erosion and accretion both up to 1.5 m. Between the February and August shoreline there is 235.759 m³ of added volume and 94.989 m³ of removed volume (Table 3.2). For comparisons of this survey area with the above historic shoreline, coastal dynamic and prediction maps, this survey is along transects 13 to 21.

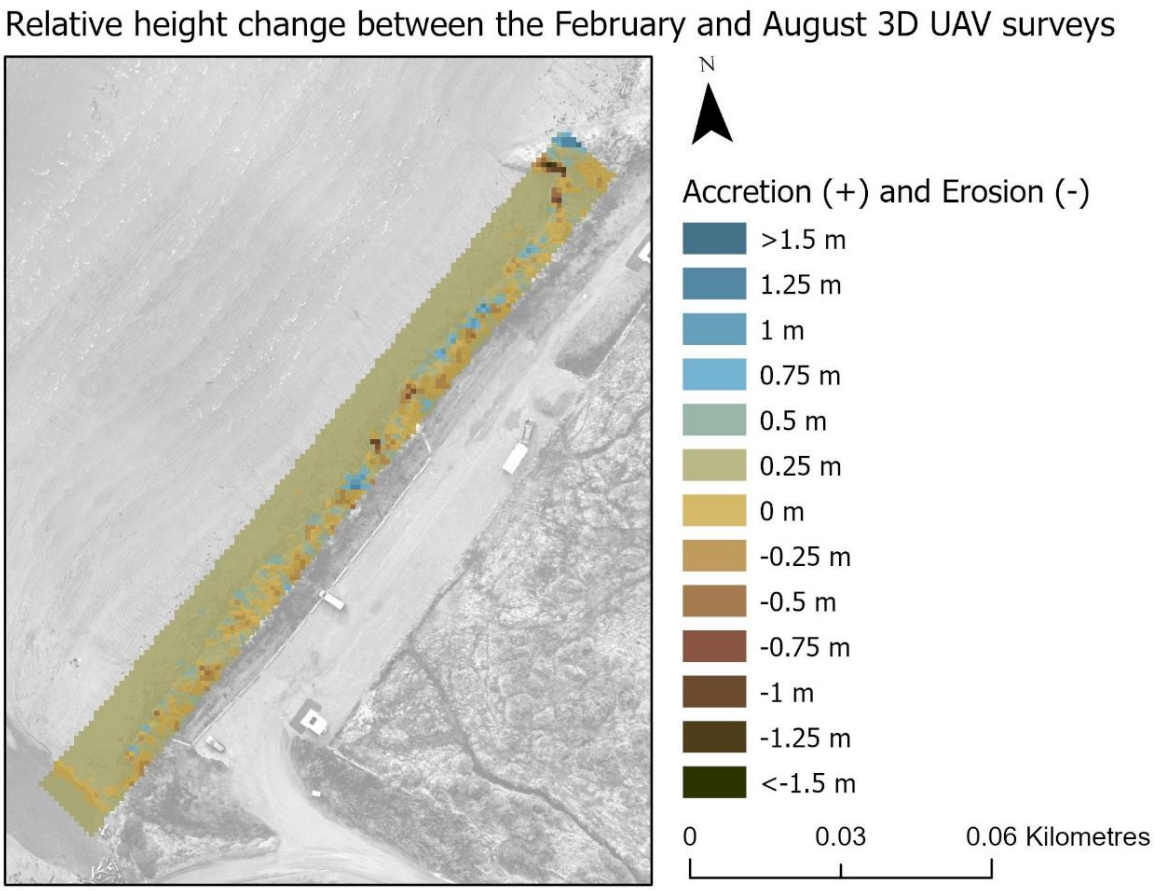

Figure 3.21. Relative height between the February and August point cloud survey at Monkey Island. There is 235.759 m³ of added volume and 94.989 m³ of removed volume. The coastline itself shows small hotspots of erosion and accretion both up to 1.5 m by the blue and dark brown patches shown in the middle and at the top of the survey area.

Between August and December surveys (Fig. 3.22) there is a distinct line of erosion along the shoreline with up to 1.75 m of negative change between the surveys shown

with the dark brown line. 731.101 m³ has been taken away between August and December where only 33.373 m³ has been added.

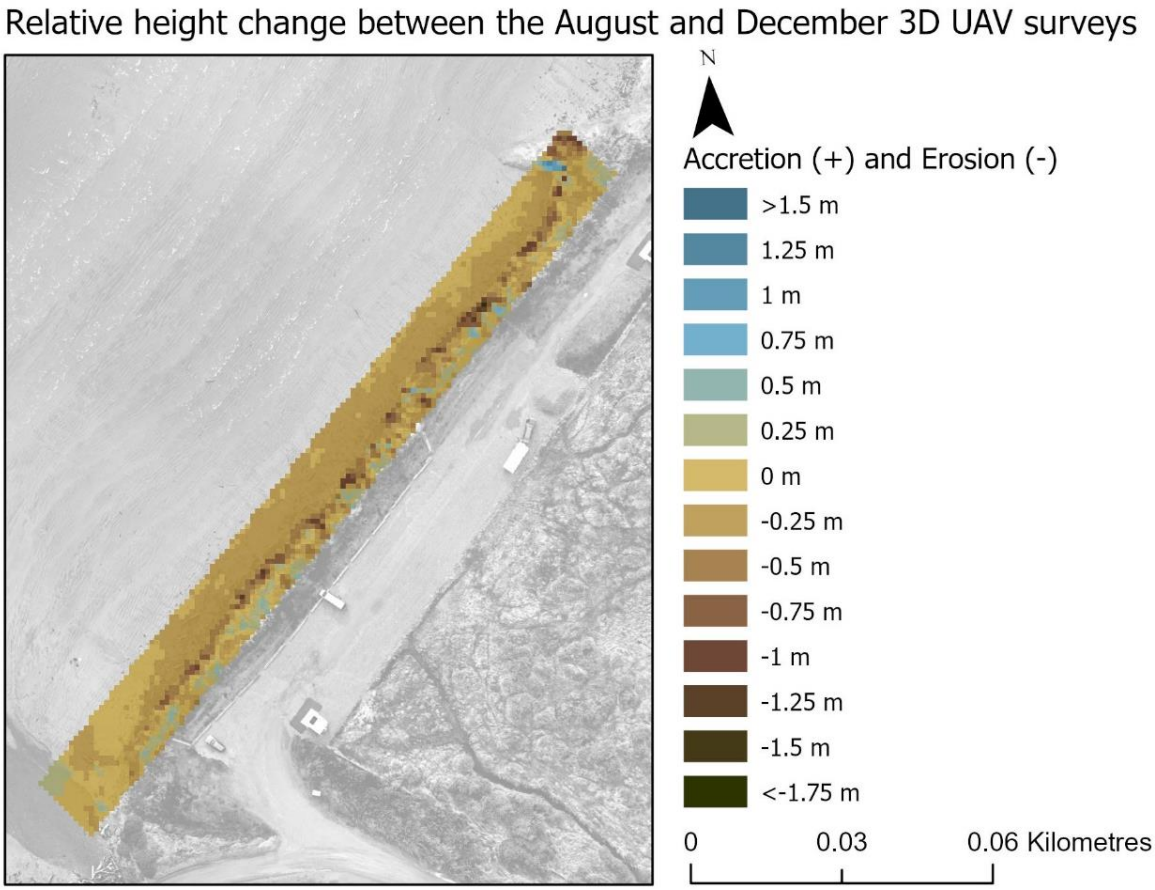

Figure 3.22. Relative height between the August and December point cloud survey at Monkey Island. 731.101 m³ have been taken away where only 33.373 m³ had been added. There is a distinct line of erosion along the shoreline with up to 1.75 m of negative change between the surveys shown with the dark brown line. The seaward site of the survey area shows slight erosion and stability with the yellow and lighter brown colours.

Table 3.2 Monkey Island removed and added volume (measured in m^3) values between each survey. The added and removed volume between each survey is standardised to $100m^2$ to simplify comparisons. Matching cells measure the certainty of the values given with a confidence percentage derived from the CloudCompare software. The 'Figure #' states the figure correspondent with the row. The final row shows the change between the first and last surveys to illustrate the sum of the change in volume.

Site	Survey	Added Volume	Standardised added volume ($100m^2$)	Removed Volume	Standardised removed volume ($100m^2$)	Matching Cells (Certainty)	Figure #
Monkey Island	February to August	(+) 235.759	(+) 9.412	(-) 94.989	(-) 3.792	96.8%	3.21
Monkey Island	August to December	(+) 33.373	(+) 1.332	(-) 731.101	(-) 29.186	97.6%	3.22
Monkey Island	February to December	(+) 17.745	(+) 0.708	(-) 574.241	(-) 22.924	98.8%	3.23

The overall change between the February and December shows only 17.745 m^3 of volume was added throughout the year and 574.241 m^3 was removed (Fig. 3.23). The yellow brown across the whole survey, shows there is little significant change of the volume. This map shows a linear change between two points of the survey years and illustrates the information that can be missed without a winter survey.

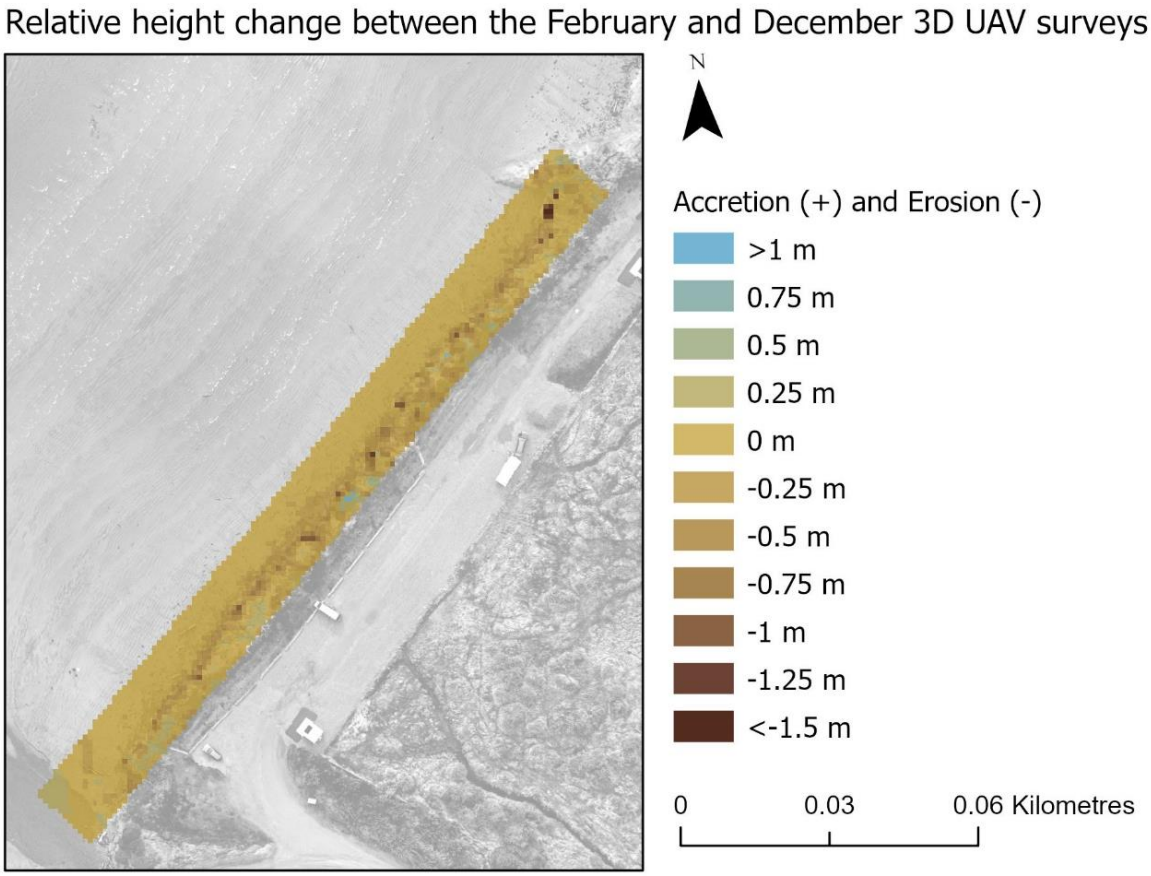

Figure 3.23. Relative height between the February and December point cloud survey at Monkey Island. 17.745 m³ of volume was added throughout the year and 574.241 m³ was removed. The yellow brown across the whole survey shows there is little significant change of the volume. There are very small patches of erosion throughout the shoreline, the most significant being at the top of the survey area. Little accretion has occurred.

3.5.2 Colac Bay Volume Maps

The results illustrate the relative height change between two temporal point clouds. There were high levels of accretion occurring along the eastern part of the survey area at Colac Bay (Fig 3.24). 152. 859 m³ of volume was added between the February and August surveys which is over double the value of removed volume at 68.780 m³ (Table 3.3). The accretion (blue) shows that there will be uncertainty in the results as the relative height between the road from the February and August surveys (likewise the August – December and February – December results) should not have changed. For comparison between the above results and the 3D UAV results, this survey captures the area between transects 75 and 83.

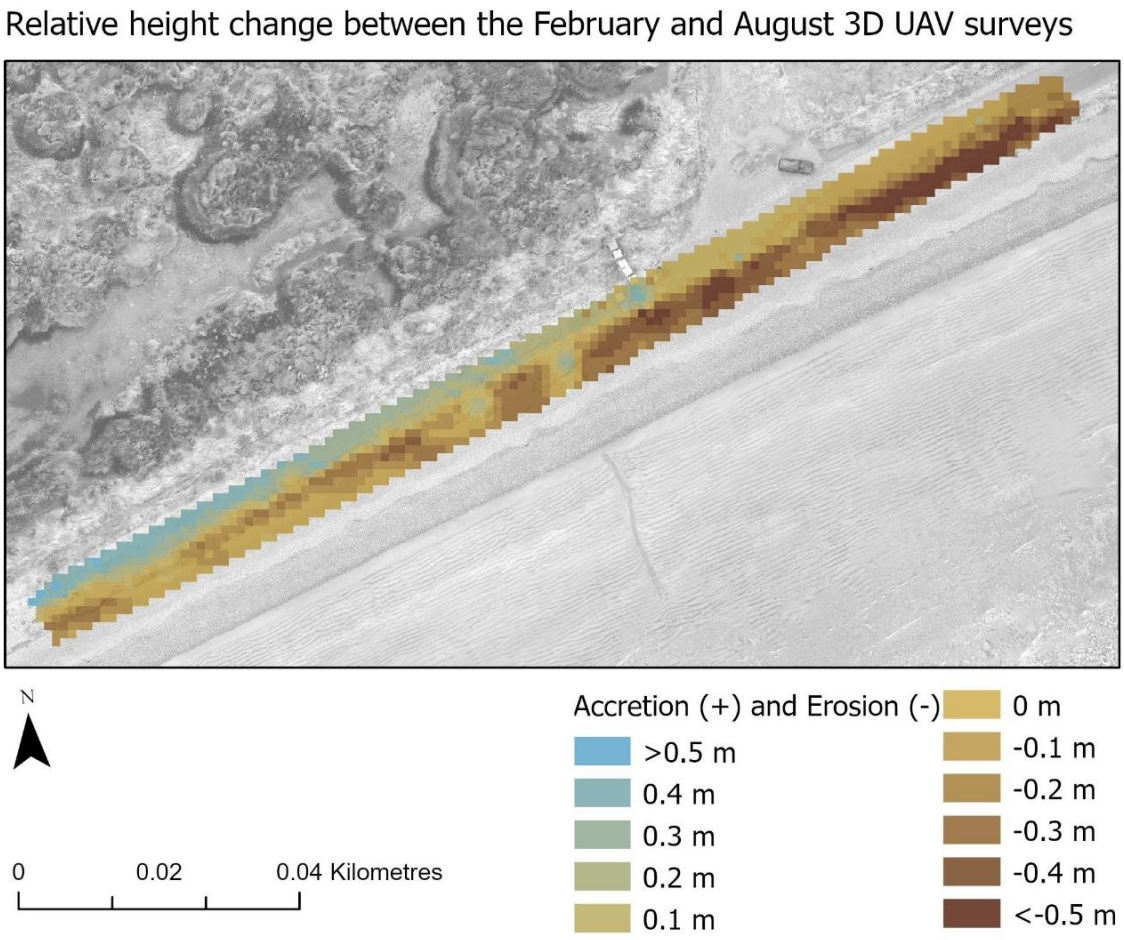

Figure 3.24. Relative height between the February and August point cloud survey at Colac Bay. 152. 859 m^3 of volume was added which is over double the value of removed volume at 68.780 m^3. there is a distinct line of removed volume along the south-eastern part of the survey shown by the darker brown areas. The blue added volume in the northern length of the survey area is overlaying the coastal road.

A large removal of volume from August to December is shown by the dark brown colour throughout the southern length of the survey area (Fig. 3.25). Brown sections in the survey area show the removal of substrate encroaching on the eroding coastal road. 301.903 m^3 of sediment is lost from the August to December survey and only 17.233 m^3 was added (Table 3.3).

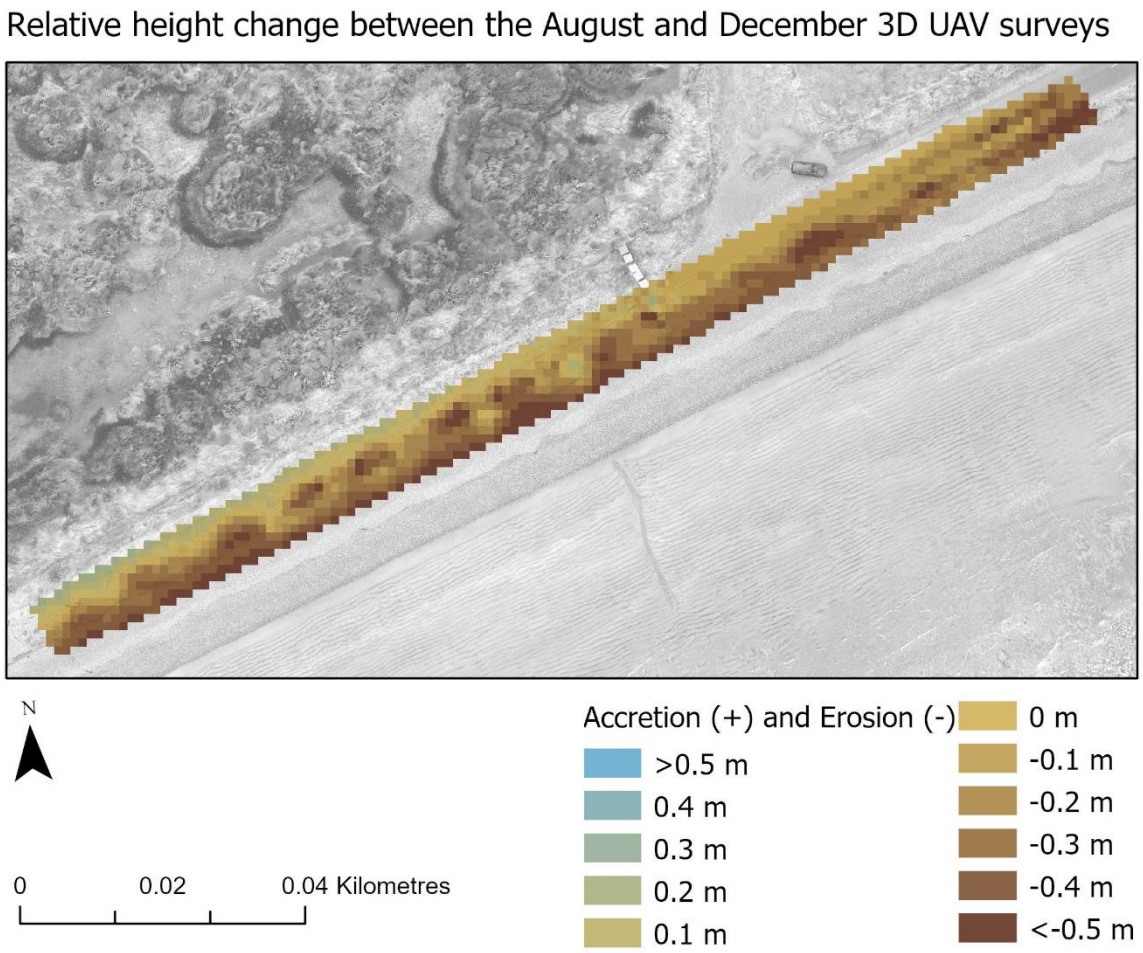

Figure 3.25. Relative height between the August and December point cloud survey at Colac Bay. 301.903 m^3 of sediment is removed shown by the dominant brown along the southern length of the survey and only 17.233 m^3 of volume was added. Throughout the middle of the survey area are rounded brown sections which show the removal of substrate encroaching on the eroding coastal road.

The relative height change between the February and December 3D UAV surveys shows the overall change from the first to last survey times (Fig. 3.26). The south-eastern corner of the survey area shows major erosion over the space of 10 months with 218.616 m^3 missing and only 9.353 m^3 added (Table 3.3).

Table 3.3 Colac Bay removed and added volume (measured in m^3) values between each survey. The added and removed volume between each survey is standardised to $100m^2$ to simplify comparisons. Matching cells measure the certainty of the values given with a confidence percentage derived from the CloudCompare software. The 'Figure #' states the figure correspondent with the row. The final row shows the change between the first and last surveys to illustrate the sum of the change in volume.

Site	Survey	Added Volume	Standardised added volume ($100m^2$)	Removed Volume	Standardised removed volume ($100m^2$)	Matching Cells (Certainty)	Figure #
Colac Bay	February to August	(+) 152.859	(+) 15.165	(-) 68.780	(-) 6.823	92.7%	3.24
Colac Bay	August to December	(+)17.233	(+) 1.710	(-) 301.903	(-) 29.951	97.5%	3.25
Colac Bay	February to December	(+) 9.353	(+) 0.928	(-) 218.616	(-) 21.688	96.2%	3.26

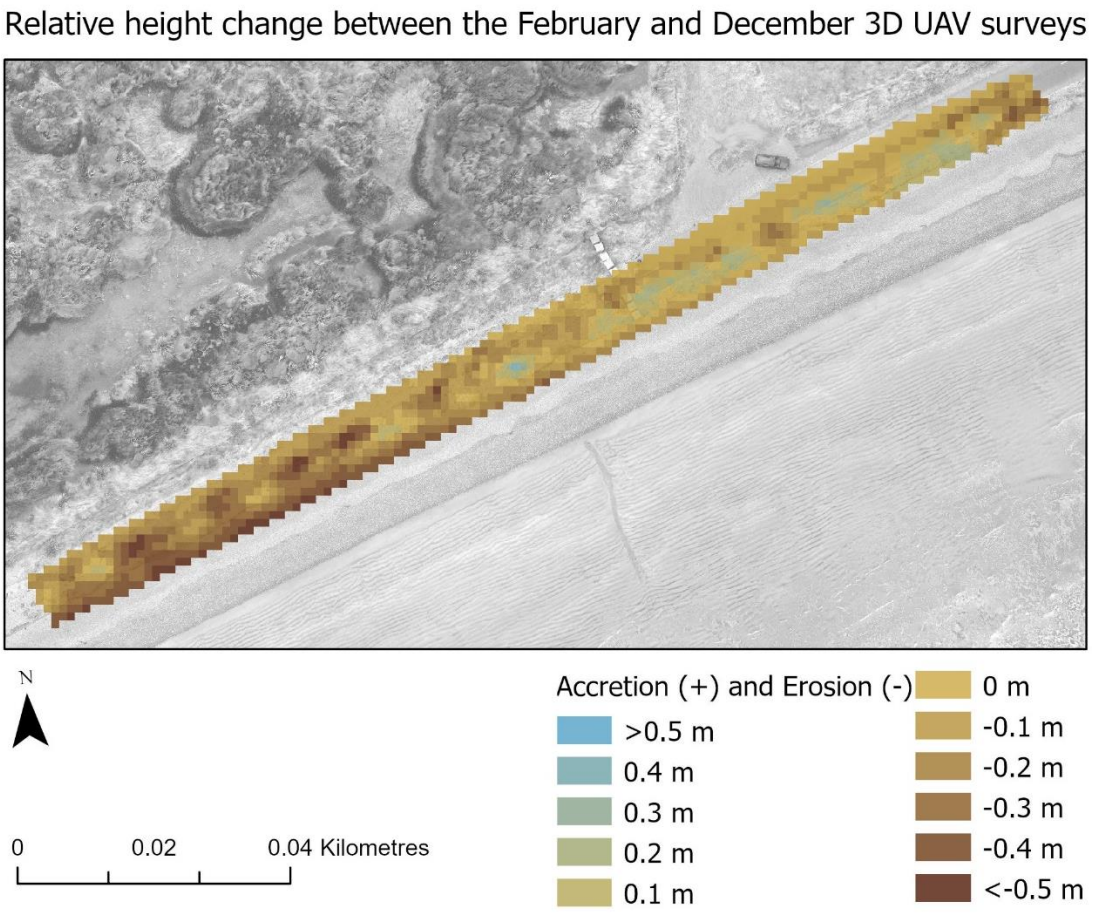

Figure 3.26. Relative height between the February and December point cloud survey at Colac Bay. 218.616 m^3 of volume was removed and only 9.353 m^3 was added. This shows that the dominant dynamic was erosion with dark brown patches shown throughout the bottom left of the survey area and minimal volume added with faint blue patches throughout the middle and right side of the survey area.

3.5.3 Fortrose Volume Maps

The results illustrate the relative height change between two temporal point clouds. For comparisons of the volumetric survey area with the above historic shoreline, coastal dynamic and prediction maps, this survey is along transects 10 – 18. Slight erosion along the estuary is shown on the seaward side of the point cloud between the February and August surveys (Fig. 3.27). Erosion is shown along the south-eastern end of the shoreline with the dark brown line spanning 30 m of the survey area. Erosion is the dominant dynamic between these surveys with 1766.031 m^3 of substrate being removed and only 23.355 m^3 added (Table 3.4). The opposite is shown in figure 57, where accretion is the dominant dynamic with 2489.657 m^3 added and 84.821 m^3 removed.

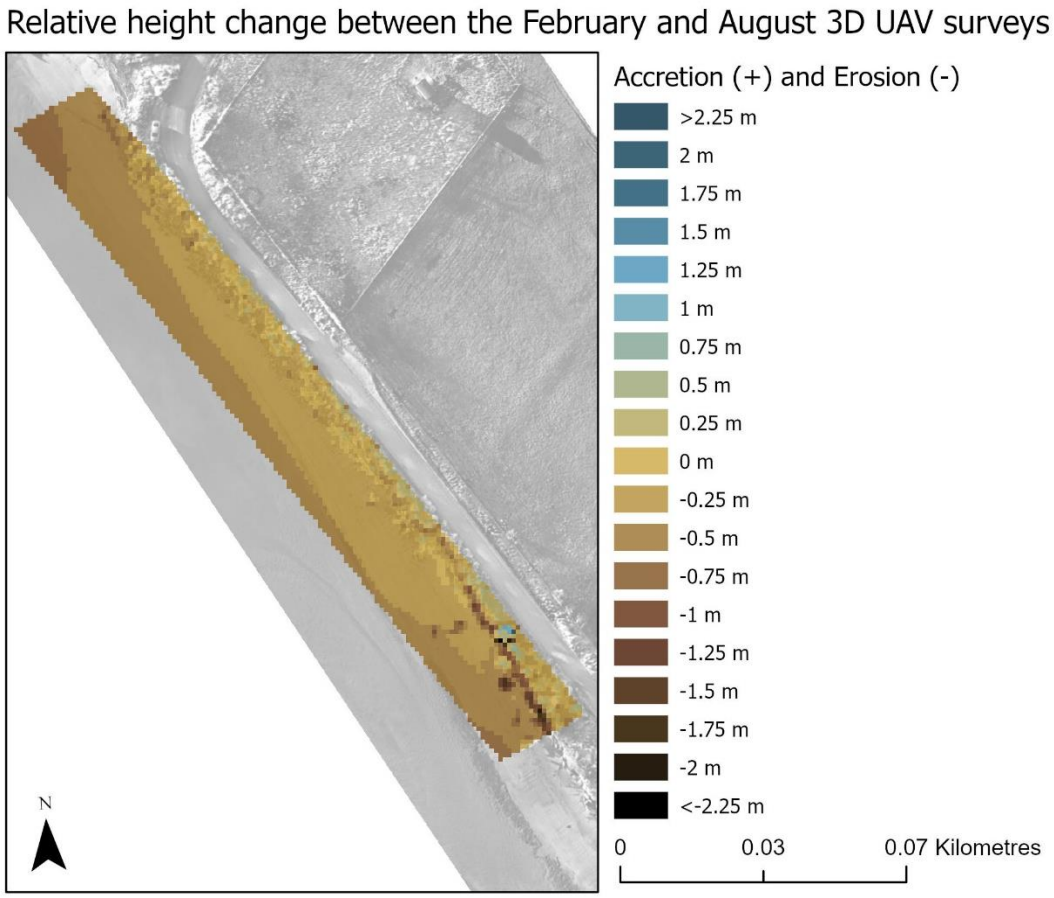

Figure 3.27. Relative height between the February and August point cloud survey at Fortrose. There is slight erosion along the estuary shown on the seaward side of the point cloud. Erosion is shown along the south-eastern end of the shoreline with the dark brown line spanning 30 m of the survey area. There are little patches of added volume in the of the survey site on the landward side of the brown line of removed volume. Erosion is the dominant dynamic between these surveys with 1766.031 cubic metres of substrate being removed and only 23.355 added

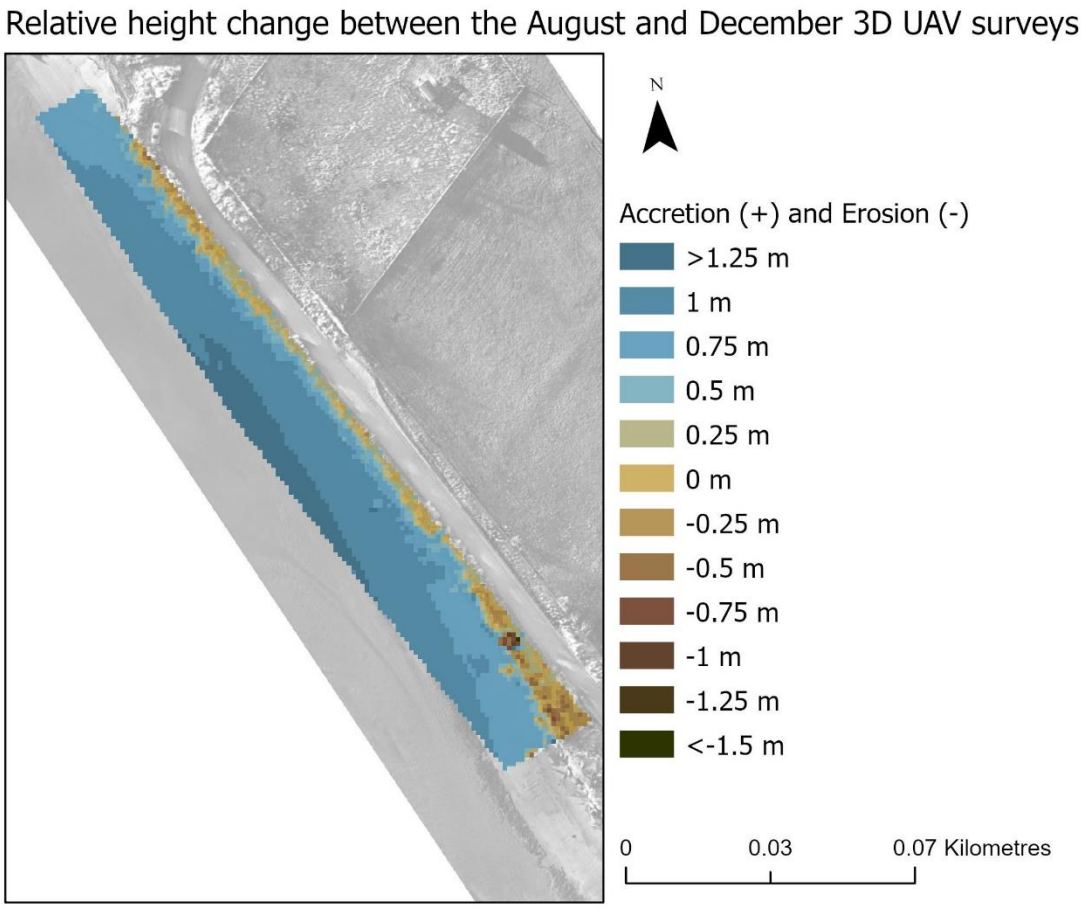

Figure 3.28. Relative height between the August and December point cloud survey at Fortrose. Major accretion is shown along the sand on the seaward side of the shoreline. This illustrates the change in volume in an estuary environment throughout the year. Accretion is the dominant dynamic because 2489.657 m^3 of volume was added and 84.821 m^3 was removed from the survey site. There is a dark brown point of removed volume which aligns with a point of accretion in the February to August point cloud.

The overall volume change between February and December was 1105.011 m^3 of added volume and 214.123 m^3 removed (Fig. 3.29). Most of this accretion was on the sand in the estuary and not the shoreline itself.

Table 3.4 Fortrose removed and added volume (measured in m^3) values between each survey. The added and removed volume between each survey is standardised to $100m^2$ to simplify comparisons. Matching cells measure the certainty of the values given with a confidence percentage derived from the CloudCompare software. The 'Figure #' states the figure correspondent with the row. The final row shows the change between the first and last surveys to illustrate the sum of the change in volume.

Site	Survey	Added Volume	Standardised added volume ($100m^2$)	Removed Volume	Standardised removed volume ($100m^2$)	Matching Cells (Certainty)	Figure #
Fortrose	February to August	(+) 23.355	(+) 0.590	(-) 1766.031	(-) 44.597	97.6%	3.27
Fortrose	August to December	(+) 2489.657	(+) 62.870	(-) 84.821	(-) 2.142	92.5%	3.28
Fortrose	February to December	(+) 1105.011	(+) 27.904	(-) 214.123	(-) 5.407	93.1%	3.29

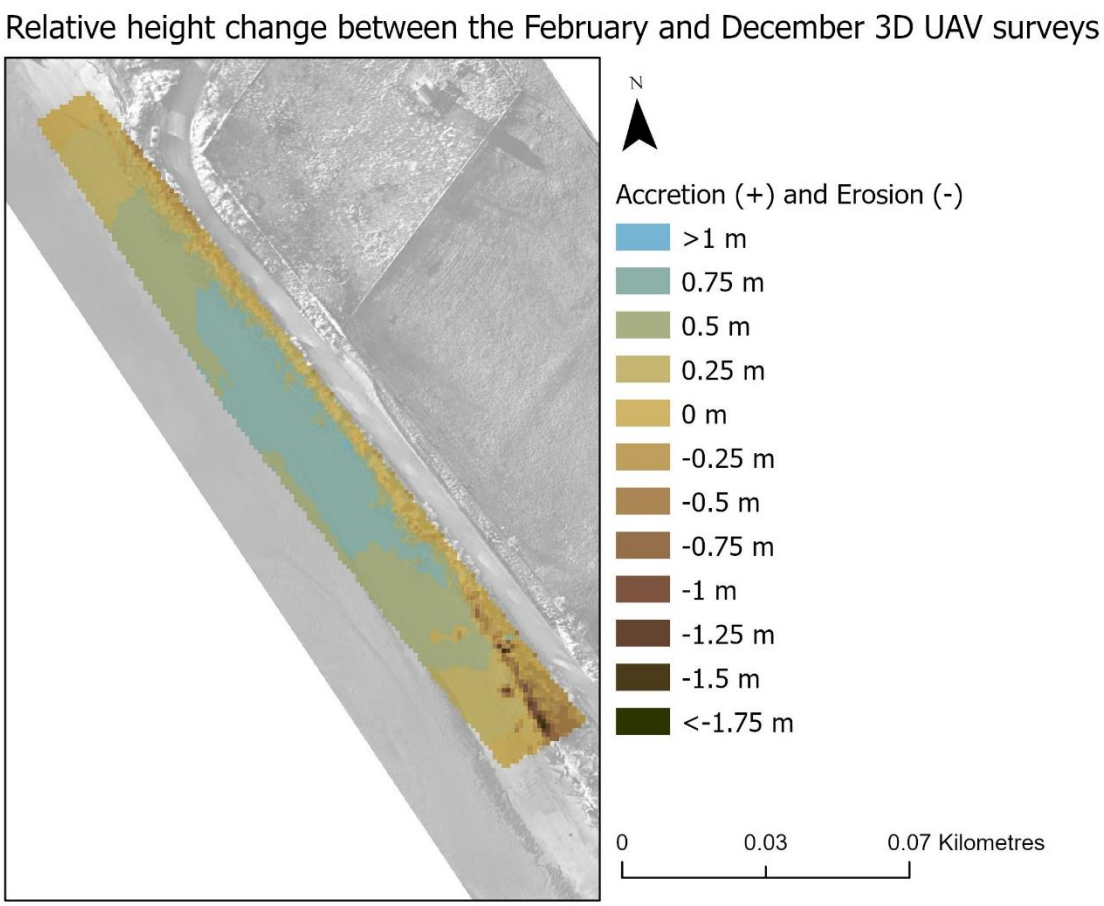

Figure 3.29. Relative height between the February and December point cloud survey at Fortrose. The overall volume change was 1105.011 m^3 of added volume and 214.123 m^3 removed. The accretion is from the sand at the base of the shoreline. The shoreline itself shows little change apart from the removed volume at the south-eastern end of the survey site shown by the brown line.

3.5.4 Porpoise Bay Volume Maps

The results illustrate the relative height change between two temporal point clouds. For comparisons of this survey area with the above historic shoreline, coastal dynamic and prediction maps, this survey is along transects 66 – 75. Major erosion is shown in the middle of the survey area both along the shoreline and the sand on the beach between February and August (Fig. 3.30). 1870.292 m³ of volume has been removed from the survey area where only 271.400 m³ has been added. The north and south ends of the survey area along the dune vegetation shows added volume.

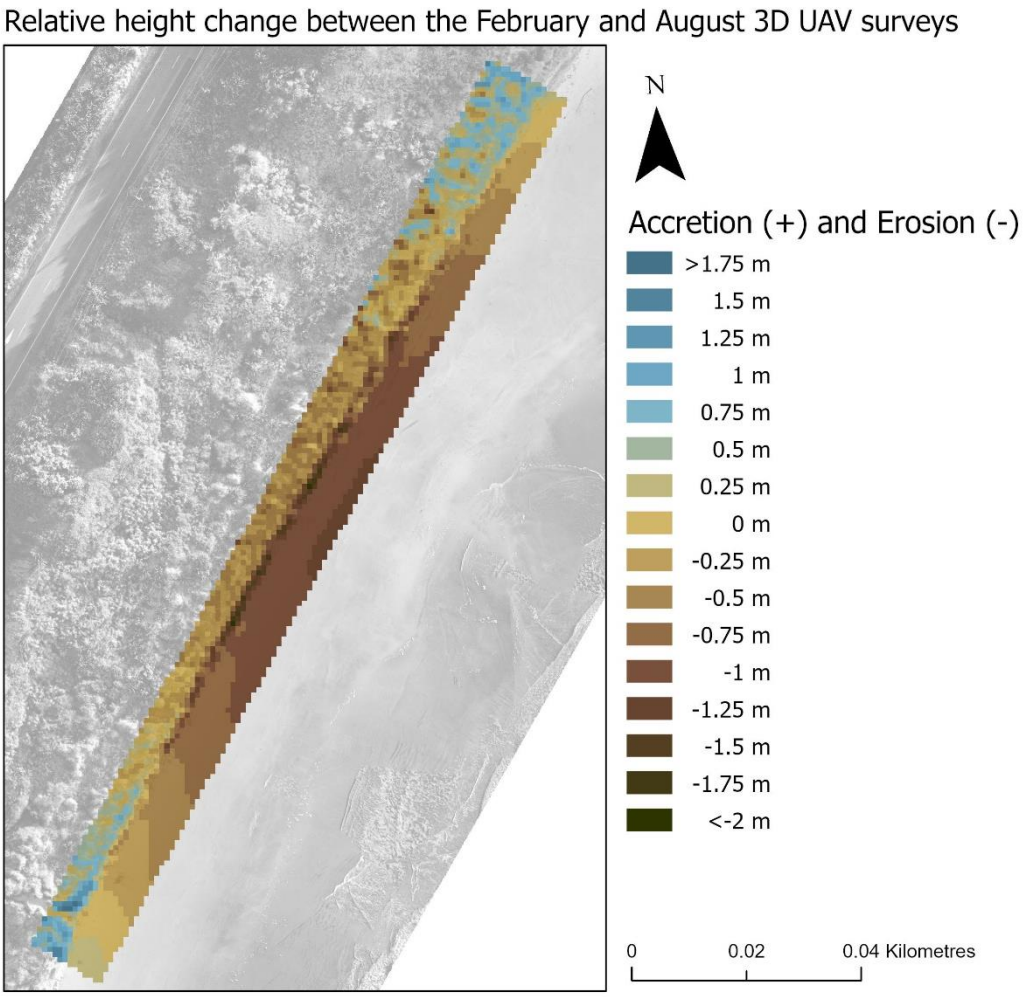

Figure 3.30. Relative height between the February and August point cloud survey at Porpoise Bay. This map shows major erosion in the middle of the survey area both along the shoreline and the sand on the beach. 1870.292 m³ of volume has been removed from the survey area and 271.400 m³ has been added.

The August to December survey shows a very distinct line of removed volume along the shoreline illustrated by the dark brown (Fig. 3.31). 1108.910 m³ of sediment is removed concentrating on the shoreline itself and 881.907 m³ of volume was added throughout the beach and vegetation around the centre of the survey area (Table 3.5).

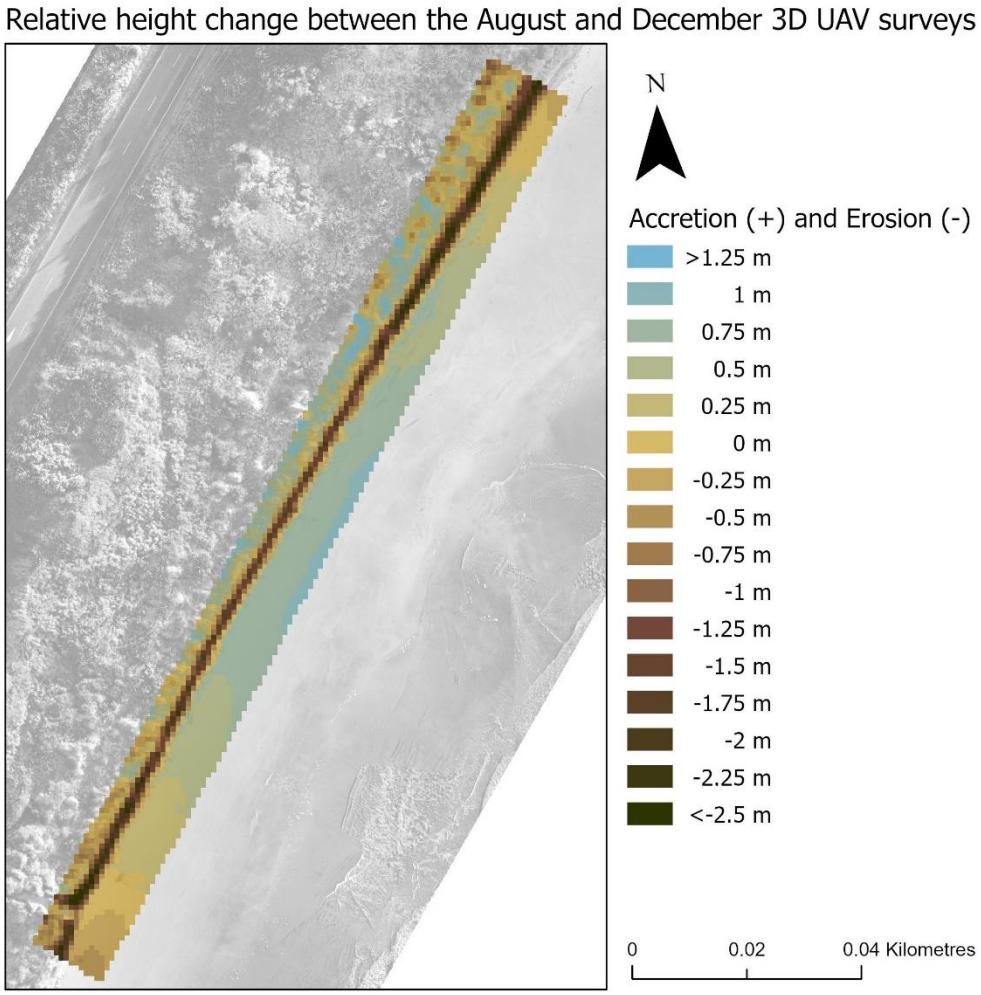

Figure 3.31. Relative height between the August and December point cloud survey at Porpoise. 1108.910 m^3 of sediment is removed shown by the dominant brown along the seaward side of the survey and 881.907 m^3 of volume was added. Added volume is shown throughout the sand on the beach and the vegetation behind the shoreline.

The yellow throughout most of the beach and vegetation shows little change over the entire span of the surveys. There is a distinctive line of volume removed along the shoreline which illustrates major erosion over the course of the survey. Overall, there was 1984.994 m^3 of volume removed from the survey area (Fig. 3.32). There are little patches of added volume at the north and south ends of the survey area which adds up to 136.234 m^3 (Table 3.5).

Table 3.5 Porpoise Bay removed and added volume (measured in m^3) values between each survey. The added and removed volume between each survey is standardised to $100m^2$ to simplify comparisons. Matching cells measure the certainty of the values given with a confidence percentage derived from the CloudCompare software. The 'Figure #' states the figure correspondent with the row. The final row shows the change between the first and last surveys to illustrate the sum of the change in volume.

Site	Survey	Added Volume	Standardised added volume ($100m^2$)	Removed Volume	Standardised removed volume ($100m^2$)	Matching Cells (Certainty)	Figure #
Porpoise Bay	February to August	(+) 271.400	(+) 9.231	(-) 1870.292	(-) 63.615	99%	3.30
Porpoise Bay	August to December	(+) 881.907	(+) 29.997	(-) 1108.910	(-) 37.718	99.1%	3.31
Porpoise Bay	February to December	(+) 136.234	(+) 4.634	(-) 1984.994	(-) 67.517	98.7%	3.32

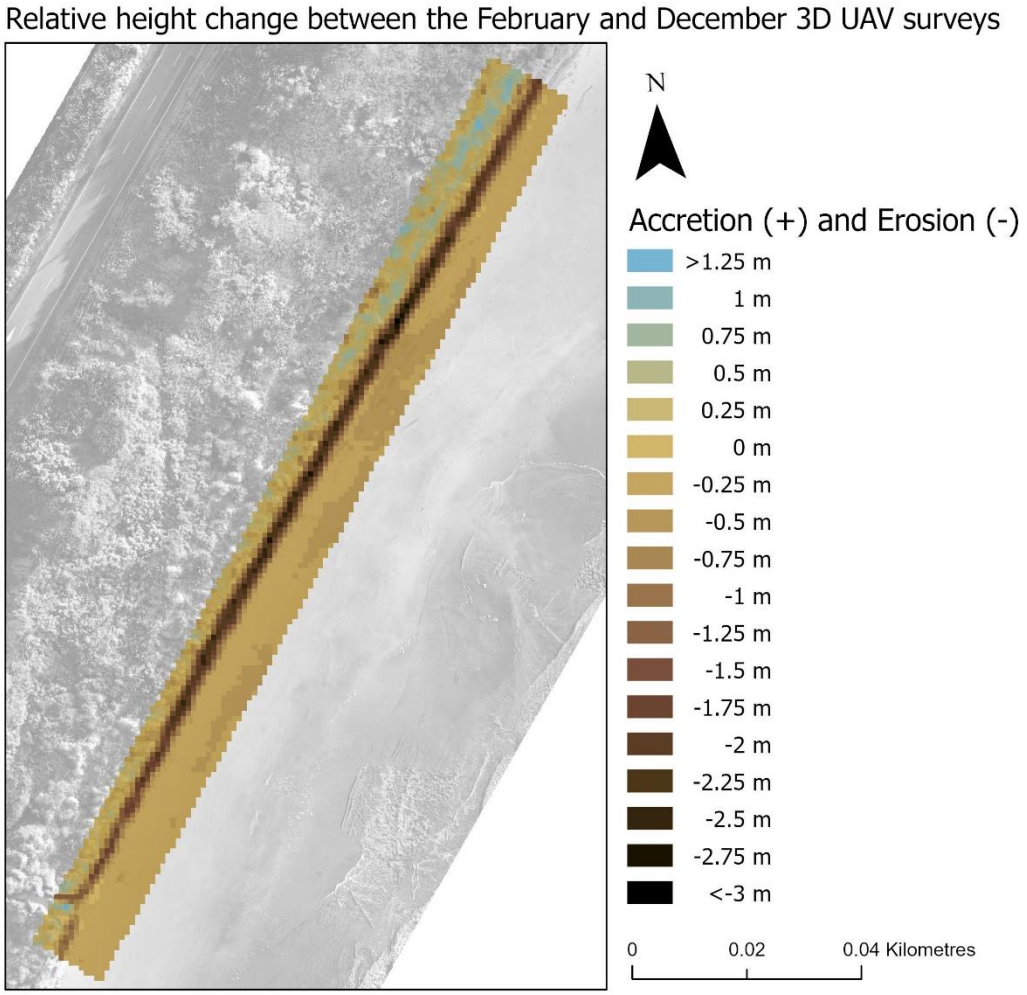

Figure 3.32. Relative height between the February and December point cloud survey at Porpoise Bay. Overall, there was 1984.994 m^3 of volume removed from the survey area. There are little patches of added volume at the north and south ends of the survey area which adds up to 136.234 m^3.

Chapter 4 Discussion

The coast is a naturally active margin that forms an important barrier system subjected to the forces of both the terrestrial and marine environment. Anthropogenic debris along the coast is at risk of being washed away or contaminating the marine environment as a result of ongoing erosion. This has the potential to cause major environmental degradation (Pascucci et al., 2018; Rouse et al., 2017). The overall aim of this research was to investigate the ability of a generalised GIS methodology to quantify coastal dynamics at different locations with anthropogenic debris. To achieve this aim, I addressed the following questions:

1. What GIS processes are applicable to characterising historic shorelines in order to understand past dynamics occurring at each site?
2. Can the past trends characterised in (1) be used to predict where future shorelines will be?
3. Does characterising the seasonal volumetric changes occurring along the coastline provide additional insight into the temporal and spatial patterns of shoreline change?

The historic shorelines at each site were georeferenced and transects generated 20 m apart extracted the magnitude and rate of change as they intersected with each shoreline. Values were extracted which aided in predicting where the shoreline will be in 20 years. These manual predictions were compared with automated predictions generated by the DSAS software for comparison of the success of both methods. Annual volumetric changes occurring along the coastline were evaluated to aid in understanding short term patterns that may occur in a 3D sense. 3D UAV imagery was collected quarterly in 2021 to measure the volumetric change between the seasons over the course of a year at each site.

This chapter is divided into three sections to evaluate the aim and questions addressed in this research. The first section holistically discusses the success and significance of this research. The second section provides recommendations and is divided into two parts. The first discusses the recommendations for how the methodology in this study can be improved and how it should be used for future research. The second part

discusses the recommendations for site specific management from the results of this research. Emphasis on the issues that Monkey Island, Colac Bay, Fortrose, and Porpoise Bay will face with future management reiterates how unique our coastlines are. The final section discusses the uncertainty and limitations of the study which will support repetition of the research.

4.1 Success and significance of research

I analysed four sites along the southern coast of the South Island of New Zealand. Each site has unique characteristics that tested my methodology for monitoring our dynamic coastlines. Further development and a site-specific approach for the methodology used at these sites made this research unique compared with previous studies. The research involved collecting historic satellite imagery and 3D UAV imagery from different time scales to understand spatial and temporal factors that influence our coastlines. I evaluated methods for understanding the coast and generated my own analysis from that evaluation. The main patterns illustrated throughout the different shorelines in the results are discussed. There were many coastal patterns shown in this study, however, I provide specific detail on the patterns resulting movement and the shoreline position fluctuations observed at Porpoise Bay. The method and success of predicting the future shorelines is debated as well as the importance of understanding human intervention and 3D UAV seasonal variability. The successes and evaluations below illustrate the significance of this research.

4.1.1 Patterns in the shorelines

As the natural margin between marine and terrestrial environments, coastlines are naturally dynamic and have eroded, accreted, or stayed the same at a range of spatiotemporal scales. Our species lives and builds infrastructure along these coastlines, resulting in an estimated 10% of the world's population inhabiting the margin up to 10 metres above sea level and 60% of the world's population inhabiting the 'coastal zone' (Boye et al., 2018; Church et al., 2006; Domingues et al., 2018; McGranahan et al., 2007). Many coastal patterns were illustrated in this study. Each site has unique geomorphological factors that contributed to the patterns occurring along the coast and the generalised methodology used, illustrated these patterns. The most important dynamic process to understand for coastline management is erosion

(Kale et al., 2019). Lengths of shoreline in the four sites showed constant erosion where human intervention was the only barrier preventing that pattern from occurring due to waves or storm surges. As well as water from the ocean, fluvial transport dramatically affected the dynamics of the coast.

4.1.1.1 Water

Water is one of the many factors affecting the position of the shoreline and the dynamics of the coast. Water sourced from inland such as from streams or rivers can show dramatic effects on the shoreline around the outlet. This was illustrated at Monkey Island, Fortrose, and Porpoise Bay. There are two stream outlets along the Monkey Island shoreline which have impacted the results of the study. The streams were 300 m away from one another and both illustrated a pattern of steady erosion occurring for 60 m to the north side of the stream mouth (Fig. 3.9). This pattern is significant because it reiterates that forms of erosion occur from inland factors instead of typical coastal factors. This is illustrated at the Fortrose study area. The maximum net change from the transect lines at Fortrose occurs on transect 4 where, due to the angle of the transect line not being perpendicular to the shore and going through a stream outlet, has a skewed result of 35.73 m of net erosion (Fig. 3.7). Transects 6, 7, 8 and 23 also have net changes above 30 m of erosion so although transect 4 has skewed results, many of the accurate transects such as transect 7 with 33.03 m of net erosion are not far off that large net change (Fig. 3.7). The flow of the Mataura River which covers the length of the study area is a major cause for the erosion along the banks at Fortrose. The curve of the estuary created by the river flow is viable to continuous erosion and it is apparent from this study that the riprap along the shoreline is preventing further erosion. Previous monitoring at Porpoise Bay recorded short term erosion around Cooks Creek from mobilising the sand with fluvial transport (Robertson & Stevens, 2012) though the historic shorelines in this study recognise little long-term change occurring around this creek (Fig. 3.8). This reiterates many factors contribute to the position of the shoreline and that it is hard to model these factors when there are many different temporal gaps with data.

4.1.1.2 Fluctuations at Porpoise Bay

Porpoise Bay showed a unique pattern that was not described at the other three sites. Porpoise Bay demonstrated major fluctuations between erosion and accretion that

occurred in ~10-year cycles that were evident along the north-eastern part of the beach. The significance of seeing this pattern reiterates the coast is naturally active and that there are many factors that affect the dynamics of the coast. Porpoise Bay is in an eroding phase where vast volumes of sand are being removed due to processes such as longshore sediment transport from waves and currents (Awad & El-Sayed, 2021). The shoreline is currently retreating at an alarming rate of up to an average of 2.62 m/y between 2013 and 2020 and a total net change of 41.72 m/y of erosion between 2005 and 2020 but the history of this coastline shows an equal period of accretion will follow. This brings to light three main points. The first is that when understanding the historic dynamics of the coast, major erosion is not necessarily a serious issue as the cycle driven by a large array of factors will eventually result in a period of accretion. In contrast to this first point, is the question of how will this cycle of erosion and accretion be impacted by rising seas and increase in storm surges in the coming years? Coastal erosion is estimated to amplify with rising seas and increased storm surges so these next few years will illustrate whether that is the case for Porpoise Bay (Hopkinson et al., 2008; Romine et al., 2013; Schweiger et al., 2020). The third point highlights that this cycle is happening in an area with no hard engineering to prevent erosion which means this pattern may be unlikely to occur in urbanised coastlines where erosion is affecting society directly. The scale of anthropogenic debris and disturbance varies at Monkey Island, Colac Bay and Fortrose and the historic imagery does not go back far enough to see if these cycles occurred before human intervention at these other sites.

4.1.2 Predicting future shorelines

Being able to predict where something may reside in the future based on past trends has been a globally used way to model. Because of this global use, a variety of shoreline model software has been developed to automate this process which results in faster data extraction to aid in management and understanding of the coast. The DSAS software is utilised globally to aid in prediction and management. For predicting the future shoreline at each site, I compared my educated forecasting with that of DSAS software. Through my research I learnt the DSAS software is significantly faster at presenting outputs for shoreline predictions, especially with large data inputs. A drawback of this software is that it cannot consider where human intervention had

created a change in the shoreline pattern, but from researching the site, I did. Although it created a bias, I incorporated that into my manual predictions for the future shorelines at each site. An example of this is at Colac Bay. Colac Bay has had rocks and hard engineering placed along the shores since the 1930s to prevent erosion. In 2015, the coastal road had to be permanently closed as the reinforced engineering was discontinued in this area. Since then, the annual rate of erosion is estimated to be over 1 m where no human intervention is occurring. The DSAS software used multiple shorelines to predict where the coast will be in 20 years' time, but I only used the estimated average since where human intervention stopped which is why the manual and automated results are different from each other (Fig. 3.6). This is significant for this area because it is in front of a coastal landfill. It is extremely important to accurately know how much time there is left to manage the site before the landfill becomes unearthed by further erosion. This research emphasises the risk of running automated models without proper knowledge of the site making it significant for the management of Colac Bay foreshore and other relevant study sites.

4.1.3 Human Intervention

Coastal systems undergo many natural processes and pressures with resilience but added pressures from anthropogenic growth and human intervention has made these systems vulnerable (Sui et al., 2020). Throughout this research, human intervention has been a reoccurring factor for determining dynamics and predicting future shorelines. This has been noted in studies around the world which has increased the difficulty of using prediction models or monitoring the dynamics of coastlines (Mishra et al., 2019; Sui et al., 2020). Humans have had a massive impact on the natural fluctuations of many ecosystems and the coast is no exception. The human intervention at these study sites were both with hard engineering and vegetation planting.

4.1.3.1 Hard engineering

Human intervention was observed in many forms at all the sites. Past infrastructure such as tarmacked coastal roads or riprap placed along a shoreline has changed the natural fluctuations of the coast. The main hard engineering occurred along Colac Bay which has been reinforced for nearly a century after storms and inundation have caused major erosion events. Hard engineering has made it difficult to understand the

dynamics of the coastline which in turn have made it hard to predict where the shoreline may be if engineering was to discontinue. Fortrose estuary has also had forms of riprap placed along its shoreline. What was apparent with collecting the 3D UAV imagery was the communities of shorebirds that reside in the estuary. In 2018, Prosser et al. stated that armouring the shoreline of an estuary can negatively influence bird communities as artificial structures lack refuge and complexity like a natural shoreline as well as reducing ecosystem services (Mishra et al., 2019; Prosser et al., 2018; Sui et al., 2020). Natural coastlines are shrinking as we aim to prevent erosion with unnatural barriers. This drive to control the naturally active margin between the marine and terrestrial environment will be detrimental to our coastal ecosystems.

4.1.3.2 Vegetation

The vegetation line was used to measure the historic shorelines in this study. Removal or planting of vegetation along the shoreline would have major effects on the results of this study and the dynamics of the coast. This introduces the concept that many of the accretion events were not really accreting in the geomorphological sense but were planted to grow, restore, or reinforce the shoreline or increase ecological services to the coastal system. This was shown at Porpoise Bay where an accretion pattern was illustrated with vegetation planting in front of the coastal houses to prevent shoreline retreat and naturally reinforce the shoreline. The dunes along Porpoise Bay show a variety of species. The historic aerial imagery show a large amount of planting / accretion occurred before 1978 at Porpoise Bay along the higher transect lines (Fig. 3.8). The dominant frontal dune species here is marram grass. Marram grass has been planted throughout all the sites at different points of time in the last 70 years because it is fast growing. Marram is a shallow rooted sand binding plant resulting in unstable dunes and thus, can be a catalyst for a lot of the erosion shown throughout the shoreline (Robertson & Stevens, 2012). None of the study sites were untouched by human intervention which is the case for most of the coastlines around New Zealand. This study reiterates that human intervention is a major factor in understanding how the dynamics of the coastline have been manipulated which can make understanding and using them as prediction models that much more difficult.

4.1.4 3D UAV seasonal data

There are many different dynamics occurring along the coast, all with different time scales. 3D UAV imagery was collected seasonally over the course of a year to understand two timescales that were occurring at each site (seasonally and annually). Seasonal changes have been noted at different beaches around the world and should be considered when attempting to understand the dynamics of the coast (Masselink & Pattiaratchi, 2001; Thanh et al., 2018). Where sand is positioned along a coastline at different times of the year may make a big difference when doing long scale time studies where satellite imagery is taken from different times of the year and decades apart. A winter coastline may remove large volumes of sand and therefore change the structure of the shoreline. Knowing where the shoreline sits throughout the year can aid in long scale studies where you can account for these changes in future research. Volume is an important variable with analysing how the coast changes because the 3D movement of sediment and sand is a major factor in shoreline positioning and dynamics. Although there were limitations with collecting the UAV data and analysing it, the results that were produced illustrate the importance of understanding different temporal patterns that can occur naturally in a coastline. The significance of this research in conjunction with further research can support future decision making and management of our naturally active coastal margins.

4.2 Recommendations

There are many coastlines around New Zealand that will face problems with coastal erosion at sites with anthropogenic debris. It is important to understand the nature of these sites with effective monitoring of the current state and the history of the coastlines. The overall aim of this research was to investigate the utility of a generalised GIS methodology to quantify coastal dynamics at different locations with anthropogenic debris. This section is divided into two parts. The first discusses the recommendations for how the methodology can be improved and how it should be used for future research. The second part discusses the recommendations for site specific management from the results of the research. Emphasis on the issues that Monkey Island, Colac Bay, Fortrose, and Porpoise Bay will face with future management reiterates how unique our coastlines are.

4.2.1 Recommendations for the Methodology

This section discusses the methodology, how it can be improved and how it is recommended to be used for future research. The methodology used to generate historic shoreline maps will be discussed first, followed by the coastal dynamic's methodology. The prediction methodology will then be discussed followed lastly by the methodology used to generate the volume maps.

4.2.1.1 Historic shoreline methodology

Shorelines extracted from historic satellite imagery has been valuable to understanding these coastlines. After conceptualising many different studies that measured shoreline change (Addo et al., 2008; Baig et al., 2020; Baral et al., 2018; Boye et al., 2018; Jeong, 2019; Kale et al., 2019; Romine et al., 2009; Sebat & Salloum, 2018; Yan et al., 2020; Y. Zhang, 2020), methods were conducted holistically for this research. Error can be generated at this first step where satellite imagery is georeferenced, so it was important to line up the satellite images as accurately as possible. From past studies, shorelines have been manually drawn based on different features such as vegetation line or high tide line (Baral et al., 2018; Pollard et al., 2019). This research generated a system when the computer would recognise the vegetation line by classifying the landcover to try and minimise bias for where the shoreline is for each satellite image. The accuracy was down to the pixel size for each image which was 40 cm for most of the satellites. Although it was time consuming, my method proved to be successful in the quality of the data generated by this process. I estimated this was more accurate than manually drawing the shoreline. This improvement in accuracy can be very significant when assessing a dynamic coastal shoreline.

4.2.1.1.1 Historic shoreline methodology improvements

It is recommended to automate this step even further where the shoreline is extracted directly from the satellite image. With a more national scale study, it would be prudent to invest time into creating a model to extract the shorelines. Awad and el-sayed published an article in 2021 explaining that shoreline extraction for their study was automated using three water indices as the high-water mark for their shoreline margin (Awad & El-Sayed, 2021). The shoreline was determined by a statistical comparison between the three indices which all used remote sensing to classify and extract the

appropriate bands with a range of sophisticated algorithms (Fisher et al., 2016; Huang et al., 2002). This technique introduces the range of geospatial approaches to solving problems which can improve extraction of layers from satellite imagery. From my research I found that gathering, georeferencing and creating the shorelines at each site was a very time-consuming part of my data preparation and could be quite costly if you must buy each satellite image. The foresight to start capturing satellite imagery as early as the 1940s is incredibly useful for temporal studies such as this. Imagery between 1940 and 2014 are freely available from Retrolens and LINZ. Not all data were freely available however, thanks to the generosity of the New Zealand's Changing Coastline project group in the National Science Challenge and Environment Southland I only needed to purchase one satellite image out of my 32. That satellite image cost $744.04 due to the minimum area of 25 km/sq. needed to purchase. Without the help of these organisations the imagery I would have needed to purchase would have cost me over $5000. A lot of information can be extracted from analysing historic shorelines and it is essential for observing the past dynamics of the coast.

4.2.1.2 Coastal dynamics methodology

There were many dynamics illustrated throughout the coast which resulted in a different variety of patterns along all the transect lines. All these patterns fell under the matrix created (Fig. 2.21) although many of the transects went through different phases of erosion, accretion, stable or unstable at different times. These temporal changes are an important factor when understanding the coast. This had to be simplified because the variation of patterns is endless and only a few exhibited the exact same patterns. These usually followed Tobler's first rule of geography where "everything is related to everything else, but near things are more related than distant things" (Tobler, 1970) where the same patterns usually occurred together in specific stretches of the coastline. Being able to group the patterns meant that management would be easier for larger areas needing similar care.

4.2.1.2.1 Coastal dynamics methodology improvements

This methodology can be improved with automating the categorisation of the coastal dynamics. This will achieve large scale, more statistically accurate results in a shorter amount of time. The DSAS software does this partially before it predicts the position of where the shoreline will be in 20 years which reiterates that automating a statistical

classification program is doable and would prove valuable when undergoing this research on a large scale. This method can be further investigated to examine the complex understanding of multiple coastlines. A multivariate analysis of all the factors of the coastline including prevailing wind, currents, compass facing as examples, would assist with understanding of the correlations contributing to the patterns that have been portrayed in this study. In-depth analysis of all the factors that contribute to the dynamics of the coast can be inputted into machine learning. This has been used in past studies and is another way to try and interpret the complexity of our coastal systems (Corbella & Stretch, 2012; Jeong, 2019; Salvadori et al., 2014). This reiterates that there is more than one way of monitoring or managing these coastlines and that the future may show different coastal dynamic patterns than what has been noticed based on rising sea levels, increased amount of storm surges and the changing climate. It is recommended that future monitoring techniques are adaptive to this changing system.

4.2.1.3 Prediction maps methodology

The concept of comparing manual with automated shoreline predictions was to evaluate the success of large-scale predictions and personalised manual predictions. In science, all possible bias is removed to create a transparent understanding of the research without human intervention. In my bespoke manual predictions, I intentionally created a bias from qualitative data I had collected to compare with the automated software that lacked this data. This part of creating a generalised GIS methodology was unique to this study and contributes qualitative analysis to predicting future shorelines.

4.2.1.3.1 Prediction maps methodology improvements

Improvements to this study would include uncertainty margins in the manual predictions to support the accuracy of the predictions. The DSAS software used to automate the future shorelines uses End Point Rate (EPR) and Linear Regression Rate (LRR) which assumes that historical rates of change are the best way to estimate the position of the shoreline in the future (Esmail et al., 2019; Mukhopadhyay et al., 2012). This has proven reliable in many studies where natural fluctuations were measured (Awad & El-Sayed, 2021; Kanwal et al., 2020; Nandi et al., 2016). Many shorelines around the world have had major anthropogenic impacts which have changed or

manipulated the natural fluctuations of a coastline. These impacts are illustrated throughout my study from coastal protection engineering at Colac Bay and Fortrose Estuary, coastal roads being built then abandoned at Colac Bay, coastal housing being built at Porpoise Bay and an inland dam affecting the sediment supply of Te Waewae Bay and indirectly Monkey Island. Studies have focused on how anthropogenic impacts have manipulated the results of automated shoreline predictions as it has significant effects on the dynamics of a coastline (Addo, 2013; Douglas et al., 1998; Karimi et al., 2021). The DSAS software was much faster than my methods for predicting future shorelines which will result in more successful large-scale research. Human intervention creating an anomaly in the natural patterns of the shorelines and should be comprehensively understood in conjunction with automated models to aid in future understanding and management plans for relevant coastlines.

4.2.1.4 Volume Maps

Volume is an important variable with analysing how the coast changes because the movement of sediment is a major factor in shoreline positioning and dynamics (Ashton et al., 2001). Although the volumetric data collected in this research could be improved (further detail in the uncertainty and limitations section), the concept of measuring volumetric change of coastlines, dune systems or coastal cliffs is still highly recommended as 3D data exacerbates the information that can be analysed in an area especially where vegetation, height and area can change so rapidly (Hayakawa & Obanawa, 2020; Le Mauff et al., 2018). Despite the limitations, I was able to produce informative maps of the volumetric changes occurring over the course of several months at each site. The UAV imagery I collected for this study was over a one-year time span which meant there was no baseline to compare the seasonal patterns with. To monitor where the sediment is high towards the shore or further out to sea, it is recommended that 3D seasonal drone imagery is collected for 3 years to create a baseline for further monitoring. This would establish if there were any anomalies that may occur in the data that was only collected in one year. There is very limited baseline information for coastlines in Southland. It is recommended that statistical evidence-based analysis measures the impacts of storm surges. 3D UAV Imagery at different locations should be captured as soon as possible. After the next major storm hits the coast or a king tide washes away a portion of coastline, 3D UAV imagery can

be captured afterwards. The impacts of this will be compared between the before and after imagery to create a baseline for the physical impacts that could occur during a storm surge. Storm surges are expected to become more frequent, and knowledge of their impacts can greatly benefit future management and planning of coastlines.

4.2.2 Site Specific Recommendations

This research investigates the success of a generalised GIS methodology for measuring coastal dynamics at different locations with anthropogenic debris. This section discusses the outcomes specific for Monkey Island, Colac Bay, Fortrose, and Porpoise Bay.

4.2.2.1 Monkey Island

A freedom camping area right on the beach with a view of Fiordland over Te Waewae Bay, Monkey Island is secluded but not out of reach from our anthropogenic footprint. There are records of iwi habitation along the coastline where remnants of coal pits have been found indicating a culturally significant area. Discarded concrete is placed throughout the shoreline, but the origin of this debris is unknown. Upon further investigation along the shoreline there is a distinct layer of rubbish 40 cm below the surface along about 200 m of the coastline. This rubbish includes bailage wraps, bits of hard plastic and old food wrappers. Luckily, the shoreline has been mostly stable over the past 70 years. Despite this, rising seas and more frequent storm surges are eroding at the shoreline, unearthing the layer of small plastics and other rubbish into the sea. It is recommended the rubbish along the shoreline is investigated so mitigation can be undertaken. Small plastics can be transported by tides, winds and are now found in the most remote places of the ocean (Fischer et al., 2015). The nature of the pieces of plastic found throughout the shoreline are harmful to marine life. Studies have identified negative effects of small plastics in fish, marine invertebrates from filter feeding and seabirds (de Sá et al., 2018; Rochman et al., 2016; Setälä et al., 2018; Wilcox et al., 2015). These animals are all present within Te Waewae Bay and so are marine mammals that are both directly and indirectly affected by plastic litter in the ocean. Ingesting plastic is a common problem for many species that reside in and around the water as it can be mistaken for food. Physical injuries, entanglement and physiological stress are common outcomes for marine life when they encounter plastics (Senko et al., 2020). As well as the issue of litter along the coastline, the land is

disappearing into the ocean at Te Waewae Bay as a vast majority of the geomorphology is eroding cliffs. Along the middle of Te Waewae Bay is the mouth of the Waiau River which the flow of water was diverted from the source when the Manapouri Dam was finished being built in 1972. Dams greatly reduce water flow of a river and therefore reduces the volume of sediment supply to a bay (Kale et al., 2019). Further investigation along the entire coast of Te Waewae Bay needs to be observed as erosion has been a dominant feature of the bay with coastal road closures at the western end and seaside property boundaries retreating. Rising seas and more frequent storm surges that are predicted will accelerate this.

4.2.2.2 Colac Bay

Colac Bay is a southeast facing bay known for its consistent surf and local Hector's dolphin community. Erosion along Colac Bay has been a recorded issue for almost 100 years with coastal engineering occurring to prevent retreat from the 1930s. Transect lines show a stable dynamic for most of the coastline because coastal engineering has prevented major erosion. The dynamics extracted from the historic shorelines allow us to identify the capabilities of the sprawling rock wall and the major erosion that occurs when replenishment of the rock wall stops. Where the rock wall repairs were halted, the shoreline is retreating at an unforgiving rate in front of where the historic coastal landfill resides. It is recommended that monitoring the shoreline in front of the Colac Bay landfill is of the utmost importance as there have been accounts from the public of waste, car batteries, pesticides, and other physical rubbish strewn throughout the area closer to the sea than is thought. If the erosion continues, chemical monitoring will have to be considered. A study investigated case studies where the challenges of coastal landfills will be increase with sea level rise (Beaven et al 2020). Leachate and solid waste products are a significant problem and completely removing the waste is the best option for mitigation of damage to the surrounding environment although removing a fraction of the waste that causes the most harm and leaving the rest to erode has been discussed in past studies as an alternative solution (Beaven et al., 2020; Brand et al., 2018). Long term management at Colac Bay is recommended as refurbishing the rock wall after every storm surge will be uneconomical. However, if nature is left to its own devices the coastline will aggressively erode (shown between transect 65 – 75 (Fig. 2.17)). The landfill is not the only site of interest along Colac Bay.

Notably some major issues will arise with further coastal erosion at the urupā, marae and the rest of the coastal town which have experienced storm inundation over the past years. The Colac Bay township is very flat and very close to sea level, so these current problems are estimated to only get worse as the sea rises and the climate becomes more extreme. Because of the expected increase in storm surges, and sea level, there may be a requirement to protect Southland's coastlines through artificial measures. However, this will reduce the ecological services of shoreline habitats. Thorough investigation to further the monitoring and management of this entire coastline is recommended and should be a priority before it becomes hazardous.

4.2.2.3 Fortrose

From the results of this study, there is a clear pattern of erosion occurring along the shoreline at Fortrose estuary. This pattern has become stable due to human intervention with old building materials and driftwood being packed up along the shoreline to prevent further erosion. At Fortrose, the DSAS software predicts the transects 18 - 27 to be the same as it is in 2021 (Fig. 2.19). This was my prediction as well as property owners that are directly affected are likely to keep using hard engineering to prevent their properties from eroding away. In the prediction map (Fig. 2.19), the manual line represents where the shoreline may be if hard engineering was to stop and the pattern of erosion that was occurring before human intervention was to continue. 3D models captured from UAV throughout the year show that this heavy debris can be mobile with enough water from king tides or high flows from the Mataura River, so this ad hoc management of the retreating shoreline is not a long-term solution. Estuaries have been manipulated globally because of their more sheltered characteristics making them suitable for anthropogenic development but have a higher rate of erosion than ocean beaches as river flows and tidal inputs creating persistent erosion patterns (Nordstrom, 1989; Prosser et al., 2018), Because of this, the erosion occurring along Fortrose estuary will be different than ocean facing shorelines. There is a lot of cultural history in this particular area, both Māori and European that would ideally be protected or thoughtfully managed as future problems arise.

4.2.2.4 Porpoise Bay

Porpoise Bay is at the far east of the Southland Coast, furthest away from the prevailing southwest swell and westerly winds though it has the most extreme patterns of movement in the coastline. Porpoise Bay shows strong dynamic cycles of erosion and accretion on about a ~10-year cycle and vast volumes of sand and sediment are being moved around the coast. The middle of Porpoise Bay has the most instability of the whole coastline, indicated by transects 60 – 124 showing the major erosion and accretion cycles. As a result of identifying this cyclical pattern, monitoring and management for most of this stretch of coast is minimal as it is predicted that these erosion and accretion periods will continue and have minimal impact as long as further coastal development does not impose on this cyclical pattern. The historic imagery shows large sections of vegetation growth or planting have occurred and resulted in some of the accretion pattern observed in recent years. This is apparent in front of the new coastal housing shown along transects 37 – 50.

4.3 Uncertainty and limitations

The final part of the discussion chapter illustrates the difficulties that needed to be overcome with the uncertainty and limitations in this research. The uncertainty with the data was around image inaccuracy, sparse data and not being able to consider storm surges in this particular methodology. Limitations with the UAV data collection and analysis part of this research is discussed as well as how these limitations were overcome.

4.3.1 Imagery inaccuracy and sparce data

Monitoring shoreline change can be cost effective through the use of GIS, using freely available satellite imagery. Like many monitoring techniques, using GIS can create errors in accuracy. Errors can be caused by the quality of georeferencing, interpretation error or datum shifts (Moore, 2000; Romine et al., 2009). Satellite imagery used for this research comprised different resolutions, from 40 to 100 cm. The imagery was manually georeferenced in ArcGIS Pro using virtually created control points between the satellite imagery to the New Zealand Imagery base map in ArcGIS Pro. Control points were placed on the corner of buildings or stable landmarks that were consistent throughout multiple layers. This had proven difficult to geo-reference

because of the lack of consistent markers between the imagery, specifically the earlier satellite images. To minimise human error with drawing the shoreline, the line was digitally created which resulted in the pixel size being the lowest resolution the layer could go. At a smaller scale this can make a big difference especially where imagery has a pixel resolution of 100 cm. When you are unable to provide exact results due to the quality of data or how it was interpreted, estimating error margins is important to establish a level of confidence in these outcomes. Based on the scale and resolution of the images, there is between 1.3 m to 5.59 m of error from the 40 cm imagery to the 100 cm imagery created by crossed over scale control from an accuracy of atoll islands study (Holdaway & Ford, 2019). Based on these margins, errors in my research can be large enough to greatly affect the results. To reduce this error, minor manual adjustments were made to my inputs. The 1972 imagery for Monkey Island was removed because the imagery was over exposed, and a 1990s image of Monkey Island does not exist. This meant there were two ~20-year gaps between the corresponding layers instead of ~10 years. The issue with large year gaps in the data is the inability to interpret anything that occurred between the years. The average gap between each satellite image was about 10 years but that may be too large a gap to extract and distinguishable patterns that are occurring along a stretch of coast. My methodology shows an interesting depiction of the dynamics of the coast as there is not information on every coast all the time in past decades. Like any research, there can be trade-offs with quality, usability, and cost of data.

4.3.1.1 Storm surges

Projections of sea level rise in Southland, New Zealand are between 0.2 and 0.3 m by 2040 (Zammit et al., 2018). Effects of climate change, such as increased storm intensity and frequency can be damaging to all coastlines, especially those with anthropogenic debris. For coastal landfills, such as that at Colac Bay, this could lead to inundation and the release of hazardous contaminants into the environment. Erosion and flooding from sea level rise and climate change would result in a decline of natural defences such as dune systems and indirectly increase the consequences of smaller storm surges (Kebede, 2009). There is major uncertainty with the methods of estimating the average annual rate of change between the historic shorelines. Colac Bay shows a limitation in my methods where the distance the shoreline moved between the years

has been averaged at an annual rate, but most of the erosion that caused damage was recorded after storm surges, events that are likely to become more frequent. In the ~10-year intervals between satellite imagery there may be only one or two events that have caused the erosion shown throughout the entire span of the decade. This may be the case for all the sites but there has not been a way to measure this so there is a large amount of speculation and uncertainty in the frequency of erosion events. One study suggested that, although storm surges can remove vast volumes of sediment in a short amount of time, they had little effect on long term erosion patterns mainly caused by factors such as sea level rise and the coasts natural sediment supply (K. Zhang et al., 2002). This reiterates how difficult the coastal system is to monitor and manage due to its unpredictability.

4.3.2 UAV data collection

Collecting UAV data for this study was a major learning curve as this was a new way of data collection for me. Because of this, I learnt and had to overcome many issues in the field which resulted in inadequate quality of some of my drone imagery. My first survey I collected ground points using an RTK (Real-time kinematic positioning) which was hired by Environment Southland, but I was unable to use this for the following flights. My elevation data were all at different heights based off the take-off of the UAV because I did not have a control elevation. To counter this field error, I registered matching parts of the surveys on CloudCompare and applied a transformation to the original so all the point clouds would line up with the other. This was explained in the methodology chapter. There were a few challenges that needed to be overcome with collecting my UAV imagery but none of the following affected the results of my research. The rest of this paragraph highlights issues that may arise when following the general methodology of UAV data collection which will aid in future replication of the study. UAVs are revolutionary for capturing local scale imagery, where atmospheric conditions, cost and observation times are not limiting factors (Berni et al., 2009; Watts et al., 2012; Wulder et al., 2004). The two main factors needed to be resolved were the weather and wildlife. Data collection could only occur when there was no rain and wind speed was under 38 kph for many UAV models. In spring months where winds are naturally high and storms occur frequently, data collecting with a UAV must be opportunistic. The higher the wind speed, the more battery is used to stabilise the

UAV. Lower temperatures also reduce the capability of the batteries. The study took place in Southland which has an average temperature of 10.1°C. It took up to four full batteries to fly some of flight plans with two elevations which meant that the batteries had to be recharged between sites. This took a significant amount of time, resulting in the possibility of wasting a good weather day doing only one site if tides and sunlight did not permit another.

4.3.2.1 Birds

A further limitation to collecting data with a UAV is the disturbance caused to surrounding animals, especially birds. Birds were present at all sites. Fortrose proved to be the most difficult to fly at due to this being an estuary where many birds settle. Oyster catchers were prominent here and are known to be quite aggressive birds. If the birds became agitated, I would pause the flight, bring the UAV back down to me and wait for the birds to settle down. Although this did not prevent data collection at most sites, the presence of birds delayed imagery collection and made some flights quite time extensive. A further site was going to be added at Riverton Rocks because there is an old landfill situated in the dune, but nesting birds occupy the site for most of the year. Department of Conservation rules with flying UAV around birds were followed but as the UAV was taking off, a swarm of birds came to circle the drone aggressively so that survey site was terminated to avoid obvious stress to the animals.

4.3.3 Imagery doming

Taking hundreds of 2D photos which are then aligned together to create a 3D model illustrates the advancement in technology with aerial imagery. Problems can arise unexpectedly when dealing with high tech software which is what I experienced when I began processing my second survey in May. I used a different UAV of the same make and model as had been used in the February survey. This UAV had come down with me from Auckland and the compass needed to be calibrated before each flight due to the significant latitude change going down to Southland. The flight plans were the same, but when I processed the imagery back in Auckland, I found a doming shape had occurred (Fig. 4.1). This systematic error referred to as “doming” and “bowling” has been reported through many studies which identified the error occurring from inaccurate camera calibration in association with ineffective radial parameters (Eltner & Schneider, 2015; James & Robson, 2012). Because no errors arose in the first survey,

I did not expect any to occur. This made all of May's survey imagery unusable. This error had to be resolved to prevent further unusable imagery. Changing the flight design to increase the number of tie points used to connect distant images has strengthened photogrammetric networks in a previous study (Sanz-Ablanedo et al., 2020).

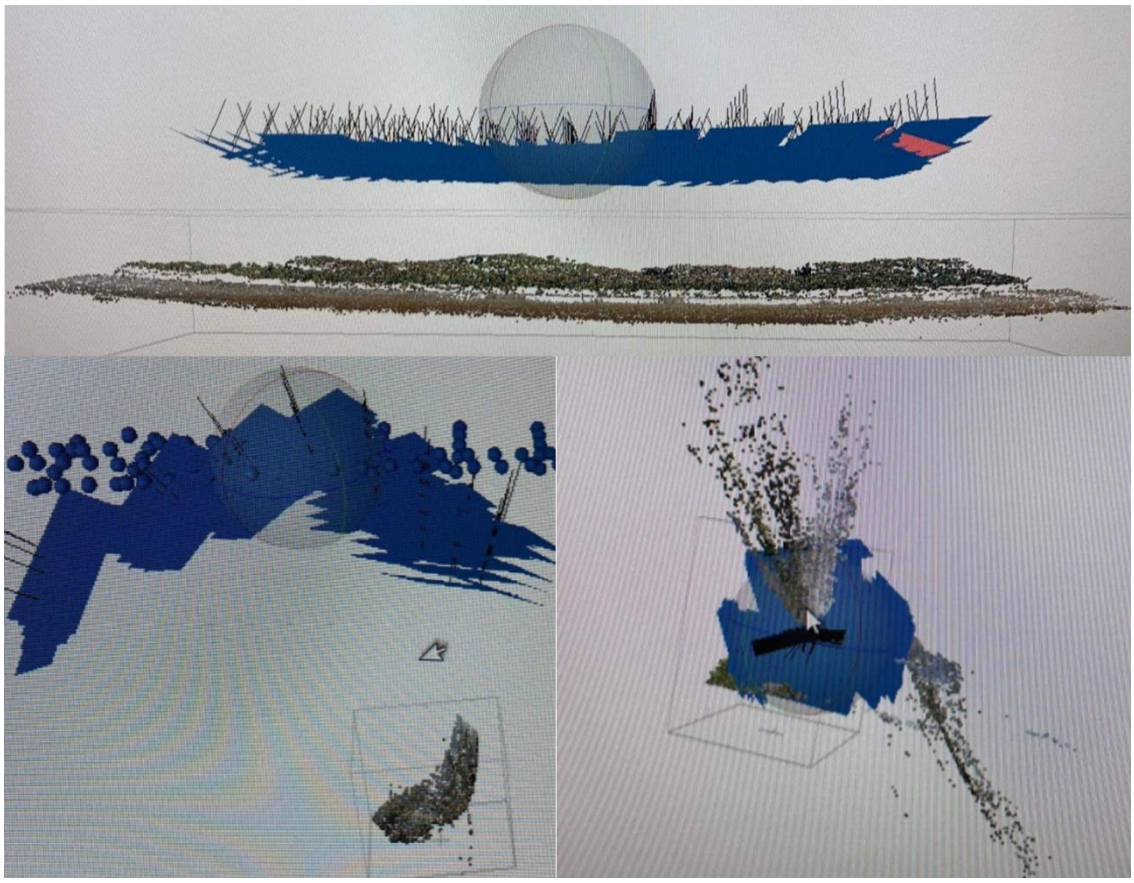

Figure 4.1. Images of the doming issue of the May. This was a result of inadequate camera calibration or lack of information for the Agisoft Metashape software to process correctly. The blue shapes are the 2D images taken from the drone and the sparce image is the point cloud created with structure from motion photogrammetry explained in the introduction. Manual tie points were added to fix the doming issues but only made it worse as shown in the bottom screenshots of this figure where the point cloud became more curved.

In August, I made the flight plan slightly larger in width and duplicated the flight so at each flight there was a survey at 50 m and 100 m elevation. The camera angle was adjusted to 80° from 45° at this second elevation. Adding a second flight at a different elevation gave the processing software more information of the scope of the site which produced a 3D model without the doming effect. This edited methodology proved successful in increasing the number of tie points between distant images and resulted in usable data.

4.4 Conclusion

This study investigated the utility of a generalised GIS methodology to quantify coastal dynamics at different locations with anthropogenic debris. Over the course of several months, historic satellite and 3D UAV imagery was collected and analysed to get a thorough understanding of the coastal dynamics of Monkey Island, Colac Bay, Fortrose, and Porpoise Bay. Maps illustrating the historic shorelines, coastal dynamics, future predictions, and volumetric changes of these sites were created from the generalised GIS methodology. Results were discussed to illustrate the success and significance of this research as well as the recommendations to better the research for future studies and site-specific recommendations. Uncertainty and limitations show where errors were made and overcome. Our coastal systems are visible hosts for anthropogenic change. Urbanisation, industrialization, or historic landfills and dumping grounds now mark a majority of retreating coastlines throughout New Zealand. Mitigating the effects that this anthropogenic debris will have on the natural environment is important and investigating the success of a generalised GIS methodology to measure the dynamics of the coast will result in better management for the future challenges our coastlines will face.

References

Addo, K. A. (2013). Shoreline morphological changes and the human factor. Case study of Accra Ghana. *Journal of Coastal Conservation*, *17*(1), 85–91. https://doi.org/10.1007/s11852-012-0220-5

Addo, K. A. (2018). Assessing Ocean Wave Dynamics, Potential Sediment Transport, and Coastal Erosion along Accra Coast in Ghana. *Journal of Coastal Research*, *81*(sp1), 86–91. https://doi.org/10.2112/SI81-011.1

Addo, K. A., Walkden, M., & Mills, J. P. (2008). Detection, measurement and prediction of shoreline recession in Accra, Ghana. *ISPRS Journal of Photogrammetry and Remote Sensing*, *63*(5), 543–558. https://doi.org/10.1016/j.isprsjprs.2008.04.001

Anderson, K., & Gaston, K. J. (2013). Lightweight unmanned aerial vehicles will revolutionize spatial ecology. In *Frontiers in Ecology and the Environment* (Vol. 11, Issue 3, pp. 138–146). https://doi.org/10.1890/120150

Anthony, E. J. (2014). L'influence de l'Homme sur les littoraux méditerranéens sur les deux derniers siècles: Unb ref aperçu à partir d'une perspective géomorphologique. In *Geomorphologie: Relief, Processus, Environnement* (Vol. 20, Issue 3, pp. 219–226). Groupe Francais de Geomorphologie. https://doi.org/10.4000/geomorphologie.10654

Ashton, A., Murray, B., & Arnault, O. (2001). Formation of coastline features by large-scale instabilities induced by high-angle waves. *Nature*, *414*, 296–300. https://doi.org/10.1038/35104541.

Awad, M., & El-Sayed, H. M. (2021). The analysis of shoreline change dynamics and future predictions using automated spatial techniques: Case of El-Omayed on the Mediterranean coast of Egypt. *Ocean and Coastal Management*, *205*. https://doi.org/10.1016/j.ocecoaman.2021.105568

Baig, M. R. I., Ahmad, I. A., Shahfahad, Tayyab, M., & Rahman, A. (2020). Analysis of shoreline changes in Vishakhapatnam coastal tract of Andhra Pradesh, India: an application of digital shoreline analysis system (DSAS). *Annals of GIS*, *26*(4), 361–

376. https://doi.org/10.1080/19475683.2020.1815839

Baker, A. N., Smith, A. N. H., & Pichler, F. B. (2002). Geographical variation in hector's dolphin: Recognition of new subspecies of cephalorhynchus hectori. *Journal of the Royal Society of New Zealand*, *32*(4), 713–727. https://doi.org/10.1080/03014223.2002.9517717

Baral, R., Pradhan, S., Samal, R. N., & Mishra, S. K. (2018). Shoreline Change Analysis at Chilika Lagoon Coast, India Using Digital Shoreline Analysis System. *Journal of the Indian Society of Remote Sensing*, *46*(10), 1637–1644. https://doi.org/10.1007/s12524-018-0818-7

Beaven, R. P., Stringfellow, A. M., Nicholls, R. J., Haigh, I. D., Kebede, A. S., & Watts, J. (2020). Future challenges of coastal landfills exacerbated by sea level rise. *Waste Management*, *105*, 92–101. https://doi.org/10.1016/j.wasman.2020.01.027

Beentjes, M. P. (2010). *Toheroa survey of Oreti Beach*. https://www.researchgate.net/publication/263580917

Bell, S., & Gibb, J. G. (Jeremy G. (1996). *Public access to the New Zealand coast : guidelines for determining legal and physical constraints*. Dept. of Conservation.

Berni, J. A. J., Zarco-Tejada, P. J., Suárez, L., & Fereres, E. (2009). Thermal and narrowband multispectral remote sensing for vegetation monitoring from an unmanned aerial vehicle. *IEEE Transactions on Geoscience and Remote Sensing*, *47*(3), 722–738. https://doi.org/10.1109/TGRS.2008.2010457

Bird, E. (2005). Coastline Changes. *Encyclopedia of Coastal Science*, 323–327.

Boye, C. B., Appeaning Addo, K., Wiafe, G., & Dzigbodi-Adjimah, K. (2018). Spatio-temporal analyses of shoreline change in the Western Region of Ghana. *Journal of Coastal Conservation*, *22*(4), 769–776. https://doi.org/10.1007/s11852-018-0607-z

Brand, J. H., Spencer, K. L., O'shea, F. T., & Lindsay, J. E. (2018). Potential pollution risks of historic landfills on low-lying coasts and estuaries. *WIREs Water*, *5*(1). https://doi.org/10.1002/wat2.1264

Burger, J. (1994). The Effect of Human Disturbance on Foraging Behavior and Habitat Use in Piping Plover (Charadrius melodus). *Biological Sciences*, *17*(3), 695–701.

Casella, E., Rovere, A., Pedroncini, A., Stark, C. P., Casella, M., Ferrari, M., & Firpo, M. (2016). Drones as tools for monitoring beach topography changes in the Ligurian Sea (NW Mediterranean). *Geo-Marine Letters*, *36*(2), 151–163. https://doi.org/10.1007/s00367-016-0435-9

Church, J., Wilson, S., & Woodworth, P. L. (2006). *Understanding sea-level rise and variability: report of UNESCO Workshop, Paris*. *15*(1), 12.

Colomina, I., & Molina, P. (2014). Unmanned aerial systems for photogrammetry and remote sensing: A review. In *ISPRS Journal of Photogrammetry and Remote Sensing* (Vol. 92, pp. 79–97). Elsevier B.V. https://doi.org/10.1016/j.isprsjprs.2014.02.013

Corbella, S., & Stretch, D. D. (2012). Multivariate return periods of sea storms for coastal erosion risk assessment. *Natural Hazards and Earth System Science*, *12*(8), 2699–2708. https://doi.org/10.5194/nhess-12-2699-2012

Costas, S., Ferreira, O., & Martinez, G. (2015). Why do we decide to live with risk at the coast? *Ocean and Coastal Management*, *118*, 1–11. https://doi.org/10.1016/j.ocecoaman.2015.05.015

Cullen, N. D., Verma, A. K., & Bourke, M. C. (2018). A comparison of structure from motion photogrammetry and the traversing micro-erosion meter for measuring erosion on shore platforms. *Earth Surface Dynamics*, *6*(4), 1023–1039. https://doi.org/10.5194/esurf-6-1023-2018

Dayton, P., Curran, S. R., & Catenazzi, A. (2005). Coastal systems. In *Ecosystems and Human Well-bring* (pp. 513–549). https://www.researchgate.net/publication/290808364

de Sá, L. C., Oliveira, M., Ribeiro, F., Rocha, T. L., & Futter, M. N. (2018). Studies of the effects of microplastics on aquatic organisms: What do we know and where should we focus our efforts in the future? In *Science of the Total Environment* (Vol. 645, pp. 1029–1039). Elsevier B.V.

https://doi.org/10.1016/j.scitotenv.2018.07.207

Domingues, R. B., Santos, M. C., de Jesus, S. N., & Ferreira, Ó. (2018). How a coastal community looks at coastal hazards and risks in a vulnerable barrier island system (Faro Beach, southern Portugal). *Ocean and Coastal Management*, *157*, 248–256. https://doi.org/10.1016/j.ocecoaman.2018.03.015

Douglas, B. C., Crowell, M., & Leatherman, S. P. (1998). Considerations for Shoreline Position Prediction. *Source: Journal of Coastal Research*, *14*(3).

Drummond, C. D., Harley, M. D., Turner, I. L., Matheen, N. A., William, ;, & Glamore, C. (n.d.). *UAV Applications to Coastal Engineering*.

Eltner, A., & Schneider, D. (2015). Analysis of Different Methods for 3D Reconstruction of Natural Surfaces from Parallel-Axes UAV Images. *Photogrammetric Record*, *30*(151), 279–299. https://doi.org/10.1111/phor.12115

Esmail, M., Mahmod, W. E., & Fath, H. (2019). Assessment and prediction of shoreline change using multi-temporal satellite images and statistics: Case study of Damietta coast, Egypt. *Applied Ocean Research*, *82*, 274–282. https://doi.org/10.1016/j.apor.2018.11.009

Everaerts, J. (2008). *The use of unmanned aerial vehicles (UAVs) for remote sensing and mapping*. www.aerobel.be

Fischer, V., Elsner, N. O., Brenke, N., Schwabe, E., & Brandt, A. (2015). Plastic pollution of the kuril-kamchatka trench area (NW pacific). *Deep-Sea Research Part II: Topical Studies in Oceanography*, *111*, 399–405. https://doi.org/10.1016/j.dsr2.2014.08.012

Fisher, A., Flood, N., & Danaher, T. (2016). Comparing Landsat water index methods for automated water classification in eastern Australia. *Remote Sensing of Environment*, *175*, 167–182. https://doi.org/10.1016/j.rse.2015.12.055

Floreano, D., & Wood, R. J. (2015). Science, technology and the future of small autonomous drones. In *Nature* (Vol. 521, Issue 7553, pp. 460–466). Nature Publishing Group. https://doi.org/10.1038/nature14542

Fraser, C., Bernatchez, P., & Dugas, S. (2017). Development of a GIS coastal land-use planning tool for coastal erosion adaptation based on the exposure of buildings and infrastructure to coastal erosion, Québec, Canada. In *Geomatics, Natural Hazards and Risk* (Vol. 8, Issue 2, pp. 1103–1125). Taylor and Francis Ltd. https://doi.org/10.1080/19475705.2017.1294114

Hamner, R. M., Constantine, R., Mattlin, R., Waples, R., & Baker, C. S. (2017). Genotype-based estimates of local abundance and effective population size for Hector's dolphins. *Biological Conservation*, *211*, 150–160. https://doi.org/10.1016/j.biocon.2017.02.044

Hayakawa, Y. S., & Obanawa, H. (2020). Volume Measurement of Coastal Bedrock Erosion Using UAV and TLS. *International Geoscience and Remote Sensing Symposium (IGARSS)*, 5230–5233. https://doi.org/10.1109/IGARSS39084.2020.9323220

Hesp, P. A. (1989). A review of biological and geomorphological processes involved in the initiation and development of incipient foredunes. *Proceedings of the Royal Society of Edinburgh. Section B. Biological Sciences*, *96*, 181–201. https://doi.org/10.1017/s0269727000010927

Holdaway, A., & Ford, M. (2019). Resolution and scale controls on the accuracy of atoll island shorelines interpreted from satellite imagery. *Applied Geomatics*, *11*(4), 339–352. https://doi.org/10.1007/s12518-019-00266-7

Hopkinson, C. S., Lugo, A. E., Alber, M., Covich, A. P., & Van Bloem, S. J. (2008). Forecasting effects of sea-level rise and windstorms on coastal and inland ecosystems. In *Frontiers in Ecology and the Environment* (Vol. 6, Issue 5, pp. 255–263). https://doi.org/10.1890/070153

Huang, C., Wylie, B., Yang, L., Homer, C., & Zylstra, G. (2002). Derivation of a tasselled cap transformation based on Landsat 7 at-satellite reflectance. *International Journal of Remote Sensing*, *23*(8), 1741–1748. https://doi.org/10.1080/01431160110106113

Ierodiaconou, D., Schimel, A. C. G., & Kennedy, D. M. (2016). A new perspective of

storm bite on sandy beaches using Unmanned Aerial Vehicles. In *Zeitschrift fur Geomorphologie* (Vol. 60, pp. 123–137). E. Schweizerbart'sche Verlagsbuchhandlung. https://doi.org/10.1127/zfg_suppl/2016/00247

James, M. R., & Robson, S. (2012). Straightforward reconstruction of 3D surfaces and topography with a camera: Accuracy and geoscience application. *Journal of Geophysical Research: Earth Surface*, *117*(3). https://doi.org/10.1029/2011JF002289

Jenks, G. K. (2018). Restoring the natural functional capacity of coastal dune ecosystems: Utilising research records for New Zealand littoral refurbishment as a proxy for analogous global responses. *Journal of Coastal Conservation*, *22*(4), 623–665. https://doi.org/10.1007/s11852-018-0598-9

Jeong, H. Y. (2019). A study on changes in coastal erosion environment by time series coastal detection using GIS. *Journal of Coastal Research*, *91*(sp1), 331–335. https://doi.org/10.2112/SI91-067.1

Kale, M. M., Ataol, M., & Tekkanat, I. S. (2019). Assessment of shoreline alterations using a Digital Shoreline Analysis System: a case study of changes in the Yeşilırmak Delta in northern Turkey from 1953 to 2017. *Environmental Monitoring and Assessment*, *191*(6). https://doi.org/10.1007/s10661-019-7535-8

Kanwal, S., Ding, X., Sajjad, M., & Abbas, S. (2020). Three decades of coastal changes in Sindh, Pakistan (1989-2018): A geospatial assessment. *Remote Sensing*, *12*(1). https://doi.org/10.3390/RS12010008

Karimi, M., Mohammad Vali Samani, J., & Mazaheri, M. (2021). Shoreline spatial and temporal response to natural and human effects in Boujagh National Park, Iran. *International Journal of Sediment Research*, *36*(5), 582–592. https://doi.org/10.1016/j.ijsrc.2021.02.004

Kebede, A. . S. (2009). *Assessing potential risks of impacts of climate change on coastal landfills*.

Le Mauff, B., Juigner, M., Ba, A., Robin, M., Launeau, P., & Fattal, P. (2018). Coastal monitoring solutions of the geomorphological response of beach-dune systems

using multi-temporal LiDAR datasets (Vendée coast, France). *Geomorphology*, *304*, 121–140. https://doi.org/10.1016/j.geomorph.2017.12.037

Lee, W. G., & Partridge, T. R. (1983). Rates of spread of spartina anglica and sediment accretion in the new river estuary, Invercargill, New Zealand. *New Zealand Journal of Botany*, *21*(3), 231–236. https://doi.org/10.1080/0028825X.1983.10428555

Ma, D., Feng, A., Wu, S., Li, P., Cai, F., Liu, J., & Lei, G. (2011). Coastal erosion risk assessment of sandy coast based on GIS and RS. *Proceedings - 2011 19th International Conference on Geoinformatics, Geoinformatics 2011*. https://doi.org/10.1109/GeoInformatics.2011.5980891

Martínez, L. M., Vázquez, G., & Colón, S. S. (2001). Spatial and Temporal Variability during Primary Succession on Tropical Coastal Sand Dunes. In *Source: Journal of Vegetation Science* (Vol. 12, Issue 3). https://www.jstor.org/stable/3236850

Masselink, G., & Pattiaratchi, C. B. (2001). Seasonal changes in beach morphology along the sheltered coastline of Perth, Western Australia. *Marine Geology*, *172*(3–4), 243–263. https://doi.org/10.1016/S0025-3227(00)00128-6

McGranahan, G., Balk, D., & Anderson, B. (2007). The rising tide: Assessing the risks of climate change and human settlements in low elevation coastal zones. *Environment and Urbanization*, *19*(1), 17–37. https://doi.org/10.1177/0956247807076960

Mishra, M., Chand, P., Pattnaik, N., Kattel, D. B., Panda, G. K., Mohanti, M., Baruah, U. D., Chandniha, S. K., Achary, S., & Mohanty, T. (2019). Response of long- to short-term changes of the Puri coastline of Odisha (India) to natural and anthropogenic factors: a remote sensing and statistical assessment. *Environmental Earth Sciences*, *78*(11). https://doi.org/10.1007/s12665-019-8336-7

Moore, L. J. (2000). Shoreline Mapping Techniques. *Source: Journal of Coastal Research*, *16*(1), 111–124.

Mukhopadhyay, A., Mukherjee, S., Mukherjee, S., Ghosh, S., Hazra, S., & Mitra, D. (2012). Automatic shoreline detection and future prediction: A case study on Puri coast, Bay of Bengal, India. *European Journal of Remote Sensing*, *45*(1), 201–213.

https://doi.org/10.5721/EuJRS20124519

Muthusankar, G., Proisy, C., Balasubramanian, D., Bautès, N., Bhalla, R. S., Mathevet, R., Ricout, A., Babu, D. S., & Vasudevan, S. (2018). When Socio-Economic Plans Exacerbate Vulnerability to Physical Coastal Processes on the South East Coast of India. *Journal of Coastal Research*, *85*(85), 1446–1450. https://doi.org/10.2112/SI85-290.1

Nandi, S., Ghosh, M., Kundu, A., Dutta, D., & Baksi, M. (2016). Shoreline shifting and its prediction using remote sensing and GIS techniques: a case study of Sagar Island, West Bengal (India). *Journal of Coastal Conservation*, *20*(1), 61–80. https://doi.org/10.1007/s11852-015-0418-4

Narra, P., Coelho, C., & Sancho, F. (2019). Multicriteria GIS-based estimation of coastal erosion risk: Implementation to Aveiro sandy coast, Portugal. *Ocean and Coastal Management*, *178*. https://doi.org/10.1016/j.ocecoaman.2019.104845

Nicholls, R. J., & Cazenave, A. (2010). Sea-level rise and its impact on coastal zones. In *Science* (Vol. 328, Issue 5985, pp. 1517–1520). https://doi.org/10.1126/science.1185782

Njue, C. N., Cundy, A. B., Smith, M., Green, I. D., & Tomlinson, N. (2012). Assessing the impact of historical coastal landfill sites on sensitive ecosystems: A case study from Dorset, Southern England. *Estuarine, Coastal and Shelf Science*, *114*, 166–174. https://doi.org/10.1016/j.ecss.2012.08.022

Nordstrom, K. F. (1989). Erosion control strategies for bay and estuarine beaches. *Coastal Management*, *17*(1), 25–35. https://doi.org/10.1080/08920758909362072

Nordstrom, K. F., Lampe, R., & Vandemark, L. M. (2000). *Reestablishing Naturally Functioning Dunes on Developed Coasts*.

Nordstrom, K. F., & Mauriello, M. N. (2001). Restoring and maintaining naturally functioning landforms and biota on intensively developed barrier islands under a no-retreat alternative. *Shore and Beach*, *69*, 19–28.

Pascucci, V., De Falco, G., Del Vais, C., Sanna, I., Melis, R. T., & Andreucci, S. (2018). Climate changes and human impact on the Mistras coastal barrier system (W Sardinia, Italy). *Marine Geology*, *395*, 271–284. https://doi.org/10.1016/j.margeo.2017.11.002

Pennings, S. C., Grant, M. B., & Bertness, M. D. (2005). Plant zonation in low-latitude salt marshes: Disentangling the roles of flooding, salinity and competition. *Journal of Ecology*, *93*(1), 159–167. https://doi.org/10.1111/j.1365-2745.2004.00959.x

Pollard, J. A., Brooks, S. M., & Spencer, T. (2019). Harmonising topographic & remotely sensed datasets, a reference dataset for shoreline and beach change analysis. *Scientific Data*, *6*(1). https://doi.org/10.1038/s41597-019-0044-3

Presswell, B., & Bennett, J. (2021). Diomedenema dinarctos n. sp. (Spiruromorpha: Desmidocercidae), a new species of lung nematode in Fiordland crested penguins (Eudyptes pachyrhynchus; Sphenisciformes), from South Island, New Zealand. *Systematic Parasitology*, *98*(3), 285–290. https://doi.org/10.1007/s11230-021-09977-1

Prosser, D. J., Jordan, T. E., Nagel, J. L., Seitz, R. D., Weller, D. E., & Whigham, D. F. (2018). Impacts of Coastal Land Use and Shoreline Armoring on Estuarine Ecosystems: an Introduction to a Special Issue. In *Estuaries and Coasts* (Vol. 41, pp. 2–18). Springer New York LLC. https://doi.org/10.1007/s12237-017-0331-1

Robertson, B., & Stevens, S. (2012). *Porpoise Bay Beach: Fine Scale Monitoring 2011/12*. www.wriggle.co.nz

Rochman, C. M., Browne, M. A., Underwood, A. J., van Franeker, J. A., Thompson, R. C., & Amaral-Zettler, L. A. (2016). The ecological impacts of marine debris: unraveling the demonstrated evidence from what is perceived. *Ecology*, *97*(2), 302–312.

Romaine, G., Balle, A., Mathieu, D., Ahouansou, M., Sintondji, L. C. O., Agbossou, E. K., & Assogba Balle, G. R. (2021). Analyses of Short- and Long-Term Shoreline Trends of the Southwest Benin Coast. *Source: Journal of Coastal Research*, *37*(2), 316–325. https://doi.org/10.2307/27000335

Romine, B. M., Fletcher, C. H., Barbee, M. M., Anderson, T. R., & Frazer, L. N. (2013).

Are beach erosion rates and sea-level rise related in Hawaii? *Global and Planetary Change*, *108*, 149–157. https://doi.org/10.1016/j.gloplacha.2013.06.009

Romine, B. M., Fletcher, C. H., Frazer, L. N., Genz, A. S., Barbee, M. M., & Lim, S. C. (2009). Historical shoreline change, southeast oahu, Hawaii; Applying polynomial models to calculate shoreline change rates. *Journal of Coastal Research*, *25*(6), 1236–1253. https://doi.org/10.2112/08-1070.1

Rouse, H. L., Bell, R. G., Lundquist, C. J., Blackett, P. E., Hicks, D. M., & King, D. N. (2017). Coastal adaptation to climate change in Aotearoa-New Zealand. In *New Zealand Journal of Marine and Freshwater Research* (Vol. 51, Issue 2, pp. 183–222). Taylor and Francis Ltd. https://doi.org/10.1080/00288330.2016.1185736

Ruiz-Beltran, A. P., Astorga-Moar, A., Salles, P., & Appendini, C. M. (2019). Short-Term Shoreline Trend Detection Patterns Using SPOT-5 Image Fusion in the Northwest of Yucatan, Mexico. *Estuaries and Coasts*, *42*(7), 1761–1773. https://doi.org/10.1007/s12237-019-00573-7

Salvadori, G., Tomasicchio, G. R., & D'Alessandro, F. (2014). Practical guidelines for multivariate analysis and design in coastal and off-shore engineering. *Coastal Engineering*, *88*, 1–14. https://doi.org/10.1016/j.coastaleng.2014.01.011

Sanz-Ablanedo, E., Chandler, J. H., Ballesteros-Pérez, P., & Ramón Rodríguez-Pérez, J. (2020). *Reducing Systematic Dome Errors in Digital Elevation Models Through Better UAV Flight Design*.

Sayers, Penning-Rowsell, & Mckenzie. (2017). *Climate Change Risk Assessment 2017 Projections of future flood risk in the UK Project A: Report prepared for the Committee on Climate Change, UK*. www.sayersandpartners.co.uk

Schweiger, C., Kaehler, C., Koldrack, N., & Schuettrumpf, H. (2020). Spatial and temporal evaluation of storm-induced erosion modelling based on a two-dimensional field case including an artificial unvegetated research dune. *Coastal Engineering*, *161*. https://doi.org/10.1016/j.coastaleng.2020.103752

Sebat, M., & Salloum, J. (2018). Estimate the rate of shoreline change using the statistical analysis technique (EPR). *Business & IT*, *VIII*(1), 59–65.

https://doi.org/10.14311/bit.2018.01.07

Seddon, P. J., Ellenberg, U., & van Heezik, Y. (2013). Yellow-eyed Penguin (Megadyptes antipodes). *In: Pablo Garcia Borboroglu and P. Dee Boersma (Eds) Penguins: Natural History and Conservation. University Pf Washington Press, Seattle & London.*, 91–112.

Seibold, E., & Berger, W. (2017). *The Sea Floor. An introduction to marine geology* (Fourth).

Senko, J. F., Nelms, S. E., Reavis, J. L., Witherington, B., Godley, B. J., & Wallace, B. P. (2020). Understanding individual and population-level effects of plastic pollution on marine megafauna. *Endangered Species Research*, *43*, 234–252. https://doi.org/10.3354/esr01064

Setälä, O., Lehtiniemi, M., Coppock, R., & Cole, M. (2018). Microplastics in Marine Food Webs. *Microplastic Contamination in Aquatic Environments*, 339–363.

Short, A. D. (1999). *Handbook of Beach and Shoreface Morphodynamics* (3rd ed., Vol. 17).

Sui, L., Wang, J., Yang, X., & Wang, Z. (2020). Spatial-temporal characteristics of coastline changes in Indonesia from 1990 to 2018. *Sustainability (Switzerland)*, *12*(8), 1–28. https://doi.org/10.3390/SU12083242

Syvitski, J. P. M. (2003). Supply and flux of sediment along hydrological pathways: research for the 21st century. *Global and Planetary Change*, *39*(1–2), 1–11. https://doi.org/10.1016/S0921-8181(03)00008-0

Taillie, P. J., Moorman, C. E., Poulter, B., Ardón, M., & Emanuel, R. E. (2019). Decadal-Scale Vegetation Change Driven by Salinity at Leading Edge of Rising Sea Level. *Ecosystems*, *22*(8), 1918–1930. https://doi.org/10.1007/s10021-019-00382-w

Taylor, R., Stephenson, B., Smith, I. W. G., Gibbs, N., Saunders, A., Cochrane, P. R., Wall, B., & Swain, D. J. (1997). *The state of New Zealand's environment, 1997*. Ministry for the Environment.

Thanh, T. M., Tanaka, H., Mitobe, Y., Viet, N. T., & Almar, R. (2018). Seasonal Variation

of Morphology and Sediment Movement on Nha Trang Coast, Vietnam. *Journal of Coastal Research*, *81*(sp1), 22–31. https://doi.org/10.2112/SI81-004.1

Thompson, L. M. C., & Schlacher, T. A. (2008). Physical damage to coastal dunes and ecological impacts caused by vehicle tracks associated with beach camping on sandy shores: A case study from Fraser Island, Australia. *Journal of Coastal Conservation*, *12*(2), 67–82. https://doi.org/10.1007/s11852-008-0032-9

Tiernan, F. (2012). *Coastal Monitoring Strategy, Marlborough*. www.marlborough.govt.nz

Tobler, W. R. (1970). "A Computer Movie Simulating Urban Growth in the Detroit Region." *Economic Geography (Supplement: Proceedings, International Geographical Union. Commission on Quantitative Methods), , 46*, 234–240.

Toffi, M. (2008). *Climate variability, man, and the dynamics of Benin coastal ecosystems*.

Van Der Meulen, F., & Salman, A. H. P. M. (1996). Management of Mediterranean coastal dunes. *Ocean & Coastal Management*, *30*(3), 177–195.

Walling, D. E. (2006). Human impact on land-ocean sediment transfer by the world's rivers. *Geomorphology*, *79*(3–4), 192–216. https://doi.org/10.1016/j.geomorph.2006.06.019

Watts, A. C., Ambrosia, V. G., & Hinkley, E. A. (2012). Unmanned aircraft systems in remote sensing and scientific research: Classification and considerations of use. *Remote Sensing*, *4*(6), 1671–1692. https://doi.org/10.3390/rs4061671

Wilcox, C., Van Sebille, E., Hardesty, B. D., & Estes, J. A. (2015). Threat of plastic pollution to seabirds is global, pervasive, and increasing. *Proceedings of the National Academy of Sciences of the United States of America*, *112*(38), 11899–11904. https://doi.org/10.1073/pnas.1502108112

Wulder, M. A., Franklin, S. E., Hall, R. J., & Coops, N. C. (2004). High Spatial Resolution Remotely Sensed Data for Ecosystem Characterization. In *BioScience* (Vol. 54, Issue 6). https://academic.oup.com/bioscience/article/54/6/511/294008

Yan, D., Yao, X., Li, J., Qi, L., & Luan, Z. (2020). Shoreline Change Detection and Forecast along the Yancheng Coast Using a Digital Shoreline Analysis System. *Wetlands*, 41–47. https://doi.org/10.1007/s13157-021-01444-3/Published

Yu, G., Xie, M., Liang, J., Farooq, A., & Williams, E. J. (2020). A GIS-based 3D slope stability analysis method based on the assumed normal stress on the slip surface. *Scientific Reports*, *10*(1), 1–12. https://doi.org/10.1038/s41598-020-61301-x

Zammit, C., Pearce, P., Mullan, B., Sood, A., Collins, D., Stephens, S., Woolley, J. M., Bell, R., & Wadhwa, S. (2018). *Southland climate change impact assessment Prepared for Environment Southland, Invercargill City Council, Southland District Council and Gore District Council*.

Zhang, K., Douglas, B., & Leatherman, S. (2002). Do Storms Cause Long-Term Beach Erosion along the U.S. East Barrier Coast? *The Journal of Geology*, *110*(4), 493–502.

Zhang, Y. (2020). An Indicator and Min-Cost Approach for Shoreline Extraction from Satellite Imagery in Muddy Coasts. *IEEE Transactions on Geoscience and Remote Sensing*, *58*(6), 4375–4386. https://doi.org/10.1109/TGRS.2019.2963460

Appendix I

Monkey Island magnitude of change between corresponding years at each transect line. The net change, total accretion and total erosion added up for each transect line are on the right three columns.

Transect Number	Year					Net Total Change	Total Gained	Total Lost
	1946-1963	1963-1984	1984-2005	2005-2013	2013-2021			
1	2.8442046	2.04398048	-1.8243986	0.6222986	-5.40706492	-1.720979916	5.510483652	-7.231463568
2	6.46935305	-10.014211	13.5740518	-2.9367056	-6.59349078	0.498997845	20.04340487	-19.54440702
3	3.76555104	-3.4398268	1.01034261	1.335258	-3.55785975	-0.886534857	6.111151683	-6.997686539
4	1.56375913	-0.0331755	-5.6092436	0.9196798	-0.64535283	-3.804332893	2.483438945	-6.287771838
5	0.93459296	-7.9227521	14.5699017	-1.4375318	0.69548272	6.839693474	16.19997735	-9.360283877
6	4.00243923	-1.7524999	-2.2576198	1.119309	-4.7899812	-3.678352662	5.121748228	-8.80010089
7	-0.7367357	0.09715669	-1.8078391	0.8787247	-6.46032359	-8.029017014	0.975881367	-9.004898381
8	-2.38770248	0.2658595	1.78879672	0.4899188	0.55570817	0.712580721	3.100283202	-2.387702481
9	4.22273815	-3.9951345	0.68618747	0.6615143	-0.40509494	1.170210477	5.570439959	-4.400229482
10	-0.95681756	-2.7789484	0.08706563	0.7125645	0.18300681	-2.753129001	0.982636989	-3.73576599
11	3.06331385	-6.1185318	2.91982438	0.8478497	-0.08460629	0.627849839	6.830987971	-6.203138131
12	-0.55887471	-8.4754853	3.53424845	2.8955521	-2.19723652	-4.801796043	6.429800513	-11.23159656
13	-6.2756601	1.4473544	-12.215117	2.6943504	0.9978405	-13.35123184	5.139545298	-18.49077714
14	-4.23522677	0.56372613	-8.1862124	0.9068263	1.26425301	-9.686633738	2.734805396	-12.42143913
15	-2.69556117	0.75186033	-6.078496	-0.3249743	0.35773337	-7.989437837	1.109593697	-9.099031534
16	8.48501919	-2.1851739	-4.1911367	2.0013375	1.70185867	5.811904759	12.18821537	-6.376310616
17	4.58521382	-1.4081238	-2.3467601	0.8683735	2.07462653	3.773329999	7.528213894	-3.754883895
18	2.01922857	-0.7405158	-0.7666187	1.7453247	0.810903	3.068321766	4.575456286	-1.50713452
19	-1.86084265	-2.2723647	-2.3144804	2.4014204	-1.87417609	-5.920443427	2.4014204	-8.321863828

20	-2.28457171	5.06972301	-6.3749556	0.6724502	1.4911899	-1.426164188	7.23336311	-8.659527298
21	0.26199196	-5.0910257	-7.0035782	-0.8001014	6.66084794	-5.97186541	6.922839895	-12.89470531
22	-2.68491637	-2.7028254	-11.047448	-0.2250605	-7.43313234	-24.09338316	0	-24.09338316
23	-0.78076939	-3.4148664	-1.4647501	-2.2451211	-5.62694406	-13.53245118	0	-13.53245118
24	-2.38966033	-6.506179	-5.1772531	-1.5854614	-2.20747522	-17.86602902	0	-17.86602902
25	-2.30704716	-1.40694	-10.89069	0.6098615	-1.13667974	-15.13149561	0.609861499	-15.74135711
26	-8.001522	-4.1551551	-2.0779396	-1.0307434	-5.92090934	-21.18626949	0	-21.18626949
27	-14.6917161	-5.152198	-0.0485232	4.7848613	-9.22786734	-24.33544323	4.784861325	-29.12030456
28	2.24580552	-1.0471517	-8.4697857	-2.5336667	2.58908964	-7.215708952	4.834895164	-12.05060412
29	-3.28399361	-0.9192814	-3.2729057	-0.5865381	-0.82989091	-8.892609659	0	-8.892609659
30	-0.88283106	0.45180003	-3.949512	-1.1183117	-0.45219205	-5.951046772	0.451800035	-6.402846807
31	-12.3662802	3.02884658	-6.3976903	-3.9298469	-0.17744064	-19.8424115	3.028846576	-22.87125807
32	-13.8205113	2.47449333	-4.5092802	-1.0305825	-0.22275873	-17.10863942	2.474493327	-19.58313274
33	-6.64188185	-2.1701569	0.28077938	-0.6556506	0.8963222	-8.290587828	1.177101573	-9.467689401
34	-3.35582809	-0.9404255	-8.2477865	4.524403	3.49298775	-4.526649381	8.017390773	-12.54404015
35	-2.36469689	3.36978817	-5.3207949	1.3952743	3.92126283	1.000833493	8.686325273	-7.68549178
36	1.83795265	-0.1348686	-5.8158019	1.9894756	4.64970771	2.52646548	8.477135996	-5.950670517
37	-3.7454485	0.33552507	4.27861107	1.4855617	-0.30893682	2.045312516	6.099697834	-4.054385318
38	-3.14739305	-3.9891425	7.06470299	-1.9867582	5.64086263	3.582271911	12.70556563	-9.123293717
39	-5.16470075	-0.7594135	3.18563541	1.1584395	4.63533514	3.055295841	8.979410056	-5.924114215
40	0.82291073	1.84209898	-1.3630845	-1.9693997	6.71009396	6.042619436	9.375103664	-3.332484228
41	-2.94031228	2.25349336	-0.575269	-0.4745011	5.72192449	3.985335425	7.975417846	-3.990082421
42	-2.30907064	-1.4893612	3.88173183	-0.7481465	7.00134047	6.336493975	10.8830723	-4.546578329
43	-2.1753682	-2.6330683	2.48684002	1.0109217	5.52983843	4.219163666	9.027600136	-4.808436469
44	-2.60698718	-5.1288334	0.31775289	3.1605265	6.45445291	2.196911725	9.93273235	-7.735820625

45	-3.98259603	-1.8229797	-0.7802468	2.8284245	6.68529548	2.927897356	9.513719957	-6.585822601
46	-5.58712151	-0.400416	3.0039397	-1.2149561	7.88466798	3.68611401	10.88860768	-7.202493668
47	-2.21123071	-1.2548757	1.26317395	1.3139253	7.0179345	6.128927284	9.595033727	-3.466106444

Colac Bay magnitude of change between corresponding years at each transect line. The net change, total accretion and total erosion added up for each transect line are on the right three columns.

Transect Number	Year							Net Total Change	Total Gained	Total Lost
	1952-1963	1963-1976	1976-1985	1985-1993	1993-2007	2007-2014	2014-2021			
1	3.5432798	-2.879009	-2.079572			-1.701577	0.296215	-2.820663397	3.839494813	-6.6601582
2	1.669108	-3.798916	-2.188559			-1.575384	0.156593	-5.737157587	1.825700681	-7.5628583
3	1.7417159	-4.33306	-1.653062			0.4329462	-1.20431	-5.015768597	2.174662165	-7.1904308
4	1.0781215	-2.109936	-1.548714			0.3428199	-2.05721	-4.294922437	1.420941426	-5.7158639
5	1.1507295	-2.497368	-2.261871			-0.448472	-0.0326	-4.089580214	1.15072949	-5.2403097
6	1.1324543	-0.376448	-4.028218			-1.848354	0.938541	-4.182024495	2.070995414	-6.2530199
7	0.6506257	-0.997569	-2.211284			0.0765206	-2.40992	-4.891631272	0.727146286	-5.6187776
8	-0.964814	-0.558751	-2.524593			-1.06811	-1.71254	-6.828807839	0	-6.8288078
9	-0.867468	0.867402	-3.714789			-1.286979	-0.039	-5.040833904	0.867402331	-5.9082362
10	-0.407294	-1.882449	-2.241315			-1.794609	0.038321	-6.287345982	0.038320767	-6.3256667
11	-0.705494	0.942604	-4.880986			-0.601604	-2.0443	-7.289783427	0.94260427	-8.2323877
12	-1.003818	-0.416457	-1.715604			-0.528932	0.464895	-3.199916135	0.464895097	-3.6648112
13	-10.28066	-6.291632	-2.982416			-2.905966	0.246183	-22.2144957	0.24618327	-22.460679
14	1.823959	1.503885	-4.705649			-0.90458	0.385719	-1.896666203	3.713562659	-5.6102289
15	-1.598188	2.970952	-6.143493			0.0847968	3.477362	-1.208570686	6.533110761	-7.7416814
16	0.9681559	1.567663	-4.850749	0.019972	0.4597102	-0.474605	4.25012	1.940266942	7.265620747	-5.3253538
17	1.0368235	-0.255833	-4.902317	-1.042551	4.4061185	-3.397575	2.755449	-1.399885962	8.198390621	-9.5982766
18	1.4103531	0.709772	-3.896187	-1.731518	3.371751	-1.848881	0.382297	-1.602412802	5.874173246	-7.476586
19	3.4751848	-1.345447	-4.303512	-0.141799	2.411251	-3.155917	1.658115	-1.402123218	7.544551178	-8.9466744
20	0.6528753	1.486475	-4.381776	-1.791657	2.2569968	-1.438211	3.613596	0.398298915	8.00994352	-7.6116446
21	2.1022193	-0.660068	-2.374436	-0.796122	1.7116306	-4.291364	5.311445	1.00330599	9.12529491	-8.1219889

22	0.6918855	1.707266	-3.664279	-1.072287	3.8725408	-3.21439	1.122012	-0.557251538	7.393704313	-7.9509559
23	-0.328788	0.350211	-3.624479	-0.829769	-0.29511	0.2325318	1.627101	-2.868302157	2.209843682	-5.0781458
24	0.2011383	0.816233	-4.224651	-1.00161	2.4778784	-2.470638	0.699938	-3.501711303	4.195187667	-7.696899
25	-0.508323	1.140005	-4.309532	-1.189481	1.3357739	-2.689357	3.043567	-3.177347091	5.519345401	-8.6966925
26	-1.255706	1.399131	-3.59669	-0.344544	1.7835874	-3.110797	1.143388	-3.981630562	4.326106156	-8.3077367
27	-0.202371	-1.300004	-2.438727	0.459939	1.2910047	-4.579204	1.848609	-4.920753635	3.599552188	-8.5203058
28	-0.371042	1.654319	-3.948807	-0.084531	2.6144342	-5.48796	1.56215	-4.061438929	5.830902347	-9.8923413
29	-1.32607	-1.274384	-1.030296	1.902543	0.0652883	-1.073117	-0.42367	-3.159707913	1.967831174	-5.1275391
30	-2.215427	-2.417076	-0.170232	1.606965	1.0068287	-2.094268	0.527676	-3.755532014	3.141470236	-6.8970022
31	0.0005372	-0.988423	-0.136748	-0.008762	0.2118273	-1.081738	0.322407	-1.680899835	0.534771714	-2.2156715
32	-0.699058	-0.523152	-2.218459	2.140033	0.2382706	-2.5081	-0.13277	-3.703234036	2.378303597	-6.0815376
33	1.60207	-0.92908	-2.307113	0.963423	2.6472186	-2.456993	0.07341	-0.407064678	5.286121438	-5.6931861
34	1.9889083	1.218272	-4.017009	2.681003	0.8555887	-2.04032	1.465625	2.15206714	8.209396681	-6.0573295
35	2.4907716	0.975885	-1.283741	0.964923	2.6193545	-4.127107	0.438842	2.078928366	7.489776206	-5.4108478
36	2.8560714	-1.848227	-0.219297	1.701337	-0.07883	-2.598472	1.256579	1.069162103	5.81398714	-4.744825
37	2.2808278	-0.86181	-1.194556	3.118456	-1.173354	-1.1916	0.214413	1.192376717	5.613696574	-4.4213199
38	1.9287028	-0.597512	-1.34417	3.652237	0.2600302	-1.959316	0.314131	2.254102315	6.155100779	-3.9009985
39	-0.625423	-1.256828	-0.140551	3.492202	-2.339567	-1.4063	1.37433	-0.902135301	4.866532123	-5.7686674
40	0.4719825	-2.198174	-0.802737	4.167701	-3.600966	-1.120882	1.066348	-2.016727772	5.706031585	-7.7227594
41	-1.238091	1.215025	-1.721895	4.322432	-4.172297	-0.749471	1.495989	-0.84830824	7.033445771	-7.881754
42	0.3108327	-0.318876	-1.138965	3.283371	-2.344801	-1.60511	1.607069	-0.206479041	5.201272443	-5.4077515
43	-1.164694	0.560804	-1.261018	4.914837	-3.797703	-1.282118	2.989979	0.960086666	8.46562109	-7.5055344
44	-1.459912	0.075789	-1.030699	5.195589	-3.119022	-3.217744	4.565829	1.009829648	9.837207165	-8.8273775

45	-0.157118	0.113176	-1.53684	4.367904	-2.435319	-2.770098	2.136005	-0.28229136	6.617084206	-6.8993756
46	-0.404967	-0.187002	-0.878601	2.479227	-3.235133	0.5667149	0.493203	-1.166558063	3.539144818	-4.7057029
47	-0.326972	0.158257	-1.503066	2.986199	-1.650709	-0.493336	1.25223	0.422603428	4.396686631	-3.9740832
48	-0.829922	-0.845354	-1.255834	3.334812	-1.254428	-0.842653	1.968014	0.274635239	5.302825934	-5.0281907
49	-0.066363	-0.78237	-0.666009	3.625666	-3.201108	-0.828368	2.232498	0.313944816	5.858163734	-5.5442189
50	-0.458468	-0.306843	-0.782	4.429881	-3.328909	-2.507075	2.537814	-0.415599578	6.967695186	-7.3832948
51	-1.213164	-0.060926	-1.284566	3.324722	-0.990641	-3.093111	1.982602	-1.335084948	5.30732365	-6.6424086
52	-1.107434	-0.628698	-0.40168	2.039463	-0.963996	-1.313389	1.819062	-0.556671567	3.858525072	-4.4151966
53	-0.850287	1.519792	-1.435519	1.765586	-3.805408	-0.200343	3.042592	0.036412538	6.32796954	-6.291557
54	-1.159195	-0.817505	0.44628	0.366372	3.2079244	-4.809185	1.970027	-0.79528142	5.990603125	-6.7858845
55	-2.482981	0.881021	-0.835892	-0.268691	1.4838998	-0.923855	1.754993	-0.391505221	4.119914654	-4.5114199
56	-2.928944	2.273175	-0.223451	-2.261192	1.9064131	-2.08217	1.346935	-1.969233963	5.526523153	-7.4957571
57	-1.832525	2.679821	-2.09551			0.3584664	-0.73807	-1.627821954	3.038287447	-4.6661094
58	-2.396812	0.639953	-0.743514			-0.789696	0.214318	-3.075751399	0.854270672	-3.9300221
59	-1.900754	0.917429	-1.526781			-0.109741	-1.30463	-3.924473014	0.917429489	-4.8419025
60	-1.846068	0.000985	0.303365			0.6250146	-2.26843	-3.18513337	0.929364646	-4.114498
61	-2.527195	0.153293	-0.79512			0.4956839	-2.68406	-5.357397689	0.648977096	-6.0063748
62	-2.710388	0.748018	-0.52247			-1.002008	-0.56949	-4.05633761	0.748018317	-4.8043559
63	-2.880016	1.513386	-0.42835	-0.09065	0.6183438	-1.856939	0.451102	-2.673123742	2.582831769	-5.2559555
64	-2.18673	0.367217	-0.326175	1.001281	-3.221254	2.0790083	-2.2159	-4.502553887	3.447507159	-7.950061
65	-3.701381	1.469654	0.463664	1.338102	-3.158898	1.8660093	-5.23807	-6.960918976	5.137429296	-12.098348
66	-5.219692	3.879193	-0.558315	0.608985	-1.495848	0.7639003	-6.76171	-8.783490114	5.252078099	-14.035568
67	-4.422477	4.642657	-1.818799	0.576864	-2.507752	1.4026208	-8.27737	-10.40425814	6.622141873	-17.0264
68	-3.368226	1.71801	-0.426037	-1.405367	1.2812386	-2.999572	-5.31332	-10.51327036	2.999248777	-13.512519
69	-2.343885	1.458511	-0.564332	-1.61562	-0.376597	-0.844618	-5.55178	-9.838321762	1.45851088	-11.296833

70	-0.902764	-0.029931	0.064083	-1.575844	-1.233808	-0.487188	-5.41661	-9.582063209	0.064082772	-9.646146
71	-1.48597	0.813873	-0.893447	-1.385755	-0.176828	-0.583743	-4.5385	-8.250374365	0.813872583	-9.0642469
72	-1.88975	1.559123	-0.374648	-1.622591	1.5194669	-0.690454	-6.72715	-8.226003624	3.078589746	-11.304593
73	-1.59846	1.002296	0.012754	-2.029891	2.5267624	-0.463359	-5.93407	-6.483967842	3.54181238	-10.02578
74	-2.851317	2.780392	0.837217	-4.411341	3.1493045	-0.998572	-4.51686	-6.011177865	6.76691335	-12.778091
75	-1.229974	0.518063	0.910288	-2.553651	3.6154815	-1.357467	-4.82837	-4.925627462	5.04383171	-9.9694592
76	-0.912232	-0.604498	2.302225	-2.880557	3.0154454	-2.682721	-2.75934	-4.52167647	5.317670182	-9.8393467
77	-1.393647	0.962394	0.425585	-2.623621	2.8803334	-1.713097	-2.01447	-3.476523822	4.26831248	-7.7448363
78	-1.509757	1.001421	-0.464808	-1.711261	3.2479515	-2.536068	0.680472	-1.292050147	4.929844482	-6.2218946
79	0.506481	0.227841	1.507929	-3.603358	1.6769023	-1.743744	1.469997	0.042048631	5.389150284	-5.3471017
80	-2.680703	1.742715	2.786537	-5.009366	3.4259223	-3.842623	1.609973	-1.967544216	9.565147316	-11.532692
81	-2.100147	3.561779	0.798966	-2.816716	2.5260918	-5.08869	1.179008	-1.939707043	8.065845114	-10.005552
82	-2.934641	1.294589	0.966778	-2.47388	3.3797989	-4.204471	1.189048	-2.782777777	6.830214145	-9.6129919
83	-1.387196	1.277938	0.62611	-3.250952	4.3068766	-4.031911	-0.78676	-3.245899594	6.210924293	-9.4568239
84	-1.798195	0.717781	0.360163	0.118783	2.2615502	-3.182703	-0.00201	-1.524634367	3.458277467	-4.9829118
85	-2.32966	1.43511	1.551795	-1.898091	3.4242695	-2.289827	-0.05285	-0.159249124	6.411174105	-6.5704232
86	-0.981517	1.135823	0.867994	-0.741277	2.3623915	-2.330986	-0.33143	-0.018998847	4.366208527	-4.3852074
87	-2.435661	2.437395	-0.195324	-0.711572	0.5110065	-1.821097	0.795541	-1.419710928	3.743942382	-5.1636533
88	-1.690035	1.778779	-0.453247	-1.244692	1.0233722	-0.79328	0.354445	-1.024657275	3.156596128	-4.1812534
89	-2.035449	2.3971	-0.329007	-1.121278	1.0890597	-1.084764	-0.11174	-1.196076841	3.486159671	-4.6822365
90	-1.180561	1.652176	0.242345	-0.648523	0.2815942	-0.389928	-0.29798	-0.340872538	2.176115653	-2.5169882
91	-1.435051	2.110861	-0.459445	-0.699893	-0.50797	0.8300179	-0.58908	-0.750560741	2.940878549	-3.6914393
92	-1.134853	2.388401	-0.570504	0.480676	-1.715254	1.3998765	-1.79844	-0.950098017	4.268953349	-5.2190514
93	-0.098116	1.927473	0.591566	-1.912457	-1.234802	1.6548465	-1.40528	-0.476765239	4.173885577	-4.6506508
94	-0.907295	1.275557	-0.015301			0.7465203	-1.45914	-0.359660787	2.022077641	-2.3817384

95	-1.716474	2.247609	-0.215455	-0.554151	-0.35164	-0.590107919	2.247608749	-2.8377167
96	-0.770662	2.593924	-1.245696	-0.981222	-0.52703	-0.930688373	2.59392377	-3.5246121
97	-0.934227	2.237099	0.047622	-1.534297	-0.5631	-0.746903769	2.284720433	-3.0316242
98	-0.296328	2.168165	0.242839	-2.533371	-1.06883	-1.487520781	2.41100431	-3.8985251
99	-1.878337	2.840405	0.342498	-3.303114	0.727854	-1.270694062	3.910756751	-5.1814508
100	-2.625227	3.923795	-1.424818	-1.841265	0.329402	-1.638113647	4.253196803	-5.8913105
101	-0.852032	0.792205	-0.109066	-0.323835	0.306721	-0.186007429	1.098926512	-1.2849339
102	-2.124895	1.282065	-1.27757	1.9623945	-2.74243	-2.900435518	3.244459652	-6.1448952
103	-0.624394	1.771925	-1.641147	3.6968902	-2.75575	0.447525365	5.468815392	-5.02129
104	-2.053735	2.393329	-2.823384	-0.700787	-1.10333	-4.287907312	2.393328871	-6.6812362
105	-1.115371	0.437074	-1.254781	-0.116478	-1.17676	-3.226310256	0.437074199	-3.6633845
106	-4.17289	0.103493	-3.809506	2.853225	-8.24279	-13.26846748	2.956717534	-16.225185
107	-3.093087	0.219423	-1.199276	-0.530504	-10.2472	-14.85066144	0.219422804	-15.070084
108	-4.851143	-0.056937	-1.243603	2.5685596	-13.5351	-17.11823765	2.568559596	-19.686797
109	-4.833556	-0.487916	-1.154164	0.3163741	3.507306	-2.651955297	3.823680561	-6.4756359
110	-2.952861	-7.199622	-0.543312	-0.212455	4.149467	-6.758783055	4.149466986	-10.90825
111	-2.310144	-6.283305	-1.113048	1.5863592	1.92233	-6.19780787	3.508689244	-9.7064971
112	-1.763077	-7.119661	0.411331	-0.952884	2.981238	-6.443053706	3.392569106	-9.8356228
113	-1.74549	-6.830663	-0.998262	0.8460243	1.924129	-6.804261772	2.770153092	-9.5744149
114	-1.235358	-6.29213	-0.940328	-0.634929	0.867443	-8.235302039	0.867442975	-9.102745
115	-1.622852	-6.315418	-0.478904	-1.058163	1.397532	-8.077804865	1.397531686	-9.4753366
116	-1.605265	-7.086279	-1.608005	4.9630564	1.090525	-4.245966809	6.05358171	-10.299549
117	-1.946324	-9.846784	-0.430803	2.9143119	2.457287	-6.852312061	5.371598705	-12.223911
118	-1.321627	-9.729608	-1.496316	0.8468784	0.871358	-10.82931349	1.71823636	-12.54755
119	-1.115187	-14.74675	14.39345	-0.105279	1.401024	-0.172739033	15.79447803	-15.967217

120	-0.3891	-1.497581	1.119715	-0.231304	0.872839	-0.125430858	1.992554306	-2.1179852
121	-1.62462	-0.150432	0.396664	-1.131279	2.989809	0.48014162	3.386472639	-2.906331
122	-0.172192	-2.142133	2.41682	3.2122805	2.953183	6.267959265	8.582284192	-2.3143249
123	0.0987037	-4.871062	1.989454	-0.34409	3.054701	-0.072294381	5.142858135	-5.2151525
124	-0.922737	1.80648	0.465827	4.2234852	2.839368	8.412422834	9.335159477	-0.9227366
125	-0.217472	1.07346	0.217202	2.2766569	1.891448	5.241294259	5.458766333	-0.2174721
126	-0.815936	3.233805	-1.461815	0.7253163	0.340616	2.021985739	4.299737312	-2.2777516
127	0.0647844	2.929575	-0.872073	0.6219869	-0.69269	2.051588023	3.61634633	-1.5647583

Fortrose magnitude of change between corresponding years at each transect line. The net change, total accretion and total erosion added up for each transect line are on the right three columns.

Transect Number	Year							Net Total Change	Total Accretion	Total Erosion
	1948-1962	1962-1978	1978-1985	1985-1994	1994-2005	2005-2013	2013-2021			
1	19.647245	24.36652	0.41645	0.1006237	-5.28509	0.8942285	-3.0381293	37.10184785	45.42506671	-8.323218866
2	19.117001	5.283838	-5.69456	-6.30368	0.5727796	2.3582589	-4.2196984	11.11393864	27.33187707	-16.21793844
3	12.685157	-0.783869	1.272243	-9.108186	6.4592091	-5.607837	-2.4580063	2.458709212	20.41660857	-17.95789936
4	-34.31859	2.4032549	-1.701879	-0.029307	-2.671542	0.8238592	-0.2368508	-35.7310594	3.227114132	-38.95817353
5	-6.318788	-4.427622	-9.76931	-4.528293	-2.226592	0.1926035	-2.8958239	-29.97382599	0.192603452	-30.16642945
6	-10.58017	-3.850957	-5.652644	-8.093457	0.3106735	-3.640583	-1.1723655	-32.67949856	0.31067352	-32.99017208
7	-9.765737	-5.264202	-1.532595	-7.649384	2.2629628	-3.811003	-5.0073302	-30.76728786	2.262962787	-33.03025064
8	-8.696611	-6.886969	-1.833441	-5.324336	0.828981	-4.418944	-5.0354914	-31.36681022	0.828980981	-32.1957912
9	-7.691406	-2.920541	-5.36515	-6.02845	0.6995102	-0.371872	-5.4405018	-27.11841085	0.69951019	-27.81792104
10	-6.589539	-7.537316	-1.803045	-4.081914	-0.338594	-0.003041	-4.0317717	-24.38522001	0	-24.38522001
11	-8.037632	-8.623426	-4.154276	-2.962812	-0.86965	0.445334	-2.0932401	-26.29570176	0.445333964	-26.74103572
12	-6.448508	-12.37198	-1.912652	-2.629651	-2.782734	1.4049705	-1.8537643	-26.59431592	1.404970498	-27.99928642
13	-7.524362	-8.235542	-3.0068	-3.619208	-1.509813	3.2894897	-0.0142667	-20.62050169	3.289489707	-23.90999139
14	-1.89464	-11.11714	-3.581282	-1.068186	-0.979778	1.0304367	-0.3872673	-17.99785446	1.030436655	-19.02829111
15	-2.887544	-5.510304	-5.364859	-1.860323	-0.787098	2.2442045	-1.6038382	-15.76976169	2.244204511	-18.0139662
16	-4.163426	-4.711893	-0.007813	-0.845989	-1.292778	1.811085	-0.3792754	-9.590089794	1.811085048	-11.40117484
17	-1.82793	-3.867348	-0.915176	-2.075817	-0.827289	2.6501217	-1.8759845	-8.739422753	2.650121704	-11.38954446
18	-8.348681	-3.699629	-8.171142	1.1552035	-4.189431	3.5259067	-0.3946667	-20.1224393	4.681110178	-24.80354948
19	-11.38481	-4.646713	-7.798462	-1.695666	-2.033148	3.8237642	-1.0640192	-24.79905095	3.823764219	-28.62281517
20	-18.58386	-6.381126	-0.608228	1.1071384	-4.550463	3.2214027	-0.1634421	-25.95857461	4.328541077	-30.28711569
21	-9.532451	-13.42539	1.481297	-2.007931	-3.923084	4.3368626	-0.2505914	-23.32128676	5.818159186	-29.13944595
22	-14.13074	-11.55376	0.910258	-1.493781	-2.593397	2.6015025	-1.9520824	-28.2120017	3.511760429	-31.72376213
23	-11.43332	-12.43377	-0.288148	-0.636935	-0.835293	-3.749865	-1.3623537	-30.73967955	0	-30.73967955

24	-10.88761	-10.80604	3.100399	-3.126552	-1.644191	-3.165169	-1.2205844	-27.74974515	3.100398506	-30.85014366
25	-11.66292	-8.835727	1.764094	-4.433994	-2.998383	0.0703736	-1.9740422	-28.0705946	1.834467934	-29.90506254
26	-8.796117	-7.092037	0.738172	-3.401806	-0.9692	1.3192596	-0.7022365	-18.90396523	2.057431307	-20.96139654
27	-9.203868	-3.151594	-2.068165	-4.277552	0.4785933	1.5716422	-0.8020589	-17.45300281	2.050235449	-19.50323826
28	-5.956401	-2.568034	-0.71032	-5.002485	1.4159362	1.0626572	-0.3518211	-12.1104671	2.478593417	-14.58906052
29	-6.067268	0.1281623	-1.877361	-3.202572	1.0729429	0.7012326	-0.363387	-9.60825075	1.902337766	-11.51058852
30	-6.463668	-0.858031	1.602996	-5.628202	3.9702656	1.0157889	-1.0665256	-7.427376334	6.589050347	-14.01642668
31	-5.770401	-0.023048	0.2475	-3.980437	4.7837091	-1.784217	-0.3280546	-6.854948908	5.031209316	-11.88615822
32	-4.462953	-0.705611	3.052688	-3.695937	5.2940555	-3.970903	-1.0207319	-5.509393545	8.346743016	-13.85613656
33	-5.527986	0.0621791	0.880454	0.4879307	1.8273256	-4.595384	-2.2423065	-9.107786175	3.257889794	-12.36567597
34	-2.648602	2.5226948	0.36767	-2.283428	-0.436994	-4.348847	-3.9712026	-10.79870982	2.890365139	-13.68907496
35	-3.180052	2.7591951	0.014244	-2.810837	0.2497453	-3.974521	-4.8654656	-11.80769134	3.023184159	-14.8308755
36	-3.083162	4.4804423	-5.91696	-8.959942	3.2548614	-3.151905	-1.3410063	-14.71767185	7.735303771	-22.45297563
37	-1.198793	4.4650344	-9.98814	-8.342963	3.1667094	-3.11861	-1.0606712	-16.07743303	7.631743742	-23.70917677
38	-1.782784	-6.632039	-11.65483	-3.85487	1.6485785	3.1453093	-3.1329067	-22.26353954	4.793887793	-27.05742734
39	-0.77416	-8.5428	-9.934036	-4.011012	1.7967519	3.9230694	-4.1391918	-21.68137762	5.719821268	-27.40119889
40	-2.51711	-2.574404	-9.528206	-5.97862	1.6121273	7.1244019	-2.8801716	-14.74198267	8.736529246	-23.47851191
41	3.310538	-2.270571	-4.821305			1.2314134	-0.5645081	-3.114432229	4.541951423	-7.656383653
42	-0.04421	0.0224641	-4.232811			-4.229393	-0.7933918	-9.277341457	0.022464059	-9.299805516
43	0.2394622	0.8537638	-3.861513			-1.685026	-0.3661989	-4.819511422	1.093226065	-5.912737487
44	0.4546399	0.6086117	-3.849129			0.3319038	-0.397361	-2.851334903	1.395155401	-4.246490304
45	2.276536	0.7498133	-3.403482			0.3636139	-0.5705126	-0.58403155	3.389963215	-3.973994765
46	4.6925163	-0.833947	-0.782755			0.2543185	-1.3410819	1.989050591	4.946834804	-2.957784212
47	-0.528815	4.2352095	-3.19493			-0.671291	-0.1904357	-0.350263498	4.235209495	-4.585472993
48	-4.324143	3.159319	-1.634739			1.6675981	-1.0684128	-2.200376795	4.826917105	-7.0272939
49	-4.622926	4.5187608	-2.762825			-0.365654	-0.2320526	-3.464695891	4.518760811	-7.983456702

Porpoise Bay magnitude of change between corresponding years at each transect line. The net change, total accretion and total erosion added up for each transect line are on the right three columns.

Transect Number	Year							Net Total Change	Total Gained	Total Lost
	1948-1967	1967-1978	1978-1985	1985-1994	1994-2005	2005-2013	2013-2020			
1						1.1142164	2.9033008	4.017517225	4.017517225	0
2	-22.980399	-0.8627374	-0.339257	5.3617132	-0.619792	-0.1639383	2.2426983	-17.36171185	7.604411507	-24.96612336
3	-16.241173	-18.894427	18.84314	6.6864617	-1.80962	-0.7052674	3.5763377	-8.544550045	29.10593767	-37.65048772
4	-14.063032	-0.6057192	0.133734	6.4659923	5.08164	-4.1552591	11.624098	4.481455243	23.3054654	-18.82401016
5	-5.8710457	8.1825832	-8.441326	11.489428	5.26334	-1.8266503	-0.2804439	8.515885564	24.9353512	-16.41946564
6	2.5401968	4.7156343	-10.26274	7.8364727	4.483714	-3.6378111	1.3350945	7.010556592	20.91111236	-13.90055577
7	1.2411082	10.371671	-10.67339	5.3189696	2.371658	0.5173112	1.8909027	11.03822926	21.71162096	-10.6733917
8	44.289541	6.7903651	-6.790365	8.2398846	0.492307	-2.7999594	3.7761196	53.99789314	63.58821759	-9.590324454
9	62.158888	7.575095	-9.470425	10.12904	0.42481	-1.6488065	3.0167257	72.18532738	83.30455882	-11.11923144
10	72.748973	1.1110628	-2.422067	3.1934396	19.28806	-4.4452036	2.5525575	92.02681899	98.89408965	-6.867270661
11	-6.0304714	7.0943186	-6.826141	6.9505966	2.216775	-3.7361393	1.615966	1.284904666	17.87765605	-16.59275139
12	-4.2411432	132.58196	-3.872246	6.3264165	3.124271	-5.3098313	2.0819162	130.6913412	144.1145619	-13.42322067
13	-4.3515329	103.22503	-6.412513	6.2907324	4.147179	-6.9576097	3.7385172	99.67980066	117.4014565	-17.72165581
14	-13.852176	6.0862509	-6.142389	5.6304115	4.261589	-5.6827465	3.6263634	-6.072697425	19.60461471	-25.67731213
15	-16.789336	8.7686639	-8.278998	5.9796864	3.619445	-10.235299	6.6334987	-10.30233921	25.00129367	-35.30363288
16	-15.579741	7.4584656	-7.037515	2.5377013	5.579644	-10.907517	6.7605378	-11.18842352	22.33634889	-33.52477241
17	-9.9087058	-1.2408014	0.869373	-1.622901	5.93222	-12.185746	5.5419828	-12.61457945	12.34357519	-24.95815465
18	-2.7439946	68.739861	66.15411	-7.535719	8.343576	-14.521503	9.4794555	127.9157819	152.7169979	-24.80121598
19	-7.436136	0.9913573	-1.286566	-2.770989	7.000422	-13.577613	7.7193053	-9.360219831	15.71108418	-25.07130401
20	-5.6821966	-0.5227918	0.461081	-2.133442	7.157279	-13.599931	4.4891407	-9.830861392	12.10749982	-21.93836122
21	-3.6039939	-0.418924	0.263913	-3.140538	8.598056	-16.135153	3.3433336	-11.09330736	12.20530226	-23.29860962
22	-7.1966443	-5.4112966	6.234018	-7.701078	12.40943	-10.553359	2.115253	-10.10367998	20.75869737	-30.86237735
23	-5.9140611	-2.2407054	0.739848	-5.800137	9.374374	-10.866802	3.116493	-11.59099027	13.23071577	-24.82170604

24	-3.5442252	-1.6697021	1.952197	0.5558278	5.085292	-9.8800405	3.083826	-4.416825563	10.67714227	-15.09396783
25	-6.9380402	-0.8094688	0.809469	-0.400247	4.693442	-8.6935046	4.3009155	-7.037434969	9.803825903	-16.84126087
26	-8.819938	-0.5705121	0.570512	-3.004789	7.446592	-5.7139419	1.1967985	-8.895278378	9.2139028	-18.10918118
27	-4.7216176	-3.4463353	2.479548	0.0160812	4.331859	-6.8957478	3.7251098	-4.511103307	10.55259735	-15.06370066
28	-7.9053853	1.0682042	-1.068204	-0.108817	14.3664	-6.1392674	5.2204468	5.433377638	20.65505119	-15.22167355
29	-9.0147556	0.660928	-5.219235	4.5583073	4.88722	-6.0281888	2.1698585	-7.985865569	12.27631412	-20.26217969
30	-6.7273965	2.4157255	-2.415726	1.5067174	5.643256	-5.1700111	2.965259	-1.78217482	12.53095828	-14.3131331
31	-7.0837284	0.1204331	-0.120433	-0.34076	4.175659	-3.372247	4.2906109	-2.330465252	8.586703394	-10.91716865
32	-8.5624017	0.779604	-0.80858	-1.023549	8.701284	-5.5849531	2.3423058	-4.156289652	11.82319418	-15.97948383
33	-8.6685357	0.5138064	-1.626684	3.3989862	4.826658	-3.8782511	1.3907951	-4.04322531	10.13024575	-14.17347106
34	-10.900154	2.477611	-2.875331	3.0813858	6.511736	-2.9331933	1.6448957	-2.993050942	13.7156282	-16.70867915
35	-9.0425192	-1.206385	1.206385	3.7965432	3.200309	0.6550871	5.5715517	4.180971441	14.42987565	-10.24890421
36	-7.2531393	1.5687991	-1.568799	3.0812225	8.191214	-4.3929378	2.3100679	1.936427285	15.15130351	-13.21487623
37	-1.1539852	0.8457249	-0.845725	5.4093648	8.441233	0.1267967	2.9109714	15.73438046	17.73409054	-1.99971008
38	-3.4512132	2.7244247	-2.724425	-0.681743	14.52596	-1.1223677	9.0725132	18.34315166	26.32290013	-7.979748471
39	-8.3259424	3.8289083	-1.885076	0.7757916	22.30777	-0.8062207	3.0064148	18.90164795	29.91888701	-11.01723907
40	-4.9357371	3.4343283	-3.434328	18.032796	14.91477	-0.6471626	3.8259398	31.19060277	40.20783077	-9.017227997
41	-2.0856808	0.7105323	-2.972024	17.842439	18.24168	1.7390829	5.6024304	39.07845772	44.13616218	-5.057704464
42	25.317803	0.0285872	1.084139	17.202399	12.30139	12.385041	4.6445919	72.96395441	72.96395441	0
43	-12.998589	2.5247614	-2.524761	12.129595	1.07455	0.7017532	4.1615345	5.068843494	20.59219406	-15.52335056
44	-10.305649	-3.5228078	3.030918	14.787751	7.256002	-2.4752513	6.5136981	15.28466136	31.58836933	-16.30370797
45	-12.830046	3.4443989	-6.794582	15.85489	9.550016	1.3529669	3.499635	14.07727861	33.70190694	-19.62462833
46	-14.091282	6.666699	-6.346784	5.8833573	12.75444	7.742327	7.5610797	20.16983364	40.60789992	-20.43806628
47	-7.6563459	3.3283944	-4.445122	1.1248528	7.777297	-2.0315652	19.01199	17.10950111	31.24253444	-14.13303333
48	-7.6922959	0.1989454	0.140144	2.0364006	18.37439	-6.0272942	-0.0966	6.933685101	20.74987525	-13.81619015
49	-5.5307128	5.1011343	-5.101134	5.2539238	13.58643	-7.1681265	0.7978906	6.939403751	24.73937737	-17.79997362
50	-2.9970375	3.4912879	-3.491288	3.5894176	10.54206	-7.3221321	-10.39211	-6.579803023	17.62276445	-24.20256748

51	-1.7522455	2.9473784	-4.104339	-1.368777	10.55496	-4.6064354	-1.2339455	0.436596792	13.50233868	-13.06574189
52	20.050673	3.0066355	-24.82772	15.638586	4.744197	0.029716	-9.6546537	8.987438603	43.4698075	-34.4823689
53	-6.8464835	-5.5045619	4.231837	-4.900744	2.169579	-2.3838486	-1.2211778	-14.4554002	6.401415913	-20.85681612
54	-7.1097953	2.2125769	-2.683775	-2.146686	4.091603	-4.5597597	0.673597	-9.522239261	6.977776719	-16.50001598
55	-4.9706363	-9.3968834	9.396883	-4.329461	2.411613	-3.777154	3.1419765	-7.523661459	14.95047335	-22.4741348
56	-0.2072172	-9.4505961	8.995739	-5.575369	1.078024	-3.334122	2.1308264	-6.362714957	12.20458963	-18.56730459
57	1.7401552	-1.7164593	1.716546	-1.988109	7.393898	-6.1948342	0.5564191	1.507615844	11.40701857	-9.899402726
58	19.002759	-2.5383885	2.102943	-2.560132	6.964692	-5.5907566	0.2565372	17.63765412	28.32693155	-10.68927743
59	13.281748	-1.7937038	-0.281561	1.1419024	4.791809	-5.1154987	-1.0659137	10.95878186	19.21545903	-8.256677166
60	11.860439	-3.0493858	3.235067	-5.483734	4.160783	-0.4425756	-2.4243074	7.856286249	19.25628891	-11.40000266
61	52.28569	-2.472898	2.472898	-9.366525	5.860082	-1.6728646	-3.274207	43.83217523	60.61867017	-16.78649494
62	26.840606	-2.8670696	2.86707	-13.13275	7.309223	-2.6038634	1.1309555	19.54417366	38.14785414	-18.60368048
63	31.68838	-4.335873	4.335873	-21.95163	10.88568	-0.3414263	2.6508496	22.93185696	49.56078428	-26.62892732
64	34.596394	-6.5217329	6.138818	-21.37814	9.990003	-0.2267318	0.3144038	22.91300907	51.0396182	-28.12660913
65	29.631864	-3.8074448	3.807445	-22.39496	5.748392	0.7549081	4.3531737	18.09337499	44.29578186	-26.20240687
66	25.399558	-3.2585494	1.304659	-21.38225	1.041837	5.5649877	10.812864	19.48310508	44.1239059	-24.64080081
67	36.232134	-2.9908391	2.990839	-20.73338	8.335884	1.09379	1.5919275	26.5203573	50.24457412	-23.72421682
68	38.156812	-3.9335025	3.933502	-17.06561	6.194709	-1.1281227	3.6375567	29.79534257	51.92258029	-22.12723772
69	50.140753	-3.0076781	3.403691	-23.7706	10.69362	1.7643901	-0.4739823	38.75019658	66.00245196	-27.25225538
70	21.814018	-5.9858978	4.641938	-19.87053	10.41173	-0.806636	0.8618829	11.06650852	37.72956807	-26.66305954
71	24.144307	-3.6063583	2.901065	-21.34088	12.83375	-5.4410642	1.7300552	11.22087134	41.60917816	-30.38830682
72	38.2342	-2.2549853	3.598941	-18.4979	10.0394	4.1169506	3.9239443	39.16054881	59.91343291	-20.7528841
73	59.57839	-6.7207921	7.668121	-20.84158	12.59116	-2.8890307	-1.0480698	48.3381954	79.83767076	-31.49947535
74	43.463004	-7.6884098	7.089943	-13.21064	7.714907	-3.1396986	0.9870619	35.21616742	59.25491554	-24.03874812
75	57.678151	-5.7784754	5.778475	-10.54996	5.879131	-3.7210565	-0.8138201	48.47244596	69.33575811	-20.86331215
76	15.236831	-0.734707	0.734707	-6.600559	5.708923	-5.8635401	0.7898574	9.271512308	22.47031805	-13.19880574
77	40.656591	-0.7127248	-1.235369	-1.527949	4.234828	-7.0908714	3.1496451	37.47415117	48.04106479	-10.56691362

78	47.027632	-2.2694388	1.872695	-1.054478	8.258843	-8.258843	2.8462808	48.42269134	60.00545073	-11.5827594
79	61.904484	2.455099	-3.900583	1.1001544	8.66675	-11.688921	2.5613373	61.09832093	76.68782469	-15.58950376
80	91.596578	-1.7052115	2.170624	-3.451269	4.861563	-8.876433	-1.6959348	82.89991656	98.62876478	-15.72884822
81	100.54987	-3.5298998	4.366673	-3.553713	3.98646	-11.747678	-0.3117086	89.76000093	108.9029994	-19.14299848
82	91.578058	-6.5016116	6.501612	-2.335293	4.852665	-8.1807112	-3.0624592	82.85225937	102.9323341	-20.08007476
83	77.526528	-9.913713	8.156427	-4.084415	4.806231	-9.4665849	-0.4297235	66.59474936	90.48918628	-23.89443692
84	84.147015	-10.076167	10.07617	-5.624915	4.189769	-9.386874	-1.6768261	71.64816902	98.41295175	-26.76478272
85	82.542989	-10.732652	10.42775	-6.804709	4.440927	-5.5174988	-5.3968739	68.95993286	97.41166731	-28.45173445
86	61.276078	-12.6526	12.6526	-9.524735	4.511912	-6.30417	-6.2463573	43.71272798	78.44059106	-34.72786307
87	84.606735	-12.614423	12.61442	-10.22542	4.302153	-4.8484745	-10.356693	63.47830507	101.5233115	-38.04500644
88	105.11836	1.5980571	9.768425	-6.594986	8.192739	-7.6288156	-13.011784	97.44199079	124.6775766	-27.23558582
89	38.450768	-16.488788	25.4499	-16.14313	10.58656	-7.7184985	-13.059097	21.07772204	74.48723403	-53.40951199
90	32.916212	-12.600497	14.88857	-14.65142	13.26791	-9.6443462	-15.06151	9.114916552	61.07268635	-51.9577698
91	106.68392	-13.425935	13.40296	-12.90073	12.75925	-10.988868	-18.39784	77.1327656	132.8461385	-55.71337294
92	112.14649	-12.725603	10.44006	-15.13677	13.72856	-10.862349	-15.899041	81.69134667	136.3151118	-54.62376515
93	115.16028	-15.265499	15.45403	-14.57872	9.214032	-6.4101021	-13.932212	89.64181659	139.8283522	-50.18653564
94	115.07902	-19.582424	19.52276	-14.50296	11.53488	-11.316758	-11.590377	89.14413529	146.136653	-56.99251776
95	124.5657	-15.272288	15.51714	-15.24968	10.56835	-11.088338	-11.089449	97.95144327	150.6511999	-52.69975661
96	122.48904	-14.794039	14.79404	-10.3535	10.40808	-13.21405	-5.8040327	103.5255396	147.6911608	-44.16562119
97	106.14565	-12.571494	12.57149	-8.473763	7.500137	-10.648491	-3.8214293	90.70210687	126.2172841	-35.51517718
98	98.560435	-19.042995	18.78354	-14.24562	9.049334	-9.6927103	-3.415713	79.9962654	126.3933056	-46.39704016
99	96.728416	-17.114168	16.89231	-15.21879	10.20627	-11.013531	-1.4065672	79.07393852	123.826991	-44.75305247
100	79.699202	-23.450519	23.7828	-16.45782	7.750142	-8.4628002	-1.5110929	61.34991536	111.232144	-49.88222868
101	68.562453	-13.405242	13.07806	-15.46748	4.440299	-3.9145408	-1.9204375	51.37310677	86.08080938	-34.70770261
102	82.182377	-15.06956	15.06956	-20.55445	7.258635	-6.0893148	-0.3980271	62.3992173	104.5105711	-42.1113538
103	78.682148	-14.927761	13.46916	-28.54375	13.82756	-6.0529708	0.5269546	56.98134126	106.5058273	-49.52448603
104	70.759558	-13.51066	13.51066	-15.20309	6.0151	-4.1071323	-1.3939847	56.07044729	90.28531786	-34.21487056

105	63.601516	-13.556535	13.18945	-4.925118	5.791739	-5.7978981	-1.5936516	56.70950252	82.58270525	-25.87320273
106	98.871288	-18.380037	17.85707	-4.663823	6.386209	-6.3844189	-3.3830246	90.3032631	123.1145674	-32.81130435
107	89.588871	-21.221869	12.54957	-2.751482	8.573496	-8.0436522	0.2248364	78.91976836	110.9367715	-32.01700315
108	122.95084	-17.820938	22.45668			-4.805891	-2.4975195	120.2831739	145.407522	-25.12434808
109	105.21585	-26.350523	28.31744			-7.6460133	-3.8266546	95.71010243	133.5332938	-37.82319138
110	66.327824	30.883666	-6.925227			-7.2157935	-8.8020547	74.26841461	97.21148995	-22.94307534
111	79.400111	22.975629	-21.44944			-5.3067621	-7.8240959	67.79544404	102.3757406	-34.58029653
112	127.47807	23.763259	-24.73166			-20.164474	-14.037194	92.30799872	151.2413249	-58.93332617
113	107.03539	44.809112	-44.8584			-21.576862	14.278118	99.68735911	166.1226186	-66.43525954
114	17.644788	18.386874	-18.60671			-24.906461	17.98383	10.50232399	54.01549168	-43.5131677
115	9.9296776	26.676089	-26.64106			-20.716346	16.677395	5.925756567	53.28316144	-47.35740487
116	1.0762022	-12.979922	12.09025			-17.286538	14.700762	-2.399242442	27.86721729	-30.26645973
117	22.94923	-29.840202	-7.831412			-11.860562	4.829218	-21.75372845	27.77844762	-49.53217607
118	46.971169	-21.295481	-8.80975			-13.599761	11.229174	14.49535019	58.2003429	-43.70499271
119	57.403353	-14.422053	5.578031			-10.811931	6.5853728	44.33277328	69.56675721	-25.23398392
120	68.440564	-4.7647412	-8.203998			-11.281975	6.9752274	51.1650765	75.41579145	-24.25071495
121	77.583988	-2.1046929	-12.77874			-7.8054222	0.3142553	55.20938517	77.89824367	-22.6888585
122	92.011994	-12.730728	-7.611463			-5.6427977	-1.0593103	64.9676959	92.01199445	-27.04429855
123	98.108198	-4.7499727	3.936516			-2.9674961	-1.5681473	92.75909845	102.0447146	-9.285616144
124	89.742493	-1.4596426	1.459643			-4.6940275	-1.9427312	83.10573469	91.20213599	-8.096401302